ABSTRACT

Title: AN EXPERIMENTAL STUDY OF SILVER PARTITIONING IN SULFIDE-OXIDE-MELT SYSTEMS AT 800° C.

Leah Englander, Master of Science, 2005

Directed By: Dr. Philip A. Candela – co-advisor
Dr. Philip M. Piccoli – co-advisor
Dr. Ann Wylie

Silver solubility, and partitioning of silver between pyrrhotite and magnetite at a(Ag) = 0.13 ± 0.04 (1σ) has been determined at 800°C, and a range of fS_2 between -4.06 and -0.18 and fO_2 between -14.90 and -11.62 . Solubility is reported at 2800 ± 700 (1σ) ppm for pyrrhotite and 200 ± 100 (1σ) ppm for magnetite, at an a(Ag) = 0.13 ± 0.04 (1σ). Data indicate that silver partitions to a larger extent into pyrrhotite as compared to magnetite, $D_{Ag}^{po/mt} = 13 \pm 14$ (1σ). Silver solubility in a melt, and vapor and brine present at 800°C, 140 MPa and fO_2 ranging between QFM and NNO in Ag-metal saturated hydrothermal experiments were quantified by using LA-ICP-MS. Approximately 1 ppm silver is soluble in peralkaline silicate melts at an a(Ag) = 0.10. $D_{Ag}^{b/v}$ is approximated at 7 at 800ºC, 140 MPa, fO_2 ranging between QFM and NNO, and a(Ag) = 0.10.

Models presented in this study indicate that Au, Ag, and Cu concentrations in silicate melts are impacted by the fractionation of magnetite and pyrrhotite. Sulfide mineral fractionation has a larger effect on ore metal budgets in silicate melts than magnetite. Magnetite does not remove as significant quantities of ore metals as does

pyrrhotite; in high fO_2 melts the minimal effects of Au, Ag, and Cu sequestering by magnetite should yield a high removal of these metals by the MVP. Small variations in fO_2 can affect metal budgets in magmatic-hydrothermal systems because of the partially overlapping stability fields of pyrrhotite and magnetite.

AN EXPERIMENTAL STUDY OF SILVER PARTITIONING IN SULFIDE-OXIDE-MELT SYSTEMS AT 800°C.

By

Leah Irene Englander

Thesis submitted to the Faculty of the Graduate School of the
University of Maryland, College Park, in partial fulfillment
of the requirements for the degree of
Master of Science
2005

Advisory Committee:
Dr. Philip A. Candela Co-Chair
Dr. Philip M. Piccoli Co-Chair
Dr. Ann Wylie

Dedication

This thesis is dedicated to The Family Englander, my Mom, Dad, David, Daniel. I would especially like to dedicate this to Dolly, my dog, who passed away in the Fall of 2004. Dolly you were the best dog, who always listened and sometimes talked back. You are missed by everyone, and will be in my heart forever. To my Mom who is my role model, thank you for all of your love and support and enduring spirit. I only hope I can be like you when I grow up. To my Dad who taught me to keep trying, and for personifying the old saying practice makes perfect, great job Coach Englander. David, without a doubt the smartest and most creative person I know, who has achieved so much already, you have greatness ahead of you. Daniel, oh Daniel you have come along way and I am proud of you. Congratulations from one member of the Class of 2005 to another.

To Mike the best stock car driver/IBM Level 2 Consoles, RRS, and Logger programmer I know who has been there with love and support since Union College, I am so glad you got locked out that fateful day. Thank you for good night, and ride home conversations, and for being the funniest guy I know. I am truly grateful for your keeping it real attitude, and always putting things in perspective. I know that we have had our problems the past three years, but none of that matters now.

Finally, I need to dedicate this thesis to the 2004 World Champion Boston Red Sox. I have been a Red Sox fan for as long as I can remember, and nothing has brought greater joy to my life than that final out on October 16th, 2004. This team exemplified fighting back in the face of adversity, and never giving on their dream, a lesson that anyone can learn from not just a Red Sox fan. There was no curse, there was just bad luck, which is something I can relate to after spending hours in Room 1116 in Geology and having nothing go my way. You have to do what works, and somehow amid failure this project found a way to work. Thank you for your determination.

LONG LIVE RED SOX NATION!!

Acknowledgements

I would like to acknowledge the NSF for providing funding for this project with the following grant #9909576
Thank you Phil Candela for being my advisor and giving me this opportunity. The amount of information that you have to teach people amazes me, you are a great educator.
Thank you Phil Piccoli, I know that taking pictures and pressing the acquire button on the EDS isn't that exciting, but to me it was the coolest thing ever. Thank you so much for all of your guidance and help with everything.
Thank you Ann Wylie for taking the time to be on my committee.
Thank you Adam Simon for giving me a great introduction to the labs, and taking the infamous L1 and L2 to Switzerland with you.

I would like to acknowledge We are We, you know who you are….SKOL!
Courtney, you are the closest thing that I have to a big sister, thank you so much for being the best officemate ever, and a great friend. You have taught me so many important things about life, things I will remember forever. This would not have been the same without you.
Dave, I feel like I have known your forever, I appreciate all of your great advice and value your friendship. Good luck with everything that you do!

Thank you to Dorothy, Jeanne, Ginnette, and Todd for having all the right answers, and all of your help.

To all the roommates at 4703 Caddo Rd, thank you for being so entertaining these past three years. To Miss Ashley from Hotlanta, don't stress about it, that's OUR motto. Brooke, to Thursday nights and neighbors, who will be your party girl now that I'm gone? Thank you for being a great friend, and putting up with me not cleaning the kitchen when I was supposed to.

Thank you to all of my friends from Union and home who were always a phone call away. I'm coming back to the Northeast…y'all get ready.

I would like to thank 94.7 The Arrow for playing all of my requests on the Eclectic Lunch, it made polishing my samples really fun… I would also like to apologize to anyone on the third floor who heard me singing along.

Thank you to the ladies at Dunkin Donuts on Route 1 for making the best Iced Coffee with extra skim milk this side of the Mason Dixon.

To the CRC at UMD for the hours of me time every week.

Table of Contents

List of Tables

List of Figures

Chapter 1: Background and Introduction

Section 1: Background

An ore deposit is a naturally occurring, spatial concentration of metal or nonmetals that can be mined at a profit. Ore deposit formation is a consequence of the sum total of the magmatic, tectonic, chemical, and hydrologic processes operating in the Earth's crust. In the magmatic-hydrothermal systems that generate porphyry and epithermal-vein type deposits, ore deposit genesis is associated with the formation of an igneous intrusive body of intermediate to felsic composition (i.e. diorites, granidiorites, granites) (Figure 1).

Porphyry ore deposits sit near the top of the causative intrusion in the upper 2-5 kilometers of the crust. The ore is hosted in fractures, veins and stockwork structures. Fracturing in the surrounding wall and roof rock is hypothesized to result from the brittle failure induced by the stress of the intruding magma and the change in internal pressure generated during exsolution of hydrothermal fluid from the related melt (Burnham, 1979). Hydrous silicate melts (liquid + volatiles) exsolve a volatile phase when the amount of water present exceeds the saturation concentration for a melt at a given temperature and pressure (Burnham, 1975). Volatile exsolution is attributed to a decrease in load pressure as the melt ascends to higher levels in the crust (first boiling), and/or crystallization of anhydrous mineral phases (second boiling). The aqueous phase, or magmatic volatile phase (MVP), is any chloride bearing vapor or brine that has exsolved from a melt (Frank, 2001). Experiments

Figure 1: Schematic of a magmatic-hydrothermal environment (Adapted from Hedenquist and Lowenstern., 1994). Not drawn to scale.

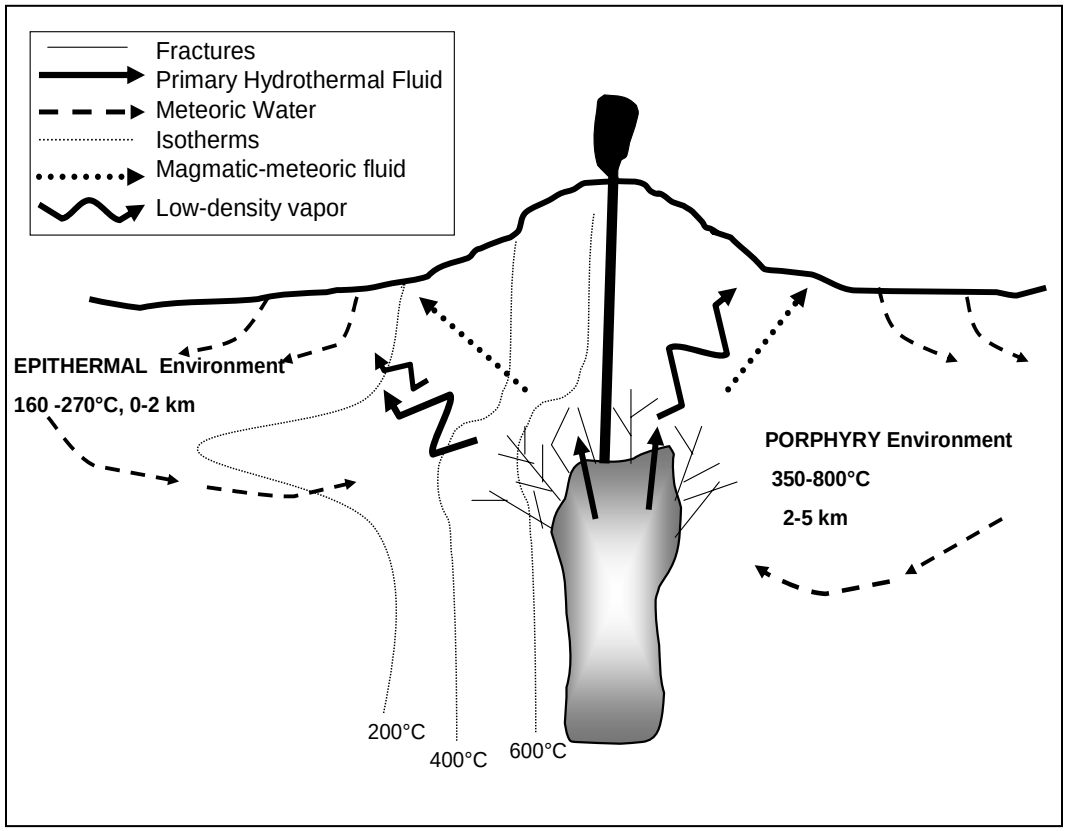

conducted in the NaCl-H_2O system show that chloride-bearing fluids can separate into an immiscible vapor + brine phase at temperatures and pressures equivalent to those found in magmatic-hydrothermal systems in sub-volcanic environments (Bodnar and Sterner., 1985, Chou, 1987, Fournier, 1987, Anderko and Pitzer, 1993). Hydrothermal fluids and volatile exsolution from hydrous silicate melts have been extensively studied because of their importance in many geologic systems. The prevailing hypothesis for the origin of magmatic-hydrothermal ore involves the concentration of ore metals in vapors and brines, later to precipitate from solution to deposit ore. As well as NaCl and H_2O, MVPs can have high solute loads of potassium, iron, and other cations, dissolved gas constituents such as CO_2, H_2, H_2S, SO_2, and ore metals such as copper, silver, and gold. Surficial analogues of these fluids include waters from active geothermal areas and gases discharged from fumaroles and volcanic vents where metals concentrations and fluxes have been measured (Brown, 1986, Hedenquist and Lowenstern, 1994, Hedenquist, 1995, Simmons 1995, Stefansson and Seward, 2003).

Brine and vapor inclusions in quartz from veins and surrounding alteration minerals are considered to include samples of hydrothermal fluids from which associated ore minerals precipitate. Advancements in analytical techniques have made it possible to determine ore metals concentrations in fluids from natural ore systems by using LA-ICP-MS (Heinrich et al., 1992, Audetat et al., 1998, Günther et al., 1998). Similar techniques have been applied to synthetic fluid inclusions grown in ore metal- saturated experimental systems (Frank et al., 2001, Simon et al., 2004). Metal solubility experiments indicate that gold and other metals are transported as

chloride, sulfide, or hydroxyl associated complexes in aqueous phases (Candela and Holland, 1984, Gammons and William-Jones, 1997, Frank et al., 2001, Stefansson and Seward, 2003). Data from experiments conducted at temperatures and pressures akin to those in magmatic-hydrothermal systems indicate that ore metals partition to a large extent into the magmatic vapor and brine phases relative to a coexisting melt (Candela and Holland, 1984, Candela and Holland, 1986, William et al., 1995, Candela and Piccoli, 1995, Frank et al., 2002, Simon et al., 2003b). The amount of Au, Cu, or Ag available to the MVP is limited by the proportion of metal remaining in the melt at the time of volatile saturation. Metal concentrations in a melt can decrease with the progressive crystallization of mineral phases such as magnetite, pyrrhotite, chalcopyrite, and bornite (Cygan and Candela, 1995, Jugo et al., 1999, Simon et al., 2003). If MVP exsolution occurs late in the crystallization history of a melt, the probability of formation of metal-rich ore deposit can decrease if a significant amount of metal has been sequestered by these crystallizing phases (Candela, 1989, 1992). Data from experimental studies can be used to model the development of an ensuing ore deposit and predict what factors enrich and diminish the potential for an ore deposit to form.

Section 2: Introduction

The Group IB, or coinage metals comprise copper, silver, and gold. Silver use dates back to the 7th century B.C., when ancient civilizations first recognized its value as a versatile metal. In the 21st century, the world demand for silver is approximately 30, 000 tons per year. Silver is mainly exploited for its ability to conduct electricity. Jewelry, photography, X-rays, and medicine also rely heavily on silver for its

different properties, including its aesthetics, sensitivity to light, and ability to kill bacteria. The price of silver in the commodities market is dramatically lower than gold, making it a more affordable metal. Silver is different from gold with respect to some physical and chemical properties, such as color and resistance. The price of silver in relation to other metals is partially a reflection of its relative abundance in the Earth's continental crust, where Cu, Ag, and Cu are present at 27 ppm, 56 ppb, and 1.3 ppb respectively. Other factors include demand and recoverability/production costs.

A proportion of the world's silver is mined from epithermal vein deposits, which are low temperature hydrothermal deposits (160-270°C) which form in the epizone of the Earth's crust (Robb, 2005). Silver and other metals in epithermal deposits are inferred to be magmatic and are sometimes related to higher temperature, deeper porphyry ore deposits (Simmons, 1995). Hydrothermal fluids in epithermal systems are derived from the mixing of low density magmatic vapor and circulating meteoric water (Hedenquist and Lowenstern, 1994). Long-lived groundwater convection cells are maintained due to heat generated from plutons. Vapors, which are more buoyant and less dense than brine, escape through the fracture network propagated during pluton and porphyry ore emplacement and are infused into the circulating groundwater. Silver can be present in high concentrations in porphyry deposits, although primary silver-bearing phases do not precipitate in these environments. Silver is found mainly in the sulfide minerals chalcopyrite and bornite and as silver-gold alloy. Silver grades in porphyry deposits are often higher than gold; for example Ag: Au ratio in two deposits in British Columbia, Copper Mountain

and Poison Mountain, is 25:1 in grams/metric ton (Singer et al., 2005). The Bingham Canyon Porphyry Copper Deposit contains approximately 15 million tons of copper, 9,000 tons of silver, and 1,300 tons of gold (Ag: Au = 7:1) (Ballantyne et al., 1997).

Epithermal vein deposits are classified as high sulphidation or low sulphidation deposits; this refers to the oxidation state of sulfur in the hydrothermal fluid and the type of hydrothermal alteration related to the deposit (Hedenquist and Lowenstern, 1994). High-sulphidation deposits are proximal to volcanic vents, and the associated hydrothermal fluids are acidic and oxidized are predominantly magmatic in origin. Low-sulphidation deposits are found in geothermal areas, distal to volcanic vents. The major constituent of hydrothermal fluids is meteoric water; they have near-neutral pH, are reduced, and have low salinity (Robb, 2005). Low-sulphidation deposits are extensively mined for silver and are generally more silver-rich than high sulphidation deposits. Silver is mainly extracted from Ag-bearing enargite, (Cu_3AsS_4) Mexico is the world's largest silver producer; silver deposits are also found in Peru, Australia, United States, and China.

The formation of epithermal vein deposits may be ultimately linked to underlying magmatic systems and associated porphyry ore deposits. Magmatic contributions to epithermal deposits have been extensively studied by using oxygen isotopes, the N_2-Ar-He system, hydrogen, helium, and fluid inclusion analysis as tracers for fluid origin (O'Neil and Silberman 1974, Sheppard and Taylor, 1974, Giggenbach and Corrales, 1992, Hedenquist and Lowenstern, 1994, Simmons, 1995, Albinson et al., 2001). Data from these studies indicate that magmatic signatures in fluid inclusions and hydrous minerals related to epithermal deposits are present. In

most cases, they are weak owing to water-rock interaction along the flowpath separating a magma from and the epithermal environment, or waning hydrothermal activity (Simmons et al., 1995).

Extensive experimental studies show that the efficiency of ore metal transport in high temperature magmatic-hydrothermal systems is a function of factors such as pressure, chloride concentration of the hydrothermal fluid, timing of MVP exsolution, and the extent of mineral crystallization prior to MVP exsolution. Assuming that porphyry-type and epithermal-type mineralization are related, the processes involved in porphyry ore deposition also control, to some extent, the probability of epithermal vein deposit formation. The focus of this study will be to target one metal, silver, which can be in high concentration in both porphyry and epithermal deposits, to begin to understand how silver behaves in magmatic-hydrothermal systems.

Chapter 2: Experimental Procedure

Section 1: Experimental Procedures: Sealed Silica glass Tube Experiments

Experiments were conducted in Heraeus silica glass (Amersil) tubing. Two thicknesses of tubing were used: 5 mm ID, 7 mm OD (1 mm wall), and 5 mm ID, 9 mm OD (2 mm wall). The silica glass tubing was sealed at one end by using an oxygen-methane torch. The tubes were loaded with pyrrhotite from Sudbury, Canada (Ward's Scientific, 46E6898), magnetite, and silver foil (99.9% Ag, thickness 0.025 mm) from Sigma-Aldrich. The primary source of silica in the experiments was the silica glass tubing. Approximately 28 mg of silver was used per experiment, and was added as several little pieces. The pyrrhotite was crushed and ground before being loaded into the silica tubing. The composition of the starting pyrrhotite and magnetite are reported in Table 1. Flattened triangle-shaped pieces of gold, weighing on the approximately 9 mg, and approximate thickness of 0.197" were added to the experiments to be used as a calibrant for silver activity. The silica glass tubing was evacuated by using a vacuum pump and sealed by using methods described by Kullerud (1971). The average length of the loaded, sealed, evacuated tubes was 40 cm. All experiments were shaken prior to being loaded into the furnaces to try and evenly distribute the starting materials. Experiments were conducted in Lindberg one atmosphere furnaces calibrated to 800°C; the temperature was monitored with Type-K (Chromel-Alumel) external thermocouples placed adjacent to the silica tubes on the floor of the furnace. The temperature gradient over the lateral extent of the furnace was determined to be 0.33°C/ cm.

Table 1: The composition of the magnetite and pyrrhotite starting material used in the silica tube experiments. Analyses were performed using the EPMA at the University of Maryland. All values are reported in weight percent element, b.d. stands for below detection. Detection limits for each element are reported in Table 6. The magnetite (Meramac) is part of the starting material collection donated to the University of Maryland by Julian J. Hemley (USGS). Values are reported with a 1σ standard deviation.

Metal	Pyrrhotite, Sudbury, Canada	Magnetite M109237
Fe	60.45 ± 0.13	(FeO) 89.40 ± 1.41
Ag	bd	bd
S	38.66 ± 0.14	0.03 ± 0.05
Mn	0.008 ± 0.005	0.018 ± 0.014
Cu	0.006 ± 0.004	bd
Si	bd	0.039 ± 0.027
Zn	0.029 ± 0.058	0.03 ± 0.05
Total	99.10 ± 0.11	89.53 ± 1.73

The sulfur and oxygen fugacities were limited to finite range by the assemblage magnetite – pyrrhotite, fO_2 ranges between -14.63 and -11.6, fS_2 ranges between -3.74 and -0.18. Experiments were rapidly quenched in a room temperature water bath. Experiments were determined to be successful after quenching if there was a 'pop' when the tube was opened and an accompanying sulfurous odor. Experiments were classified as 'failed' if the tubing filled with water upon quenching. A comprehensive summary of all the experiments is in Table 2.

Table 2: Summary table of the experimental design for silica tube experiments completed in this study; gray shading denotes failed experiments. Experiments 17-51 were conducted in Furnace 1, and experiments 52-60 were conducted in Furnace 2. Silica tubing with a 2 mm wall thickness has a 5 mm ID and 7 mm OD, silica tubing with a 1 mm wall thickness has a 5 mm ID and a 9 mm OD. Gold was added as 2 triangles (4 mm^2) or 4 triangles (8 mm^2), and had a thickness of 0.197". The silver foil was added as small pieces, amounting to 28 mg of total weight.

Sample #	T (C)	Pyrrhotite (mg)	Magnetite (mg)	Silver Foil	Gold	Duration (hrs.)	Silica tube size
17	800	200	50	Y	N	96	2 mm wall
18	800	200	50	Y	N	96	2 mm wall
19	800	200	50	Y	N	96	2 mm wall
20	800	200	50	Y	N	96	2 mm wall
21	800	200	50	Y	N	96	2 mm wall
22	800	200	50	Y	N	96	2 mm wall
23	800	200	50	Y	N	96	1 mm wall
24	800	200	50	Y	N	96	1 mm wall
25	800	200	50	Y	N	96	1 mm wall
27	800	200	50	Y	N	144	1 mm wall
28	800	200	50	Y	N	144	2 mm wall
29	800	200	50	Y	N	144	2 mm wall
30	800	200	50	Y	N	144	1 mm wall
31	800	200	50	Y	N	144	1 mm wall
32	800	300	60	Y	N	144	1 mm wall

Sample #	T (C)	Pyrrhotite (mg)	Magnetite (mg)	Silver Foil	Gold	Duration (hrs.)	Silica tube size
33	800	300	60	Y	N	144	1 mm wall
34	800	300	75	Y	N	168	2 mm wall
35	800	300	75	Y	N	168	2 mm wall
36	800	300	75	Y	N	168	2 mm wall
37	800	300	75	Y	N	285	2 mm wall
38	800	300	75	Y	N	285	2 mm wall
39	800	300	75	Y	N	523	2 mm wall
40	800	300	75	Y	N	523	2 mm wall
41	800	300	75	Y	N	696	2 mm wall
42	800	300	75	Y	N	696	2 mm wall
43	800	200	50	Y	2x2 mm	227.5	1 mm wall
44	800	200	50	Y	2x2 mm	227.5	1 mm wall
45	800	200	50	Y	N	227.5	1 mm wall
46	800	200	50	Y	4x4 mm	227.5	1 mm wall
47	800	200	50	Y	2x2 mm	227.5	1 mm wall
48	800	200	50	Y	N	227.5	1 mm wall
49	800	200	50	Y	4x4 mm	227.5	1 mm wall
50	800	200	50	Y	2x2 mm	227.5	1 mm wall
51	800	200	50	Y	2x2 mm	227.5	1 mm wall
52	800	200	50	Y	2x2 mm	336	1 mm wall
53	800	200	50	Y	2x2 mm	336	1 mm wall
54	800	200	50	Y	2x2 mm	336	1 mm wall
55	800	200	50	Y	2x2 mm	504	1 mm wall
56	800	200	50	Y	2x2 mm	504	1 mm wall
57	800	200	50	Y	2x2 mm	504	1 mm wall
58	800	200	50	Y	2x2 mm	696	1 mm wall
59	800	200	50	Y	2x2 mm	696	1 mm wall
60	800	200	50	Y	2x2 mm	696	1 mm wall

Section 2: Experimental Procedures: Hydrothermal Experiments

In these experiments an aqueous phase, melt, silver, and magnetite (Fe_3O_4) were equilibrated at 800°C and 140 MPa at oxygen fugacities ranging between QFM and NNO. The capsule material was gold (4.8 mm ID, 5.0 mm OD, 0.197" wall, 30 mm length) with an annealed silver lining occupying approximately one-half the length of the capsule. The silver was annealed to the gold over a Meeker Burner. The starting materials, 40 mg of a synthetic rhyolite melt (GR-1), 40 mg magnetite, 100 μL of aqueous solution, and a small rectangular piece of pre-fractured inclusion-free Brazilian quartz were loaded into the charge. The synthetic rhyolite, GR-1, was prepared from the components $NaAlSi_3O_8$, $KAlSi_3O_8$, and SiO_2, at the USGS (Reston). The composition of the starting materials is reported in Table 3. The magnetite is from Essex County, New York. The aqueous solution was prepared to have a composition of 15 wt. % NaCl equivalent, with a molar ratio of Na:K:H of 1.0:1.0:0.5. The starting solution composition was selected to lie in the vapor plus brine stability field in the binary H_2O-NaCl system at the designated experimental pressure and temperature (Figure 2). The quartz chip was added to trap vapor and brine at run conditions for later fluid inclusion analysis. The capsule bottoms were welded into a 'tri-crimp' configuration with a carbon arc welder. The starting material and capsule were weighed, placed in copious amounts of dry ice, and top welded. To verify that no aqueous solution was lost during welding, the capsules were placed in a drying furnace at 120°C overnight, and then reweighed. Capsules were used if the weight remained constant ± 0.1 mg.

Experiments were carried out in René-41 cold-seal pressure vessels composed of a nickel-based alloy. Water was used as a pressure medium. Vessels were externally heated in doubly-wound tube furnaces fitted with Kanthal windings and were inclined 12° to minimize convection at the hot end of the vessel (Frank, 2001). The furnaces were calibrated to 800°C, and the temperature was monitored by Type-K (Chromel-Alumel) external thermocouples. The vessels were calibrated with internal thermocouples to estimate the temperature gradients across the length of the capsules, which were ± 4°C. Pressure was generated by using an air-driven water compressor. In order to accommodate for the expansion of water upon heating past the boiling point, the vessels were initially brought up to temperature and pressure in two steps approximately 30 minutes apart: 1) 100 MPa and 800°C, 2) 140 MPa and the calibrated temperature. Final adjustments were made to achieve the pressure of 140 MPa in the vessel after the initial heating phase. The temperature was monitored during the course of the experiment to ensure that there were no signigicant fluctuations from the calibrated temperature. The experiments were quenched isobarically. First a steady stream of compressed air was employed until the vessel was approximately 200°C, and then the vessel was placed in a room temperature water bath. The vessel was left in the water bath for approximately one hour to cool down room temperature. A summary of all successful experiments is in Table 4.

Table 3: The composition of the starting synthetic rhyolite, GR-1, used in the hydrothermal experiments. The analysis was performed using the EPMA at the University of Maryland (Simon, 2003). All concentrations are reported in weight percent oxide, with the exception of Cl and are reported with a 1σ standard deviation.

Oxide	GR-1
SiO_2	80.4 ± 1.4
K_2O	4.67 ± 0.43
CaO	0.02 ± 0.01
Na_2O	3.58 ± 0.24
Al_2O_3	10.9 ± 1.1
FeO	bd
Cl	0.05 ± 0.05
Total	99.6 ± 0.9

Figure 2: 800°C isotherm in the NaCl(eq.) – H_2O system, adapted by using data presented in Bodnar (1985). The red dot represents the starting aqueous fluid loaded into the hydrothermal experiments with a 15 wt.% NaCl equivalent composition.

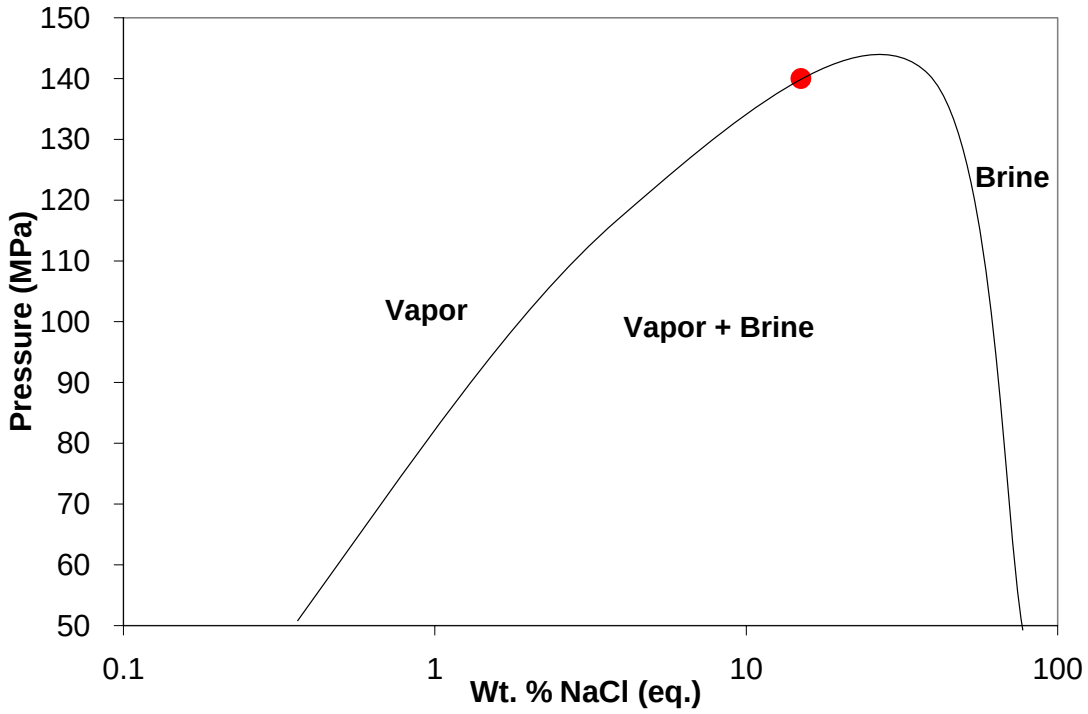

Table 4: A summary table of the successful hydrothermal experiments conducted in this study. GR-1 is the starting synthetic rhyolite melt, and the composition of the starting aqueous fluid was 15 wt. % NaCl equivalent. The molar ratio of Na: K: H in the aqueous fluid is 1.0 : 1.0 : 0.5.

	Capsule material	GR-1 (mg)	Magnetite (mg)	Aqueous fluid	P (MPa)	T (°C)	Duration (hrs.)
L1	Gold w. silver foil	40	40	100 µL	140	800	168
L2	Gold w. silver foil	40	40	100 µL	140	800	168

Section 3: Failed Silica Tube and Hydrothermal Experiments

Silica tube and hydrothermal experiments failed during the course of this study. Silica tube experiments were designated failures if there was water present in the silica tube after quenching. The water leaked into the cylinder syn-quench, leaving the run products irreparable. They did not physically resemble the run products produced in successful experiments, and were not considered viable for analysis.

Sixty-seven hydrothermal experiments were conducted as part of this study. Two are included in this thesis. Experiments conducted in platinum capsules (1-36) failed due to iron-silver-platinum interaction. Iron loss to the platinum capsule caused a weakening of the capsule walls, which instigated cracks to develop and as a consequence the capsule leaked during the course of the experiment. Twenty milligrams of magnetite were added to the initial experiments, but not magnetite was found in the run products. By adding more magnetite, to try and procure run product magnetite, the iron caused excessive weakening of the platinum capsule.

The second set of high temperature experiments was conducted in gold capsules, which was later changed to gold capsules with a silver foil lining. The successful experiments reported in this study were part of this group.

$Ag_{75}Pd_{25}$ tubing was used for later experiments, where silver for the experiments was provided by the capsule material. The material developed micropores and leaked as silver was shed from the capsule into the vessel during the course of the experiment (Figure 3).

Figure 3: Secondary electron image of micropores in the wall of the AgPd capsule material used for hydrothermal experiments.

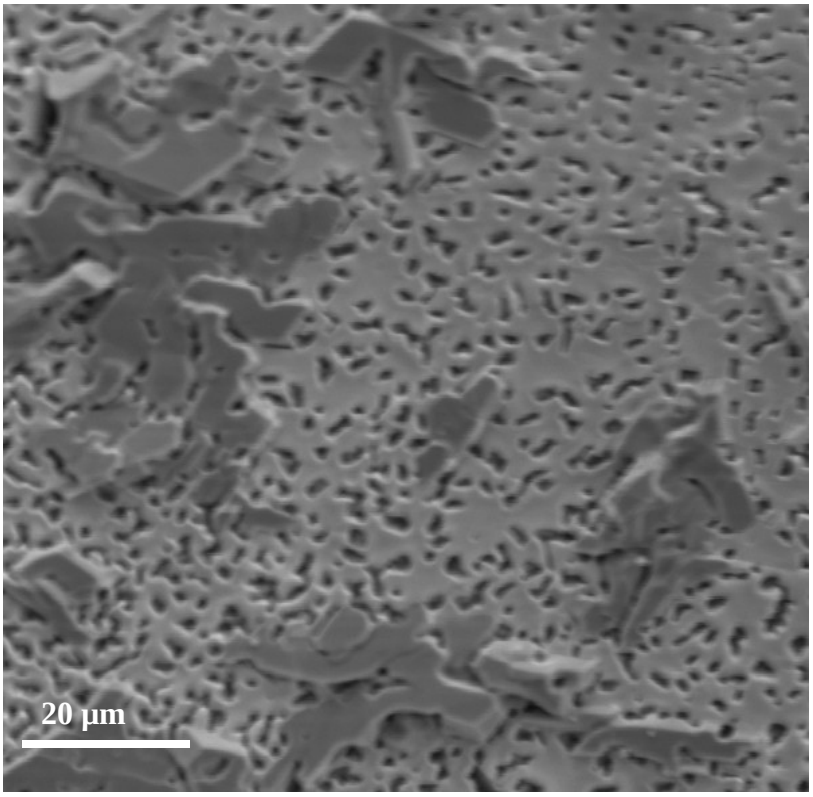

Chapter 3: Analytical Methods

Section 1: Sealed Silica Tube Experiments

Sample Preparation for Electron Probe Analysis

Immediately following quenching, run products were removed from the silica tubing, given sample numbers and placed in glass vials. Each sample was inspected using a binocular microscope to identify phases present. A representative group of run products from each experiment was mounted in epoxy, and cured overnight. Epoxy mounts were polished by using an automatic polisher with 320 grit SiC paper, hand polished with 600 grit SiC paper, and then polished with successive steps of diamond paste including 15 micron, 9 micron, 6 micron, 3 micron, and 1 micron. This was done to ensure a flat surface on each of the grains mounted to achieve good analyses; samples were checked under a reflected light microscope to make sure the polish was adequate. The mounts were prepared for further analysis by applying 300 Å of carbon using standard thermal evacuation techniques.

Analysis of Run Products

Grains in the polished epoxy mounts were then analyzed visually, qualitatively and quantitatively by using a JEOL 8900R Superprobe (Electron Probe Microanalyzer; EPMA) at the Center for Microscopy and Microanalysis at the University of Maryland. Backscatter electron (BSE) imaging was used, in conjunction with energy dispersive spectroscopy (EDS), to first identify the phases present. Phases identified in all experiments include pyrrhotite, magnetite, quartz, a silicate phase, silver-iron sulfide, and electrum (electrum in experiments 44-59, exc. 45 and 48).

Wavelength dispersive spectroscopy (WDS) was used for quantitative phase characterization of starting materials and run products. Backscatter electron images were used as reference guides for every sample. Points were identified on each image corresponding to a grain in the sample mount that was analyzed. Traverses comprised of several points taken on larger grains to identify compositional changes. Distinct morphologies of the same phase were identified in several experiments, and were analyzed seperatly. Pyrrhotite, magnetite, silver-iron sulfide, and electrum were analyzed for Fe, Ag, S, Mn, Si, Cu, Pb, Zn, and Au. Analyses were performed at 20 kV, sample current of 10^{-7} A, a beam diameter of 2 μm, and a count time of 180 seconds. Standards were used to correct the X-ray intensity of each element. PbAgSbS was used as a primary standard for silver: acanthite and silver metal were used as secondary standards to ensure the correction factors were accurate. Magnetite from Minas Gerais, Brazil was used as a standard for iron for magnetite, pyrrhotite from Santa Eulalia, Mexico was used as a standard for iron and sulfur. Rhodonite, (Mn- Fe-Mg, Ca)SiO_3, from Broken Hill, NSW, Australia was used as a standard for manganese and silicon. Chalcopyrite from Inguaram, Michoacam, Mexico was used to standardize for copper, and Sphalerite from Balmet, New York was used as a standard for zinc. Gold metal was used as a standard for gold. The compositions of the standards are listed on Table 5. Raw intensities were corrected using a standard ZAF algorithm. Detection limits for microprobe analysis for the elements of interest for this study are provided in Table 6.

Table 5: The chemical composition of the standards used for EPMA analyses of the run products from the silica tube experiments conducted in this study. Mineral abbreviations were used for the minerals in the following table: rhodonite (Rhd), magnetite (Mt), galena (PbS), pyrrhotite (Po), sphalerite (Sp), chalcopyrite (Ccp).

	Rhd	Mt	Ag	Au	PbS	PbAgSbS	Po	Sp	Ccp
SiO_2	46.7								
Al_2O_3	0.9								
Fe_2O_3	0.1	67.50							
FeO	12.3	30.20							
MgO	0.4	0.05							
CaO	5.6								
Na_2O									
K_2O									
TiO_2		0.16							
P_2O_5									
MnO	33.3	<0.01							
Cr_2O_3		0.25							
F									
Cl									
H_2O									
CO_2									
SO_3									
Ag			100			23.80			0.10
As									0.40
Au				100					
Bi									0.01
Cu									34.6
Fe							61.28		30.4
Pb					13.40	30.47			0.01
S					86.60	18.86	39.01	32.9	34.9
Sb						26.86			0.30
Zn								67.1	0.03
Total	99.60	98.16	100	100	100	99.99	100.2	100	100.8

Table 6: The detection limits (ppm) for the elements of interest for this study for EPMA analysis. Detection limits are presented as ranges because they varied throughout the analyses. Detection limits are reported at the 1σ level.

Element	Magnetite	Pyrrhotite
Fe	(FeO) 230- 240	160-180
Ag	20-30	20-30
S	50-60	25-30
Mn	60-70	55-65
Si	42	20-25
Pb	115-125	115-130
Cu	40-45	30-40
Zn	520-600	440-480
Au	200-210	200-210

Section 2: Hydrothermal experiments

Sample Preparation for Electron Probe

Capsules were removed from the René vessels, cleaned and weighed to determine whether or not the system remained closed during the course of the experiment. Successful capsules were pierced with a hypodermic needle, and the fluid was removed. The run products were removed and separated from the capsule material and washed with deionized and distilled water. For sample preparation methods for microprobe analysis please refer to "Sample preparation for electron probe analysis" in the experimental procedure section for sealed silica tube experiments.

Analysis of Run Products (EPMA)

The grain mounts were analyzed by using EDS to identify the phases present, which include a silicate glass (quenched melt), magnetite, and fayalite in experiment L1. BSE images were taken of each phase, which were used to identify points in each grain that would be characterized using WDS. The glass was analyzed for major elements, including Si, Al, Fe, Na, Ca, K, and Cl. Operating conditions for major elements in the glass are as follows, accelerating potential of 15 keV, beam current of 5 nA, and beam size of 15 microns. Yellowstone Rhyolite was used to correct X-ray intensities for Si, Al, Na, and K in the melt, Kakanui hornblende was used to standardize iron, and scapolite (Meionite, Brazil) was used to standardize chlorine.

Analysis of Fluid Inclusions (Microthermometry)

Quartz chip processing and microthermometry was done at the University of Maryland by Dr. Adam Simon. The recovered chips were washed in deionized and distilled water to remove contaminants, and then set in epoxy. The mounts were sectioned into discs ~ 500 microns thick, and polished for microscopic examination, microthermometry, and LA-ICP-MS analysis. The microthermometry was done by using a USGS-gas flow heating-freezing stage manufactured by Fluid, Inc. using methods described in Simon et al. (2004).

Analysis of Fluid Inclusions (LA-ICP-MS)

Synthetic fluid inclusions trapped in the quartz chips and silicate glasses were analyzed via Laser Ablation-Inductively Coupled-Mass Spectrometry (LA-ICPMS) at ETH in Zurich, Switzerland for Na, Al, Si, K, Fe, Ag, and Au by Adam Simon. All analyses were externally calibrated with a National Institute of Science and Technology (NIST) SRM 610 silicate glass standard. Element ratios determined by LA-ICP-MS were converted to absolute element concentrations using sodium as an internal standard. The analyses were done by using similar methods described in Heinrich et al., (2003), and Audétat and Pettke, (2003).

In situ laser ablation of individual inclusions was done with a 193-nm ArF excimer laser (Complex 110i, Lamda Physik) with an output energy of 100-120 mJ. The beam diameter was large enough to envelope the entire inclusion, which ranged between 13 and 26 microns. Ablations pits, approximately 75 and 90 microns in diameter, were drilled into the glasses. The ablated material was flushed from the sample chamber and carried in a helium gas aerosol to the plasma torch. An Elan

6100 (Perkin-Elmer) quadrapole mass spectrometer was used to analyze for the isotopes of interest, including ^{23}Na, ^{27}Al, ^{29}Si, ^{39}K, ^{57}Fe, ^{107}Ag, and ^{197}Au.

Section 3: Demonstration of Equilibrium

The conclusions reported in this study are predicated upon the fact that equilibrium was attained in the experimental system before quenching. The demonstration of equilibrium for silica tube experiments hinges on time invariance of the partition coefficient for silver between the magnetite and pyrrhotite. The duration of the silica tube experiments was varied between 96 and 696 hours, with at least three replicate experiments for each duration of time (96, 144, 168, 227.5, 285, 336, 504, 696) at identical experimental conditions. Values for silver concentration in magnetite and pyrrhotite, partition coefficients, activity of silver, and fugacity presented in this thesis are for sealed silica tube experiments that were run for 144 hours or longer. Experiments that were run for 96 hours did not attain equilibrium, and therefore data generated from these experiments will not be used in any of the presented values. Hydrothermal experiments were conducted for 168 hour; previous studies have shown that this is sufficient time for the systems to attain equilibrium (Candela and Holland, 1984, Frank et al., 2002, Simon et al., 2003b).

Chapter 4: Results: Silica Tube Experiments

Section 1: Exclusion of Data and Observations

Magnetite analyses were evaluated based on specific criteria to determine whether they were suitable for inclusion in the final data set (Figure 4a). Pyrrhotite analyses were refined based on a similar set of criteria more applicable to ideal pyrrhotite compositions (Figure 4b). Analyses were excluded from partition coefficients and other relevant calculations if they did not meet the criteria. BSE images were used to identify each point analyzed by using EPMA, and to evaluate the integrity of that point based on its relationship with bordering phases. A possible source for contamination in phase analyses is from simultaneously hitting two phases with the electron beam when the desired target was only one phase.

Data from thirty-seven successful sealed silica tube experiments are included in this thesis. In all of the silica tube experiments pyrrhotite, magnetite, a silicate phase (Figure 5), quartz, silver-iron sulfide, and electrum (experiments 44-60) were identified from BSE images, and visual observation of the run products with a fiber optic light source and a binocular microscope (Table 7).

Figure 4a: The criteria used for evaluating individual data points in the magnetite data set; data points are corrected analyses generated by the EPMA.

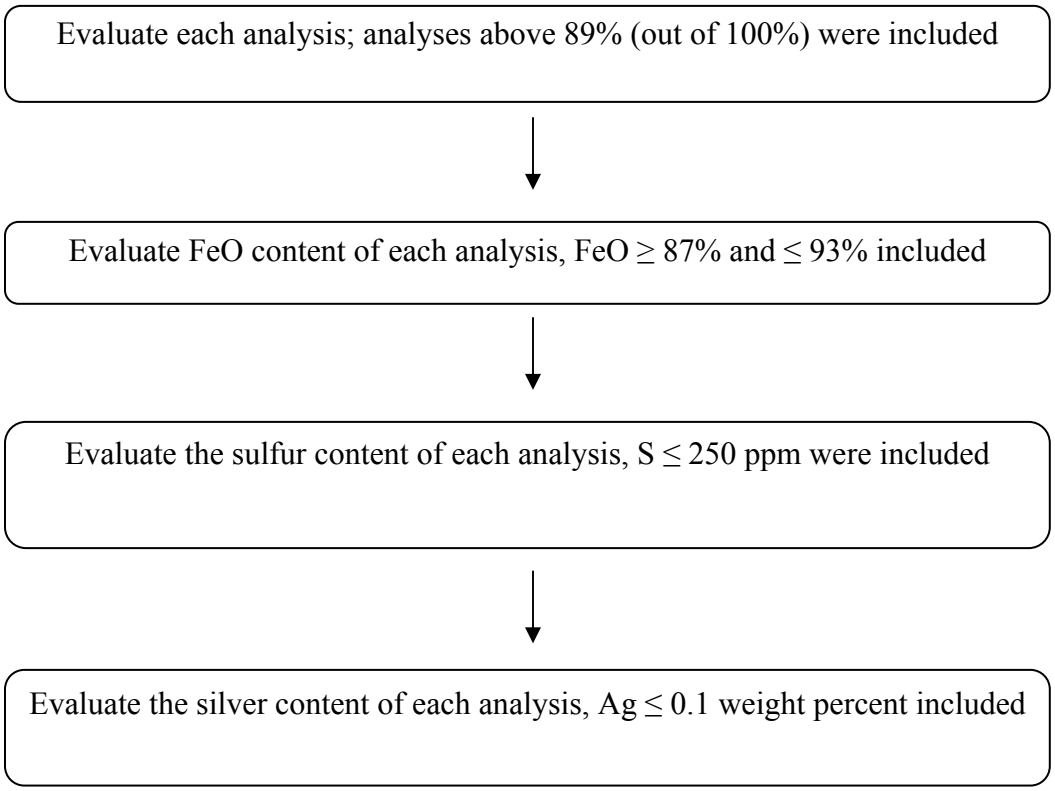

Figure 4b: The criteria used for evaluating the individual data points in the pyrrhotite data set; data points are corrected analyses generated by the electron probe.

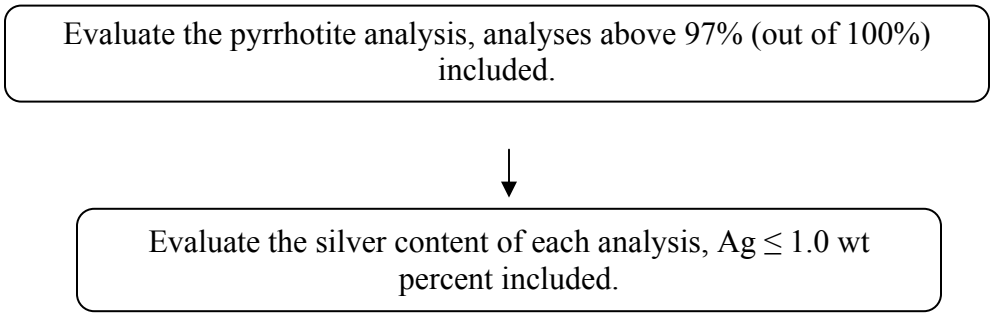

Table 7: Visual observations of the run products from silica tube experiments 17-60; observations were done using a binocular microscope and fiber optic light source. All observations were taken immediately after quenching the experiments.

Sample #	Observations
17	Large black colored fine-grained pieces, metallic luster, magnetic with metallic bronze colored drops on top, white silica with small pyrrhotite crystals on side in contact with the tubing walls. Silicate phase present
18	Dark staining on sides of tubing, no small pyrrhotite, larger pieces have metallic colors (blue, green, red, yellow)
19	Similar to 17
20	Similar to 17
21	Similar to 17
22	Similar to 17
23	Run products are not consistent with other failed experiments; resemble the assemblage present in 17. FAILED
24	Similar to 17
25	Similar to 17
27	Similar to 17
28	No white silica with small pyrrhotite grains on side of tubing, large black, fine-grained pieces, magnetic, with metallic bronze drops. Silicate phase present.
29	Similar to 28
30	Similar to 28
31	Similar to 28
32	Large black pieces (2-3), tubing filled with water FAILED
33	Large black pieces (2-3), tubing filled with water FAILED
34	Black, some bronze pieces, fine-grained, metallic luster and magnetic, no white silica with small pyrrhotite grains. Silicate phase present.
35	Similar to 34
36	Similar to 34
37	Similar to 34
38	Similar to 34
39	Large black pieces, tubing filled with water FAILED
40	Similar to 34

Sample #	Observations
41	Exploded during quench, few grains were stuck to side of tubing
42	Large black pieces, tubing filled with water FAILED
43	Silica tubing coated in metallic substance, run products were very similar to other experiments. EXCLUDED
44	Run products are black/grey fine-grained masses with metallic luster. Bronze grains with metallic luster also present. Gold pieces present at the end of experiment similar in shape/size to starting gold material. Silicate phase present
45	Run products are black/grey fine-grained masses with metallic luster; and relatively bigger bronze grains with metallic luster. Silicate phase present.
46	Similar to 44
47	Similar to 44
48	Similar to 44
49	Similar to 44
50	Similar to 44
51	Similar to 44
52	Run products include black/grey fine-grained masses with metallic luster, and relatively bigger bronze grains with metallic luster. Gold pieces present at the end of the experiment but are covered in black run product. Pieces of silver foil (?) left, although difficult to tell, and are covered in black run product. Silicate phase present.
53	Similar to 52
54	Similar to 52
55	Similar to 52, no evidence of silver foil
56	Similar to 52, no evidence of silver foil
57	Similar to 52, no evidence of silver foil
58	Similar to 52
59	Similar to 52
60	Similar to 52, no gold added

Figure 5: Backscatter electron image of a silicate phase (grey) in a pyrrhotite grain (white) (Experiment 52).

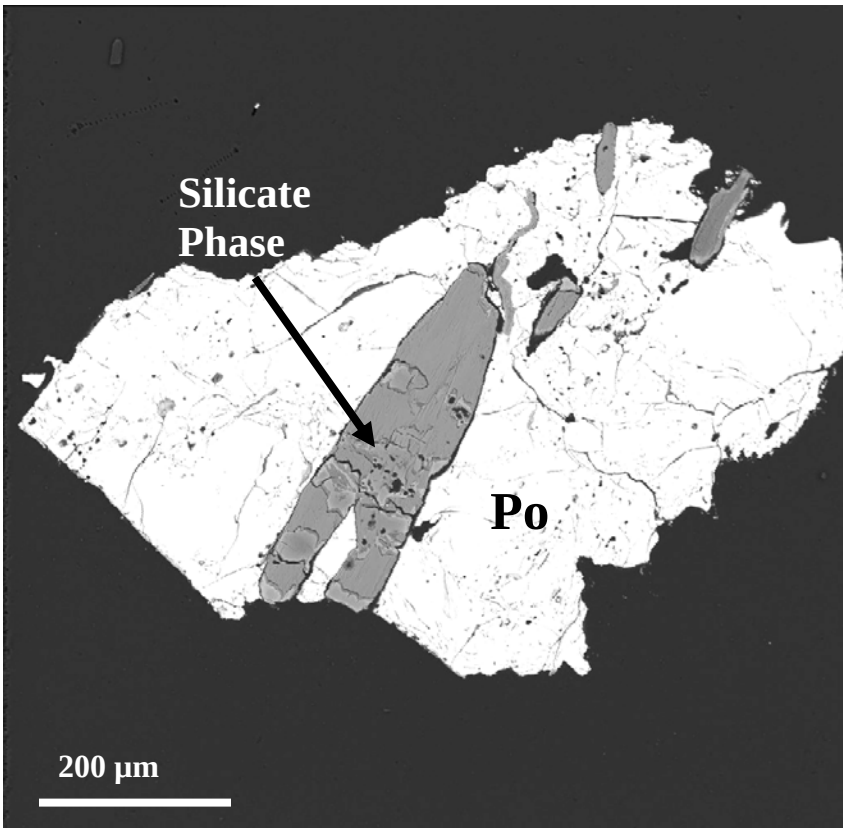

Observations of the run products by using BSE images and optical microscopy were made to identify phase characteristics, including color, size, textures, crystal habit, zoning, and phase relationships.

There were two morphologies of pyrrhotite identified in the run products from these experiments. The first morphology was present in all experiments (17-60). It occurred as millimeter sized angular pieces, and is interpreted as being starting (original) pyrrhotite grains that underwent a change in composition during the course of the experiment (Figure 6a). EPMA analysis of the run product pyrrhotites showed increased concentrations of trace elements (i.e. Ag, Zn, Cu, Pb) relative to the starting pyrrhotite. The second morphology of pyrrhotite was present as well-formed crystals or as clusters of crystals with defined grain boundaries on silica coating the inside of the silica tubewall in experiments 17-31 (Figure 6b and 6c). Grains of the second morphology were located approximately one inch above the bottom of the tube, not in direct contact with the reactants in the experiment (Figure 7). These are interpreted to be pyrrhotite that nucleated on the side of the silica tube and precipitated during quenching. The composition of both morphologies of pyrrhotite from experiments 18 and 21 is within error; compositions from both morphologies of pyrrhotite in 22 are dissimilar (Table 8). With the exception of 22, these represent equilibrium compositions of the two morphologies of pyrrhotite.

There were two morphologies of magnetite identified in these experiments. One type was associated with Ag-Fe-sulfide (Figure 8A). Based on phase relationships and appearance of the magnetite these are interpreted to have exsolved from the Ag-Fe-sulfide phase during quench. The second morphology of magnetite

Table 8: The composition of quench pyrrhotites from experiments 18, 21, and 22, and the composition of altered pyrrhotite grains from experiments18, 21, and 22; analyses were done by using EPMA, all compositions are reported in weight percent. Silicon is present at levels below detection. Original pyrrhotite refers to the starting pyrrhotite, loaded into the experiments, which underwent a change in composition during the course of the experiment. Quench pyrrhotites nucleated and precipitated on the sides of the silica tube during quenching. B.D (bd) stands for below detection.

Sample #	Fe	Ag	S	Mn	Cu	Si	Zn	Total
Quench Po								
18 (avg)	59.9	0.245	36.77	0.025	0.33	bd	0.13	97.4
Original Po								
18 (avg)	59.9	0.256	36.52	0.026	0.42	bd	0.17	97.2
18 (stdev)	0.7	0.065	0.96	0.008	0.07	bd	0.08	1.5
Quench Po								
21 (avg)	60.3	0.314	38.26	0.026	0.37	bd	0.13	99.4
21 (stdev)	0.4	0.028	0.39	0.003	0.01	bd	0.04	0.5
Original Po								
21 (avg)	60.4	0.286	38.08	0.027	0.29	bd	0.10	99.1
21 (stdev)	0.5	0.070	0.58	0.007	0.08	bd	0.06	0.9
Quench Po								
22 (avg)	60.0	0.132	37.97	0.033	0.25	bd	0.50	98.9
22 (stdev)	0.5	0.048	0.54	0.012	0.09	bd	0.04	0.5
Original Po								
22 (avg)	59.9	0.340	37.52	0.030	0.39	bd	0.47	98.7
22(stdev)	0.5	0.080	0.30	0.010	0.02	bd	0.08	0.5

Figure 6a: A backscatter electron image of an original pyrrhotite grain (polished) (Experiment 44).

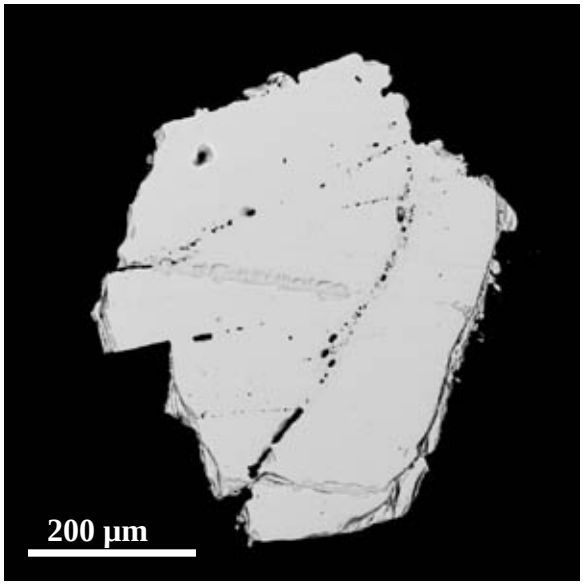

Figure 6b: A backscatter electron image of quench pyrrhotites (white) on quartz (grey) (polished) (Experiment 22).

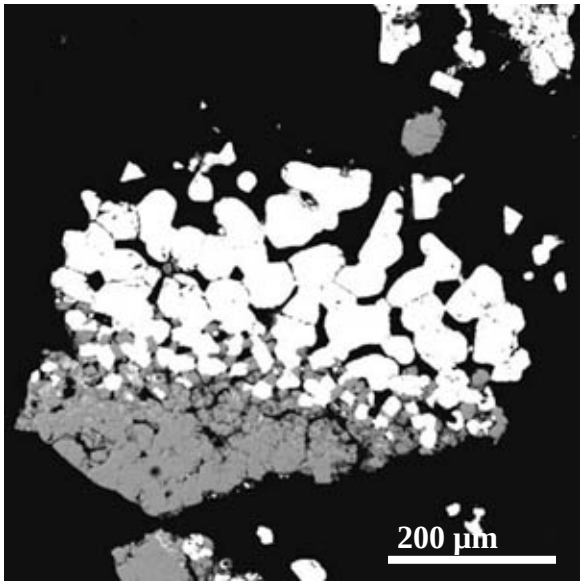

Figure 6c: A backscatter electron image of quench pyrrhotites on quartz (Experiment 9).

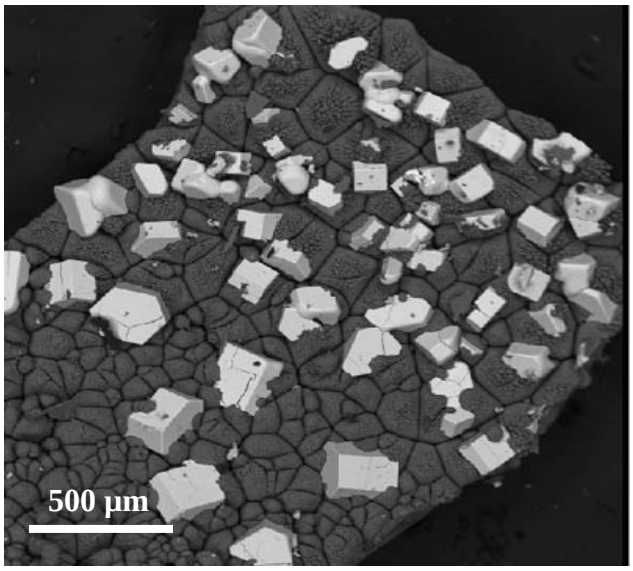

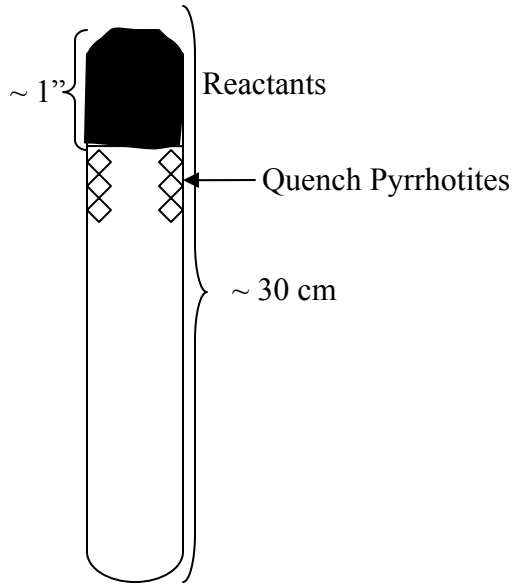

Front of furnace

Figure 7: Plan view of a silica tube resting on the floor of the furnace. Pictured is the relationship of quench pyrrhotites to the rest of the reactants in the silica tube.

was commonly found on the edge of grains of pyrrhotite or as individual grains in the mount (Figure 8b). These are interpreted to be starting magnetite that has undergone a change in composition during the course of the experiment, similar to the original pyrrhotite. A cluster of well-formed octahedral magnetites was identified in experiment 53 (Figure 8c).

Figure 8a: A backscatter electron image of the quench magnetite associated with the Ag-Fe-sulfide (Experiment 44).

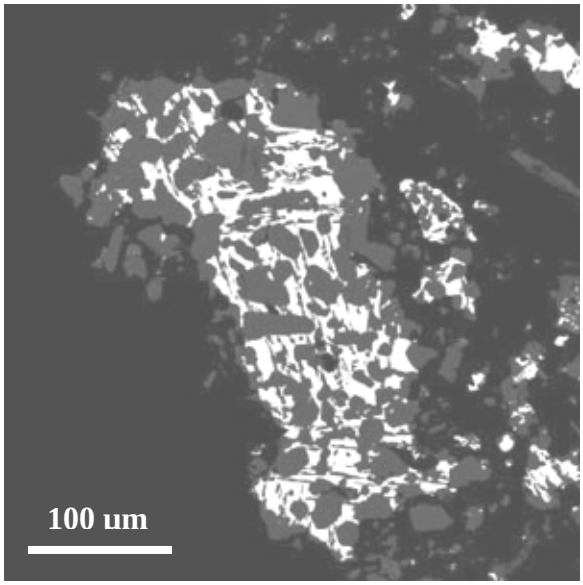

Figure 8b: A backscatter electron image of original magnetites (outlined in red) with pyrrhotite (Experiment 40)

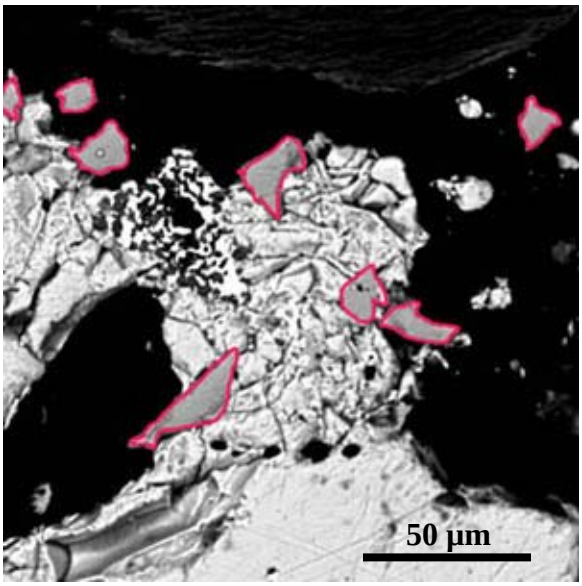

Figure 8c: A backscatter electron image of well formed magnetite crystals in a hole in a pyrrhotite grain (Experiment 53).

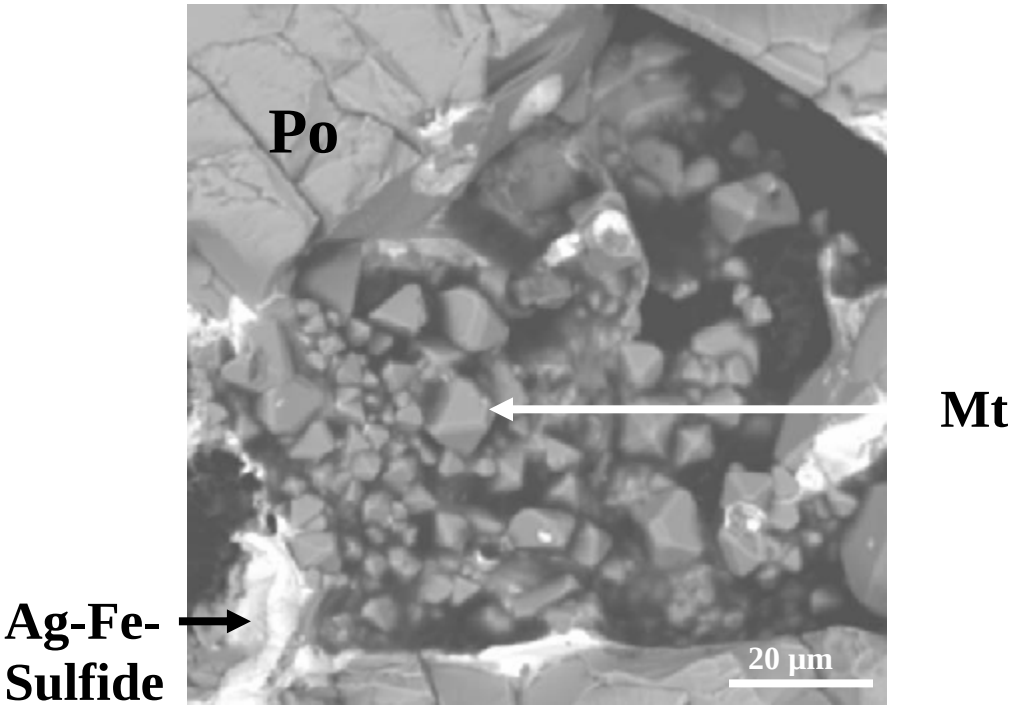

Section 2: Silver concentrations in magnetite and pyrrhotite

Analytical results for concentrations of Fe, Ag, S, Mn, Si, Pb, Cu, Zn, and Au in magnetite and pyrrhotite run products are reported in Appendices I and II. Analyses yielded average silver concentrations of 200 ± 100 ppm (1σ) in magnetite, and 2800 ± 700 ppm (1σ) in pyrrhotite at an average a(Ag) = 0.13 ± 0.04 (1σ). These include data from all samples except 52, 53, 54, 58 and 59. There was no magnetite data generated from 17, 20, 40, and 58.

Experiments completed in this study were conducted at the vapor pressure of the run product assemblage. The partial pressure of oxygen in these experiments is negligible, ~ 10^{-13} bars, the dominant gaseous species is sulfurous, which generated approximate partial pressures of 10^{-2} bars. At these minimal pressures, the concentration of silver measured in magnetite and pyrrhotite may represent the upper limits at which silver can be soluble in these phases. Based on this, it is interpreted that at the crustal pressures present in magmatic-hydrothermal systems, the C_{Ag}^{Po} and the C_{Ag}^{Mt} are expected to be lower to some extent than those reported in this study.

Section 3: Partition coefficients for silver between pyrrhotite and magnetite

Experimentally determined partition coefficients for silver between pyrrhotite and magnetite, $D_{Ag}^{Po/Mt}$, are reported in Table 9. Nerst partition coefficients (D) are defined by:

$$D_{Ag}^{Po/Mt} = C_{Ag}^{Po} / C_{Ag}^{Mt} \quad (1),$$

where concentration (C) is measured in parts per million (ppm).

The average $D_{Ag}^{Po/Mt}$ calculated for the silica tube experiments is 14 ±3 (1σ), at an average a(Ag) = 0.13 ± 0.04 (1σ). The $D_{Ag}^{Po/Mt}$ for experiment 29, 70 ± 0.98, is not included in this average; it is anomalously high due to low C_{Ag}^{Mt}. The $D_{Ag}^{Po/Mt}$ for samples 52, 53, 54, and 59 are not included in this average because of differences in the data from these experiments relative to data from the majority of the experiments (see discussion on Experiments 52, 53, 54, 58, and 59 in Results section).

Section 4: Silver-iron sulfide and silver-gold solid solution run products

Silver was added to the experiments as silver foil (99.9% pure silver). The chemical composition of the silver-bearing run products can be found in Appendix III. The composition of the silver-iron sulfide run product can be approximated by the formula $Ag_{1.3}Fe_{0.24}S$, with approximately 68 ± 9 (1σ) wt. % Ag, 7 ± 4 (1σ) wt. % Fe, and 15 ± 3 (1σ) wt. % S.

Natural mineral phases present in the Ag-Fe-S system include argentopyrite ($AgFe_2S_3$), sternbergite ($AgFe_2S_3$), and lenaite ($AgFeS_2$) (Figure 10). The initial breakdown products of argentopyrite (sternbergite) are acanthite + pyrrhotite + pyrite, further annealing produces the stable assemblage silver metal + pyrite (Czamanske, 1969). No phases were identified in this study that were stoichoimetrically equivalent to argentopyrite (sternbergite) or lenaite; furthermore, acanthite (Ag_2S), pyrite, and silver metal were not identified in any experiment. The melting point of pure silver is 961.78°C. During the course of the experiments the silver foil was most likely present in a molten (liquid + solid) form maintaining structural ordering allowing

Table 9: The $D_{Ag}^{Po/Mt}$ for samples 18-60. Samples 17, 20, 40, and 58 did not generate adequate magnetite data for analysis and calculating partition coefficients. Samples 18-25, 29, 52, 53, 54, and 59 were left out of the calculated average. Samples that are in bold denote gold-bearing experiments. Standard deviation for individual experiment partition coefficients was calculated using the following formula: STDEV = SQRT $(\text{stdev}^{mt}/\text{average}^{mt})^2 + (\text{stdev}^{po}/\text{average}^{po})^2$, standard deviations for averages were calculated using the STDEV function in Microsoft Excel, n= number of experiments conducted for a length of time (hrs.), and the total # of experiments.

Sample #	$D_{Ag}^{Po/Mt}$ ± 1σ	Length of Experiment (hrs.)	Average $D_{Ag}^{Po/Mt}$ ± 1σ (n)
18*	14 ± 0.55	96	-
19*	33 ± 0.38	96	-
21*	24 ± 0.73	96	25 ± 13 (6)
22*	40 ± 1.00	96	-
24*	8 ± 0.76	96	-
25*	33 ± 0.56	96	-
27	22 ± 0.38	144	-
28	8 ± 1.15	144	-
29*	70 ± 0.98	144	15 ± 6 (4)
30	15 ± 1.19	144	-
31	13 ± 1.19	144	-
34	5 ± 1.02	168	-
35	15 ± 0.54	168	21 ± 19 (3)
36	41 ± 0.88	168	-
37	18 ± 1.18	285	13 ± 7 (2)
38	8 ± 0.97	285	-
44	**22 ± 1.46**	**227.5**	-
45	6 ± 0.68	227.5	-
46	**8 ± 0.76**	**227.5**	-
47	**27 ± 1.32**	**227.5**	-
48	8 ± 0.33	227.5	19 ± 13 (8)
49	**11± 1.74**	**227.5**	-
50	**33 ± 1.53**	**227.5**	-
51	**38 ± 0.60**	**227.5**	-
52*	**1 ± 1.10**	**336**	-
53*	**3 ± 0.00**	**336**	**2 ± 2 (3)**
54*	**1 ± 0.50**	**336**	-
55	**9 ± 1.10**	**504**	-
56	**13 ± 1.29**	**504**	**12 ± 2 (3)**
57	**14 ± 1.37**	**504**	-
59*	**6 ± 1.38**	**696**	**14 ± 0.62 (1)**
60	**14 ± 0.62**	**696**	-
		Average $D_{Ag}^{Po/Mt}$	14 ± 3 (20)

Figure 9: $D_{Ag}^{Po/Mt} \pm 1\sigma$ versus time. $D_{Ag}^{Po/Mt}$ for experiments 17-25, and 29 are represented by the black box, and are not included in the average $D_{Ag}^{Po/Mt}$. Experiments 17-25, which were run for 96 hours, are not included in the average partition coefficient, because 96 hours is not sufficient time for the silica tube experiments to obtain equilibrium. The partition coefficient for experiment 29 is anomalously high.

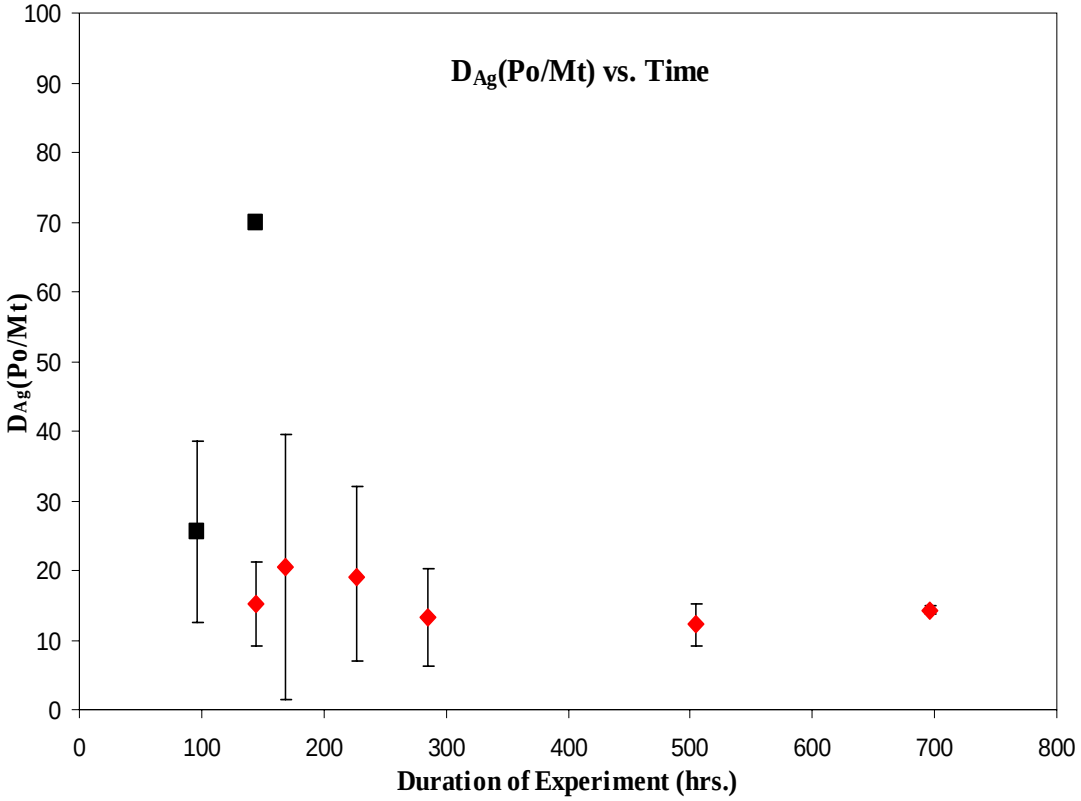

diffusion of iron, sulfur, and oxygen. The Ag-Fe-sulfide run products had iron-rich exsolution textures with pyrrhotite composition and an associated morphology of magnetite, which are interpreted as being exsolved during quenching procedures (Figure 11a, 11b).

Gold was added to experiments 44-59 (excluding 45, and 48), to form electrum; electrum compositions were used to calculate the activity of silver by using the electrum tarnish method described in Barton and Toulmin (1964). Silver-gold alloy, electrum, was synthesized in every experiment that contained gold; the mole fraction of silver in electrum ranged from 0.0002 to 0.28 (Appendix IV).

Figure 10: Ternary diagram of the major phases present in the Ag-Fe-S system. The red dots represent the composition of Ag-Fe-sulfide generated in the silica tube experiments. Phases represented by the squares include acanthite, sternbergite, lenaite, pyrrhotite, and pyrite (Adapted from Czamanke, 1969).

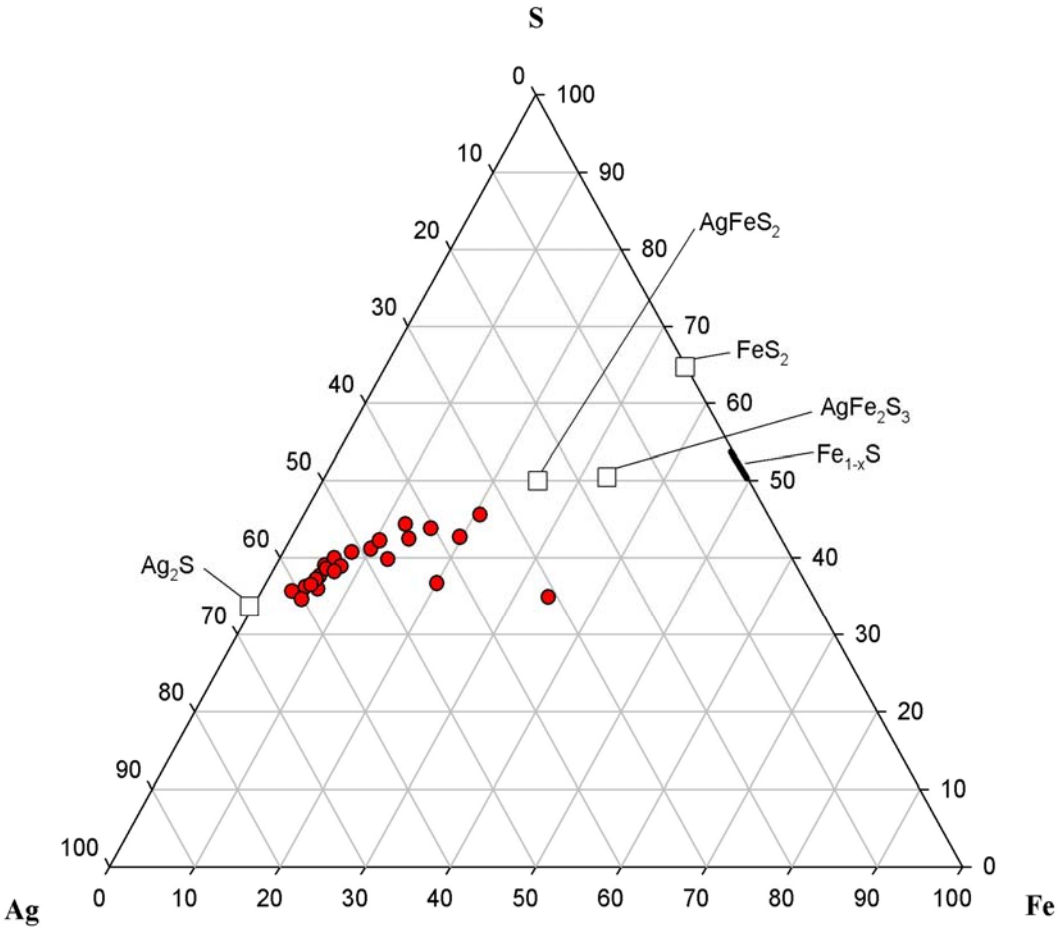

Figure 11a: A backscatter electron image of Ag-Fe-sulfide (white) with pyrrhotite exsolution textures (grey)(Experiment 31).

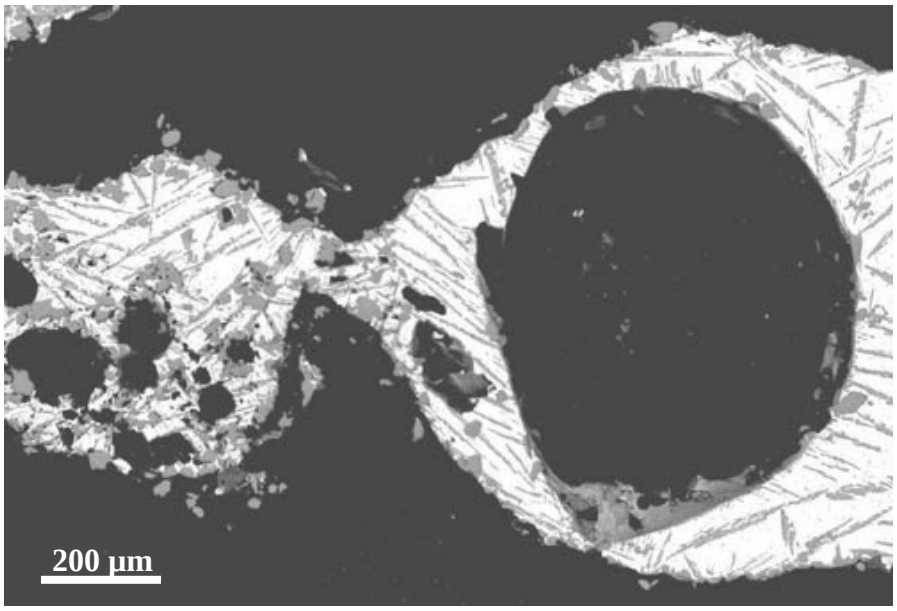

Figure 11b: A backscatter electron image of Ag-Fe-sulfide (white) with magnetites (black) pyrrhotite (grey), and pyrrhotite exsolution textures (grey) (Experiment 55).

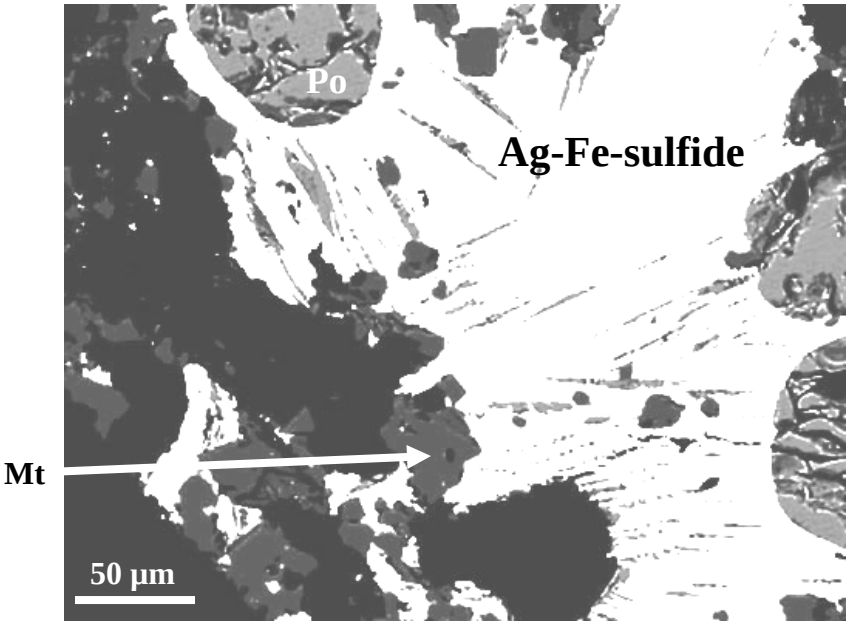

Section 5: Thermodynamics

Thermodynamic parameters need to be defined for these experiments in order to understand the interaction between the different components of the system. Determining sulfur fugacity, oxygen fugacity, the activity of silver, and equilibrium constants is integral to understand what influences equilibrium in this system.

The total mechanical pressure inside the quartz tubes is the sum of the individual vapor pressures of the gaseous species present. In these experiments the presence of a sulfurous species is assumed based on the smell emitted from the freshly broken tubing. The tubing was evacuated before it was sealed, but oxygen was most likely present on oxidized surfaces of pyrrhotite; magnetite may also be a point source of oxygen in these experiments. The gases present in these experiments are inferred to be O_2, S_2, and SO_2, $P_{total} = P_{O2} + P_{S2} + P_{SO2}$, where SO_2 is generated from the reaction $\frac{1}{2}S_2 + O_2 \longrightarrow SO_2$. One group of experiments (8-14) ruptured in the furnace during the course of this study. This was caused by the large amount of vapor generated due to the large volume of starting material loaded into the tubing.

Oxygen and sulfur fugacity

Fugacity, the corrected vapor pressure for a nonideal gaseous component in a system, was calculated for both oxygen and sulfur in these experiments. Oxygen fugacity, $\log_{10}fO_2$, is classically defined by the equation:

$$\mu_i = \mu_i^o + RT \ln fO_2 \qquad (2)$$

where μ_i is the chemical potential of component i at 1 bar (in KJ/mol), μ_i^o is the chemical potential of i at a standard state (KJ/mol), R is equal to 0.008314 KJ K^{-1} mol^{-1}, T is in absolute temperature (K).

Oxygen fugacities for the silica tube experiments in this study were calculated by using the equation for the magnetite-pyrrhotite boundary curve at 800°C. The data used to construct the magnetite-pyrrhotite boundary curve were reported in Whitney (1984). Experimental data indicate that oxygen fugacity was variable in these experiments, with the average $\log_{10}fO_2$ of -13.14 ± 0.88, where $\log_{10}fO_2$ ranges between -14.90 to -11.63 for all silica tubes experiments completed. This approximates oxygen fugacities between QFM and NNO. This range is similar to the range of fO_2/fS_2 in pyrrhotite-bearing silicic volcanic rocks (Whitney, 1984).

Sulfur fugacity (fS_2) for each experiment was calculated from pyrrhotite compositions by using the equation from Toulmin and Barton (1964):

$$\log_{10}fS_2 = (70.03 - 85.83N)(1000/T) + 39.30(1-0.9981N)^{.5} - 11.91 \qquad (3)$$

where N = mol fraction of FeS in pyrrhotite in the system FeS-S_2, for this calculation N = mol fraction of FeS. T is equal to 1073 K. The equation used to calculate sulfur fugacity from pyrrhotite composition was derived from experiments by using the electrum-tarnish method (Barton and Toulmin, 1964, Toulmin and Barton 1964). The electrum tarnish method can be used define the relationship between the fugacity of sulfur and the composition of electrum that can exist with a sulfide tarnish in experimental systems (Barton and Toulmin, 1964). Calculated $\log_{10}fS_2$ for all of the silica tube experiments completed in this study range between -0.18 and -4.06. Variations in sulfur fugacity are a function of pyrrhotite composition, where lower X_{FeS}^{Po} reflect higher sulfur fugacity.

The calculated $\log_{10}fS_2$ and $\log_{10}fO_2$ appear as an array of numbers projected along the magnetite-pyrrhotite boundary curve (Figure 12). There are three

populations of samples that lie along the curve; samples fall in regions representing $\log_{10}fS_2$ of -2.4 and -0.18, -3.01 and -3.30, and -4.06 and -3.65. The total amount of error associated with calculating $\log_{10}fS_2$ from N_{FeS} is approximately ± 0.35 log units (Toulmin and Barton, 1964). The error associated with the $\log_{10}fO_2$ is also ± 0.35 log units.

Activity of silver

Activity (a) is defined as a product of $X_i * \gamma_i$, where X = mole fraction of a component (i) in a solution, and γ is the activity coefficient, the ratio of activity of a species to its molar concentration and is a correction factor used for non-ideal solutions. Activity is an indicator of reactivity; for these experiments silver reactivity needs to be quantified to put meaningful context on $D_{Ag}^{Po/Mt}$ in natural and experimental systems. The activity of silver was calculated by using silver-iron sulfide (Ag-Fe-sulfide) compositions, electrum compositions, and equations presented in Barton and Toulmin (1964).

The calculation for activity of silver based on electrum compositions was facilitated by using the following equation from Barton and Toulmin (1964) (Figure 13):

$$a_{Ag} = N_{Ag} * \exp\left\{\frac{\{5650\text{-}1600(1\text{-}N_{Ag}) - 1.375T\} * (1\text{-}N_{Ag})^2}{RT}\right\} \quad (4)$$

Figure 12: The $\log_{10}fS_2$ vs. $\log_{10}fO_2$ for the silica tube experiments. Sulfur fugacity was calculated from pyrrhotite compositions, and by using equation (3) from Toulmin and Barton (1964). Oxygen fugacities were calculated from the equation for the slope of the magnetite-pyrrhotite boundary curve, which is based on data from Whitney (1984). Error on the $\log_{10}fS_2$ and $\log_{10}fO_2$ is ± 0.35 log units (Toulmin and Barton, 1964). fS_2 and fO_2 data for Bishop, Fish Canyon, and El Chichon are plotted to show the range of fugacities in pyrrhotite-bearing silica volcanic rocks (Whitney, 1984).

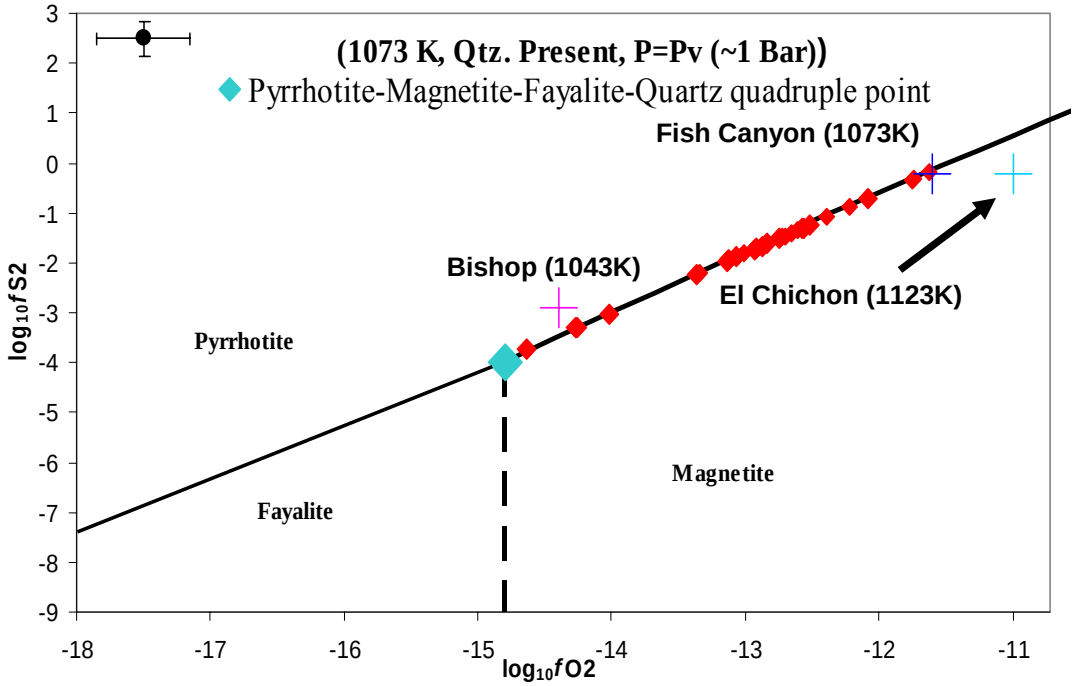

Figure 13: Activity of silver calculated from electrum compositions by using equation (4) presented in Barton and Toulmin (1964).

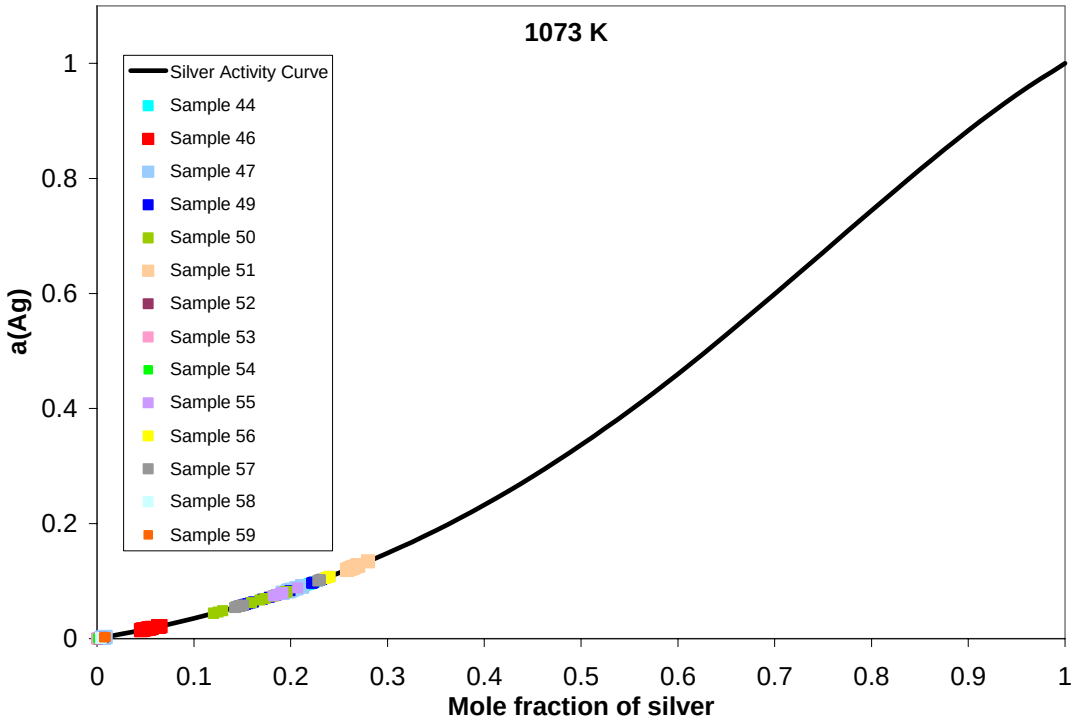

where N_{Ag} = mole fraction (X) of silver in electrum, which is calculated via the following equation (wt% Ag/107.86g)/{(wt% Ag/107.86g) + (wt% Au/196.66g). R is equal to 1.987 cal K^{-1} mol^{-1}, temperature is equal to 1073K. Equation (4) was derived from the equation for the chemical potential of Ag in electrum from a study done to elucidate the thermodynamics of silver-gold alloys completed by White, Orr, and Hultgren (1957) (Barton and Toulmin, 1964). a(Ag) calculated from electrum compositions ranges between 0.00008 and 0.12.

The activity of silver, in experiments that did not contain electrum, was calculated by using the ideal composition of acanthite (Ag_2S) corrected for each sample based on Ag-Fe-sulfide compositions, and the following equation from Barton and Toulmin (1964) :

$$\ln fS_2 = \frac{\Delta G}{RT} + \ln \frac{(a_{Ag2S})^2}{(a_{Ag})^4} \qquad (5)$$

Where ΔG = -41,680 + 16.52T cal, where T is between 452-1115 K, T = 1073 K, R = 1.987 cal K^{-1} mol^{-1}, $a_{Ag2S} = X_{Ag2S}$, and ln fS_2 = calculated from (3). This equation is based on the formation of argentite (high-T acanthite), which occurs via the following reaction:

$$4Ag_{(c)} + S_2 = 2Ag_2S \qquad (6)$$

The a(Ag) calculated for these experiments from equation (5) and corrected Ag-Fe-sulfide compositions ranges between 0.10 and 0.57 and is a function the sulfur fugacity of the system (Figure 14). Samples with low fS_2 (and fO_2) have the highest calculated activity of silver.

The *a*(Ag) calculated for all of the silica tube experiments range from 0.00008 to 0.58 (Figure 15). The transition point in *a*(Ag) between the gold-free and gold-bearing experiments is well constrained, and occurs at an activity of silver between 0.09 – 0.12; 0.12 being the maximum *a*(Ag) in gold-bearing experiments and 0.09 is minimum *a*(Ag) calculated for non-gold bearing experiments. The lower *a*(Ag) calculated for experiments containing gold is function of this addition; the gold removes silver from the system and reduces its potential to react with the other components.

A comparison of *a*(Ag) calculated by using Ag-Fe-sulfide and electrum compositions from the same sample shows that both methods can be used to approximate the reactivity of silver in this experimental system; a(Ag) for these samples are the same within error; the only exception being sample #46 (Table 10).

C_{Ag}^{Po} is highest in experiments with the highest calculated *a*(Ag) (Figure 16). The average *a*(Ag) calculated for these experiments is 0.13 ± 0.04 (1σ). With increasing activity silver concentrations in pyrrhotite pyrrhotite should increase. The concentrations provided in this study may represent only a fraction of amount of silver that can be found in natural and synthesized pyrrhotites that are in equilibrium at low pressures.

Figure 14: Activity of silver calculated from corrected Ag-Fe-sulfide compositions using equation (5) vs. $\log_{10} fS_2$ calculated from pyrrhotite compositions (3).

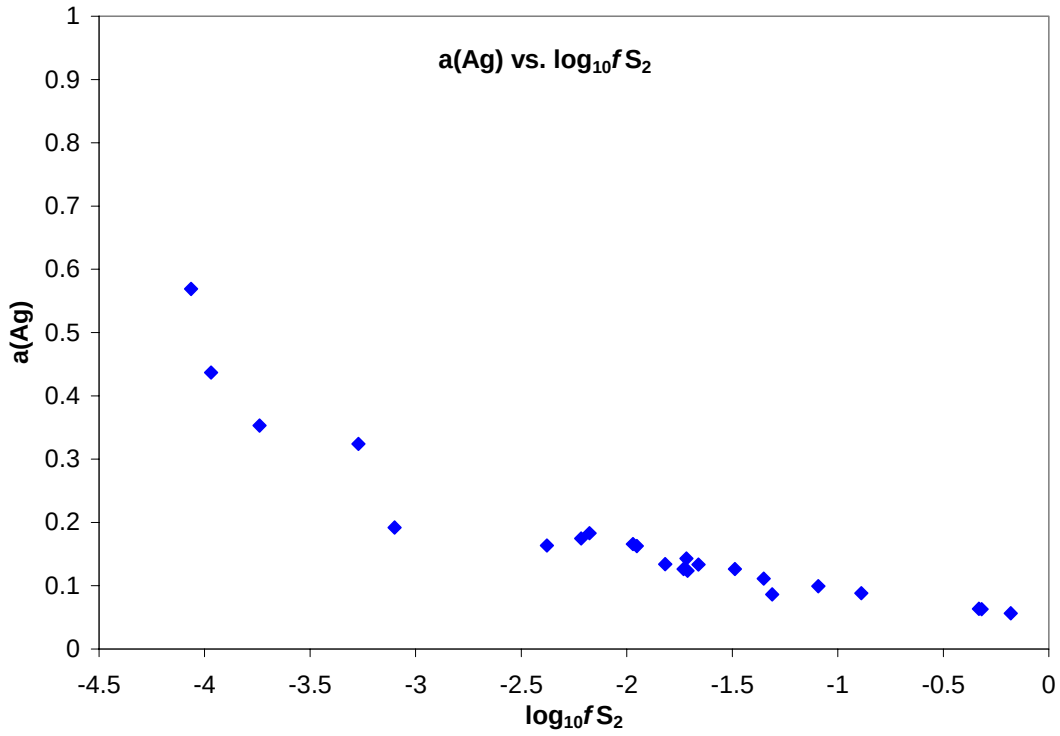

Figure 15: The calculated activity of silver for all samples. The samples that are circled have *a*(Ag) calculated from both electrum and corrected Ag-Fe-sulfide compositions.

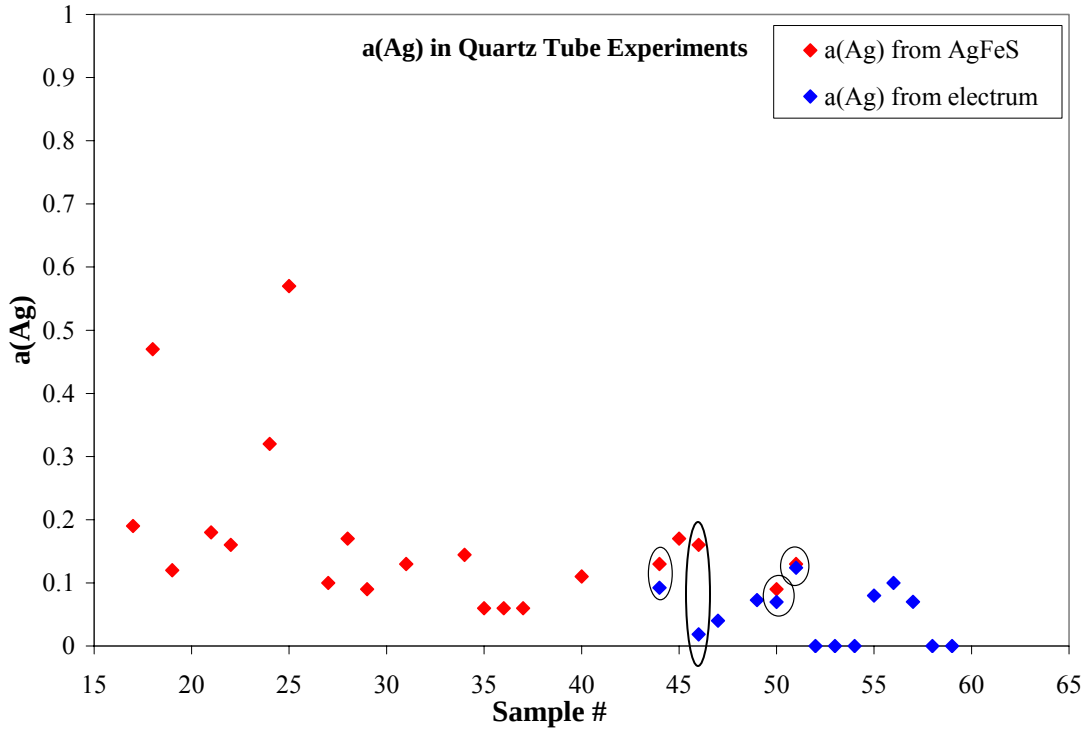

Table 10: A comparison of activity of silver calculated from corrected Ag-Fe-sulfide and electrum compositions from the same sample. Activity of silver was calculated by using equations presented in Barton and Toulmin (1964).

Sample #	*a*(Ag) Ag-Fe-sulfide	*a*(Ag) electrum
44	0.13	0.09
46	0.16	0.02
50	0.09	0.07
51	0.12	0.12

Figure 16: C_{Ag}^{Po} vs. a(Ag) * $\log_{10}fS_2$ for silica tube experiments, a(Ag) values were normalized using $\log_{10}fS_2^{1/2}$.

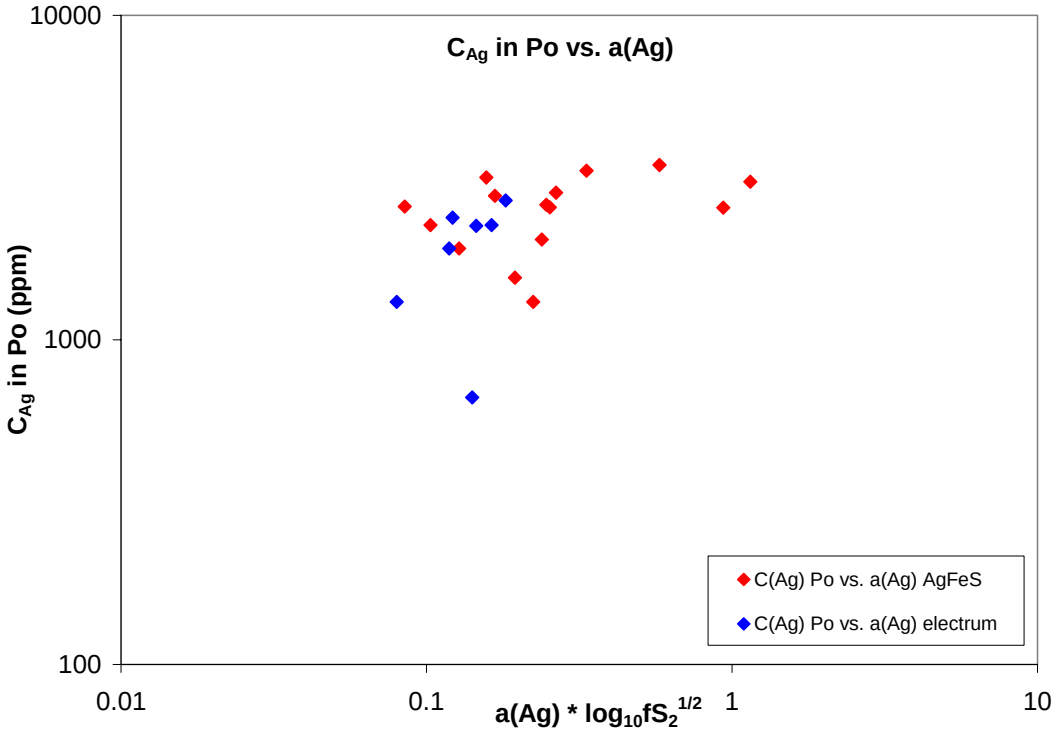

Equilibrium Constants

Attainment of equilibrium between the components of the experimental system can be assessed by calculating equilibrium constants. The major system components of the silica tube experiments are magnetite ($Fe_3O_{4)}$, pyrrhotite (FeS), silver (Ag), sulfur (S_2), and oxygen (O_2), other components include gold (Au), quartz (SiO_2), and fayalite (Fe_2SiO_4).

Pyrrhotite-Silver Equilibrium

Pyrrhotite, $Fe_{1-x}S$ ($FeS – Fe_7S_8$), can occur as monoclinic or hexagonal crystals, or as a solid solution of monoclinic + hexagonal, where the variable amount of iron defines the crystal structure of pyrrhotite. Vacancies in the iron sites give rise to the monoclinic pyrrhotite where the maximum iron content is ~ 46.67%, (Morimoto, 1970). Troilite, end-member hexagonal FeS, is commonly found in meteorites; there are no iron vacancies present in the structure of troilite. Metal cations, Au, Ag, Ni, Cu, and Mn, substitute for iron in pyrrhotite or are present as impurities in the structure of the mineral (Deer et al., 1966).

The following equilibrium describes the partitioning of silver between pyrrhotite and the metal phase in the quartz tubes experiments:

$FeS^{Po} + Ag^0 + ½\ S_2 = AgFeS_2^{Po}$, where $C_{Ag}^{AgFeS2} * 107.87 = X_{AgFeS2}^{Po}$

$$K' = \frac{X_{AgFeS2}^{Po}}{aAg^0 * fS_2^{1/2} * X_{FeS}^{Po}} \qquad (7)$$

This equilibrium is calculated assuming that silver forms a ‘chalcopyrite-like’ component in pyrrhotite. The calculated values for the apparent equilibrium constants (log K’) are reported in Table 11.

Table 11: Compilation of a(Ag) from Ag-Fe-sulfide and electrum compositions, $\log_{10}fS_2$, X_{FeS}^{Po}, X_{AgFeS2}^{Po}, and apparent equilibrium constants (log K').

Sample	a(Ag) [Ag-Fe-sulfide]	a(Ag)[elect]	X_{FeS}^{Po}	X_{AgFeS2}^{Po}	$\log_{10}fS_2$	logK'
17	0.19	NO GOLD	0.96	0.0031	-3.10	0.60
18	0.43	NO GOLD	0.97	0.0024	-3.97	0.55
19	0.12	NO GOLD	0.94	0.0029	-1.71	0.19
20	-	NO GOLD	0.97	0.0029	-3.66	-
21	0.18	NO GOLD	0.95	0.0026	-2.18	0.19
22	0.16	NO GOLD	0.95	0.0024	-2.38	0.24
24	0.32	NO GOLD	0.96	0.0032	-3.27	0.45
25	0.57	NO GOLD	0.97	0.0028	-4.06	0.55
27	0.10	NO GOLD	0.94	0.0029	-1.09	0.11
28	0.17	NO GOLD	0.95	0.0024	-2.22	0.19
29	0.09	NO GOLD	0.93	0.0024	-0.89	0.08
30	-	NO GOLD	0.94	0.0030	-1.40	-
31	0.13	NO GOLD	0.94	0.0031	-1.49	0.14
34	0.14	NO GOLD	0.95	0.0014	-1.82	0.09
35	0.06	NO GOLD	0.92	0.0039	-0.32	0.10
36	0.05	NO GOLD	0.92	0.0033	-0.18	0.09
37	0.06	NO GOLD	0.95	0.0034	-0.33	0.09
38	-	NO GOLD	0.94	0.0023	-1.46	-
40	0.11	NO GOLD	0.92	0.0029	-1.35	0.14
44	0.13	0.09	0.94	0.0018	-1.66	0.10
45	0.17	NO GOLD	0.94	0.0026	-1.97	0.15
46	0.16	0.02	0.94	0.0019	-1.95	1.0
47	-	0.04	0.95	0.0029	-2.24	1.0
48	-	NO GOLD	0.95	0.0033	-1.23	-
49	-	0.07	0.97	0.0006	-3.74	0.65
50	0.08	0.07	0.94	0.0012	-1.31	0.08
51	0.12	0.12	0.94	0.0021	-1.73	0.13
52	-	0.00063	0.95	0.0004	-1.89	6.4
53	-	0.00008	0.94	0.0027	-1.72	250
54	-	0.00042	0.93	0.0004	-0.72	2.3
55	-	0.08	0.96	0.0021	-3.31	1.2
56	-	0.10	0.96	0.0025	-3.30	1.2
57	-	0.07	0.96	0.0022	-3.02	1.1
58	-	0.00150	0.94	0.0001	-1.51	0.47
59	-	0.00269	0.94	0.0011	-1.62	2.9
60	-	-	0.94	0.0032	-1.30	-

Apparent equilibrium constants were calculated based on the assumption that the activity coefficient for the $AgFeS_2$ and FeS components in pyrrhotite is 1; Raoultian behavior was assumed for these components. Activity of silver and sulfur fugacity has the largest impact on the apparent equilibrium constants calculated for the experiments completed as part of this study.

Magnetite-Silver Equilibrium

The extent to which trace elements can partition into mineral phases is a function of the charge and size of the element relative to the charge, size of the lattice site it is entering, the activity of the element, and the kinetics of reaction. It is interpreted that magnetite, Fe_3O_4 ($Fe^{2+}Fe^{3+}{}_2O_4$), undergoes coupled heterovalent substitution of silver (Ag) and ferrous iron (Fe^{2+}) for ferric iron (Fe^{3+}) in the experiments included in this study. Magnetite is a reverse spinel, which has the structure AB_2O_4, where A = Fe^{3+}, B = 1:1, Fe^{3+}: Fe^{2+}. The A site is a tetrahedral, with IV-fold coordination, and the B site is octahedral, with VI-fold coordination. Substitution in the magnetite structure occurs at the B site; this is the most desirable site because it accommodates a mixture of elements with different size and charge (Deer et al., 1966). The VI-fold coordination site can better accommodate the larger Ag^{1+} cation, which has a Shannon-Prewitt ionic radius of 1.29Å. Fe^{2+} has a Shannon-Prewitt radius of 0.92 Å, Fe^{3+} has a Shannon-Prewitt radius of 0.79 Å. Possible equilibria that describe the partitioning of silver between the B site of magnetite and silver metal include:

$$2O_2 + 3Ag^0 = 3(AgFe^{3+}Fe^{2+}{}_{-2})^{mt} + Fe^{2+}Fe^{3+}{}_2O_4 \quad (8)$$

The amount of silver that is able to partition into magnetite is limited due to the large ionic radius of Ag^{1+} ions, as well as the noble behavior of silver metal. The structure of magnetite does not accommodate 1+ ions easily, because charge balance needs to be maintained. Lattice strain models describe trace elements as charged point defects, where ions with different charges and sizes cause the most strain in crystal lattices (Blundy and Wood, 2003). For this reason, the maximum partition coefficient occurs for ions that fit into the lattice with the least associated strain (Blundy and Wood, 2003). It is hypothesized that silver would cause substantial strain on the lattice of magnetite; therefore the partition coefficient for silver in magnetite would be lower than ions such as magnesium, titanium, or chromium which readily substitute for iron in the structure of magnetite. The following is a possible representative formula for silver-bearing magnetite:

$$AgFe_2^{3+}O_4$$

Experiments 52, 53, 54, 58, and 59

Data from experiments 52, 53, 54, 58, and 59 are not represented in the average solubility, and $D_{Ag}^{Po/Mt}$ calculations presented earlier in this thesis. The a(Ag) in these experiments is significantly lower than the rest of the experiments; C_{Ag}^{Po} and C_{Ag}^{Mt} are not typical (Table 12). These data are interpreted as being a reflection of conditions that are inherently different from those that took place in the other experiments. Visual observations taken from the run products indicate a presence of intact silver foil, which is not seen in any other experiments. It is concluded that the silver foil remained almost inert during the course of these experiments, and contrary to other data in this study, was most reactive with the magnetite component based on the high C_{Ag}^{Mt}.

Table 12: Complied data for samples 52, 53, 54, 58, 59.

Sample #	$C(Ag)_{Mt}$	$C(Ag)_{Po}$	$D_{Ag}^{Po/Mt}$	fS_2	fO_2	a(Ag)
52	435	469	1	-1.88	-13.06	0.00063
53	850	2960	3	-1.71	-12.92	0.00080
54	630	424	1	-0.72	-12.07	0.00042
58	-	125	-	-1.51	-12.75	0.00150
59	200	1230	6	-1.62	-12.8	0.00270

Experiments with low sulfur fugacity

There were two groups of experiments that had low sulfur/oxygen fugacities. The average $\log_{10}fS_2$ of the silica tube experiments is -2.0 ± 1.0. These values were calculated from pyrrhotite compositions according to the equation (3) presented by Toulmin and Barton (1964), low sulfur fugacities are a function of high mole fraction FeS in pyrrhotite (X = 0.96-0.97).

The first set includes samples 17, 18, 20, 24, and 25 and have sulfur fugacities of -3.1, -4.0, -3.7, -3.3, -4.1, and -3.7, respectively. The starting pyrrhotite has a X_{FeS}^{Po} of 0.98, which corresponds to a $\log_{10}fS_2$ of ~ -5.0. Experiments 17, 18, 20, 24, and 25 were conducted for 96 hours (4 days). These experiments had the highest calculated activity of silver 0.20, 0.50, 0.33, and 0.58 (no data for #20). Based on these results and high calculated partition coefficients for silver between pyrrhotite and magnetite, it is interpreted that experiments conducted for 96 hours did not attain equilibrium.

Experiments 55, 56, and 57 had $\log_{10}fS_2$ of -3.30, -3.29, and -3.01 based on pyrrhotite compositions. These experiments were run for 504 hours. Concentrations of silver in magnetite and pyrrhotite and calculated activity of silver of 0.08, 0.10, and 0.07, based on electrum composition, are comparable to data from other gold-bearing experiments. Low sulfur fugacity in these experiments may have been a function of the pyrrhotite loaded into the experiments. The pyrrhotite was crushed and ground prior to being used in the experiments. Some compositional variability existed in the starting pyrrhotite used for these experiments, which contributed to the variability in the final measure fugacity of sulfur. This may also be the case of experiment 49, which had a $\log_{10}fS_2$ of -3.74.

Section 6: Zn, Pb, Cu, and Mn data

The source of zinc, lead, copper, and manganese in the silica tube experiments was inclusions of sphalerite, galena, and chalcocite present in the starting pyrrhotite (Figure 17A). The starting pyrrhotite also contained inclusions of an Al-Mn-Fe-silicate. In some experiments, sphalerite precipitated around pyrrhotite grains (Figure 17B). More commonly zinc as well as lead, copper, and manganese, were found as trace constituents in all the phases, excluding silicate phases, in the run products of the silica tube experiments. $D_{Zn}^{Po/Mt}$, $D_{Pb}^{Po/Mt}$, $D_{Cu}^{Po/Mt}$, $D_{Mn}^{Po/Mt}$ were calculated and are reported in Table 13. Copper and lead partition into pyrrhotite relative to magnetite. Copper has the highest partition coefficient, ~120, for a metal between pyrrhotite and magnetite calculated in this study; these results are similar to data presented in Cygan and Candela (1995) and Jugo et al. (1999). Zinc and manganese partition in favor of magnetite as compared to pyrrhotite; this is illustrated by the average $D_{Zn}^{Po/Mt}$ and $D_{Mn}^{Po/Mt}$ being less than 1 for experiments completed for any length of time.

Figure 17a: Backscatter electron image of starting pyrrhotite from Sudbury, Ontario, Canada.

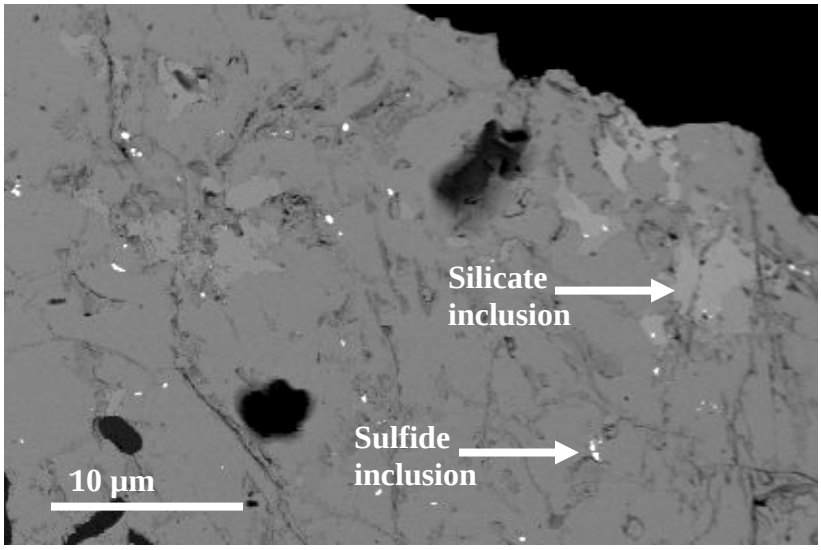

Figure 17b: Backscatter electron image of sphalerite (Sp) (white) in run product pyrrhotite (grey) (Experiment 38).

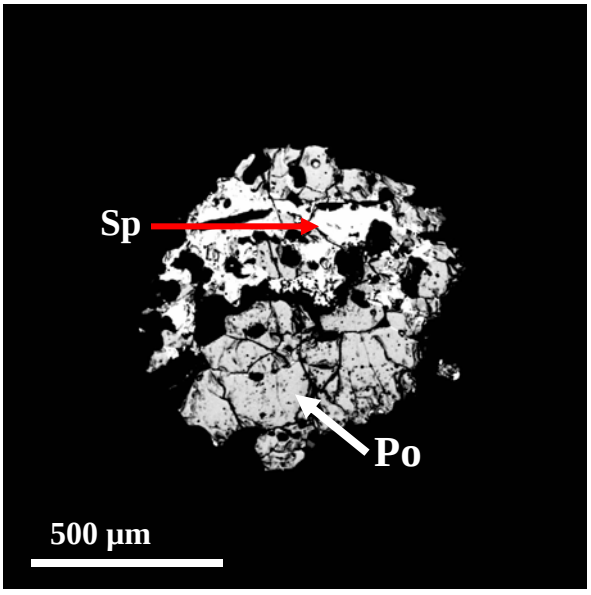

Table 13: Approximate $D_{Zn}^{Po/Mt} \pm 1\sigma$, $D_{Pb}^{Po/Mt} \pm 1\sigma$, $D_{Cu}^{Po/Mt} \pm 1\sigma$, and $D_{Mn}^{Po/Mt} \pm 1\sigma$ calculated for silica tube experiments for 96, 144, 168, 227.5, 285, 336, 504, 523, and 696 hours.

Duration (hrs.)	$D_{Zn}^{Po/Mt} \pm 1\sigma$	$D_{Pb}^{Po/Mt} \pm 1\sigma$	$D_{Cu}^{Po/Mt} \pm 1\sigma$	$D_{Mn}^{Po/Mt} \pm 1\sigma$
96 (n = 6)	0.81 ± 0.38	No data	76 ± 47	0.51 ± 0.23
144 (n = 5)	0.58 ± 0.13	3.5 ± 0.67	105 ± 44	0.57 ± 0.15
168 (n = 3)	0.44 ± 0.17	3.2 ± 0.95	92 ± 25	0.31 ± 0.19
227.5 (n = 8)	0.61 ± 0.38	2.7 ± 0.62	130 ± 53	0.70 ± 0.28
285 (n = 2)	0.50 ± 0.14	2.7 ± 0.30	80 ± 26	0.41 ± 0.02
336 (n = 3)	0.38 ± 0.10	4.4 ± 2.30	270 ± 248	0.21 ± 0.02
504 (n = 3)	0.34 ± 0.08	2.8 ± 0.32	66 ± 7	0.36 ± 0.10
523 (n = 2)	0.49 ± 0.01	7.7 ± 0.40	22 ± 7	0.25 ± 0.01
696 (n = 2)	0.30 ± 0.00	2.6 ± 0.18	320 ± 336	0.28 ± 0.07

Chapter 5: Results: Hydrothermal Experiments

Data for two successful hydrothermal experiments, L1 and L2, are presented in this study. The experimental system permitted the exchange of major and trace elements between a silicate melt, magnetite, silver metal, immiscible vapor + brine phase, and gold metal at 800°C and 140 MPa.

Section 1: Silicate Glass Chemistry

Average major element compositions and calculated ASI (aluminum saturation index) data for silicate glasses produced in experiments L1 and L2 are reported in Table 14. ASI values were calculated via the following equation:

Molar concentration: $[Al_2O_3/ (CaO+K_2O+Na_2O)]$

The composition of the starting synthetic glass (GR-1) is ASI of 1.0 (metaluminous). The glasses produced in experiments L1 and L2 are peralkaline and have ASIs of 0.80 and 0.50 respectively. Analytical totals for both run product glasses do not equal 100.00 because of water that can not be accounted for by EPMA techniques.

Compositional variations in L1 and L2 glasses were caused by differences in the experimental system at run conditions (800°C and 140 MPa). Fayalite quench crystals were identified in L1 glass in close proximity to magnetite (Table 15) (Figure 18). The formation of fayalite from magnetite and quartz occurs at $\log_{10}fO_2$ at or below QFM via the following reaction

$$3Fe_2SiO_4 + O_2 \leftrightarrow 2Fe_3O_4 + SiO_2 \quad (9)$$

Table 14: Composition of glass run products and ASIs from hydrothermal experiments L1 and L2 as determined by EPMA, data for individual points can be found in Appendix V. Concentrations are reported in weight percent oxide, except for chlorine which is reported as weight percent of the element.

Sample	SiO_2	Al_2O_3	Na_2O	K_2O	CaO	FeO	Cl	Total
L1								
Average	72.3	10.6	3.3	7.3	0.03	2.3	0.18	96.0
STDEV	2.9	1.6	0.4	1.4	0.04	1.7	0.06	1.7
ASI	0.80							
L2								
Average	67.7	7.1	3.9	6.6	0.06	9.4	0.57	95.2
STDEV	0.7	0.7	0.1	0.2	0.05	0.8	0.04	1.0
ASI	0.50							

Figure 18: Backscatter electron image from L1 of quenched fayalite crystals in a matrix of glass and magnetite.

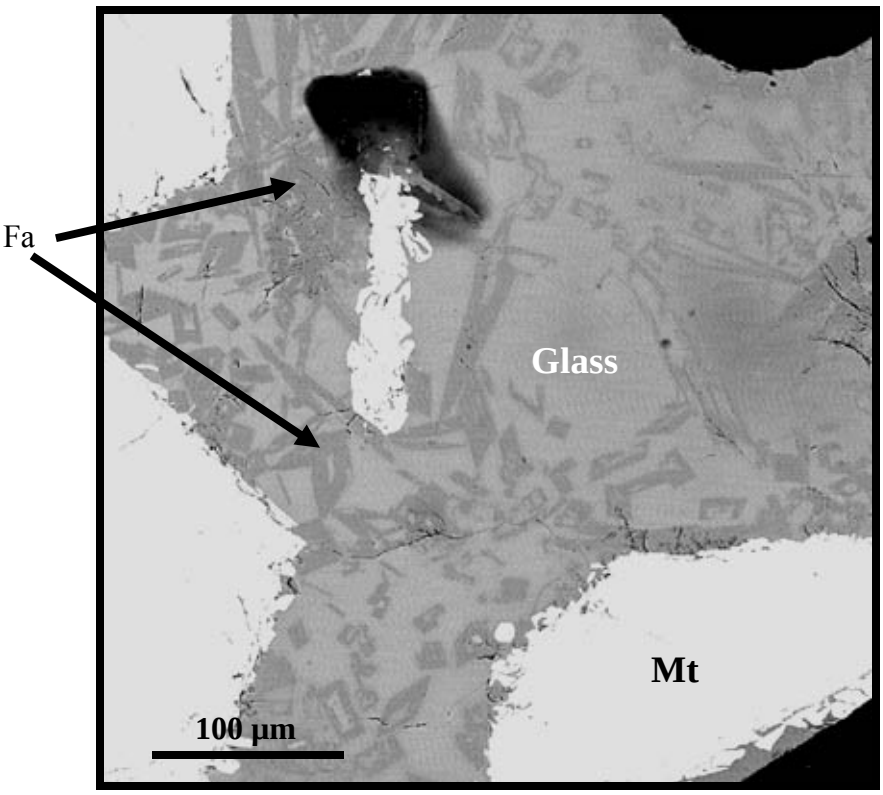

Table 15: EPMA analysis of fayalite from L1, and a fayalite standard.

	Olivine Standard-Fa	L1-Fa
FeO	67.55 wt.%	69.60 wt. %
SiO_2	29.22 wt. %	29.27 wt. %
MnO	2.14 wt %	0.02 wt. %

Iron concentrations in the glass are relatively high, ~2.5 wt. %, as compared to data from similar studies where mean iron concentrations are reported at the ppm range (Jugo, 1997, Frank et al., 2002). Glass chemistry is similar to data presented for glasses in Simon et al. (2004).

There was no fayalite present in the glass from L2 (Figure 19). Frank (2001) indicated that René - 41 vessels buffer oxygen fugacity near nickel- nickel oxide ($\log_{10} fO_2 = -13.8 \pm 0.1$); fayalite is not a stable phase at $fO_2 \sim$ NNO.

Run product aluminosity is a function of melt-aqueous phase interaction. Peralkaline melts are characterized as having an increased activity of alkali elements (Na, K) relative to aluminum. It has been suggested that the concentration of chlorine in hydrous silicate melts increases with the activities of Na, K, Ca, as well as Fe at the expense of Si (Metrich and Rutherford. 1992, Webster and DeVivo., 2002). In experiments conducted by Frank et al. (2003) and Simon et al. (2004b), the HCl concentration of the prepared aqueous solutions was varied to vary final melt aluminosity. Ancillary to these results was demonstrating the more important affect of iron on the chloride concentration of silicate melts. Data from synthetic glass shows that an increase in iron concentration positively correlates with an increase in Cl concentration in melts, suggesting Fe-Cl complexation in silicate melts (Simon et al., 2004b); data from this study reinforce this conclusion (Figure 20). In the hydrothermal experiments presented in this study the calculated ASIs are 0.80 and 0.50, where the glasses with the highest Fe and Cl concentrations had the lowest ASI and Si concentration. The cause of the difference between the two glasses is unknown because the experiments were designed to be identical.

Figure 19: Backscatter electron image of glass surrounding the quartz chip from experiment L2.

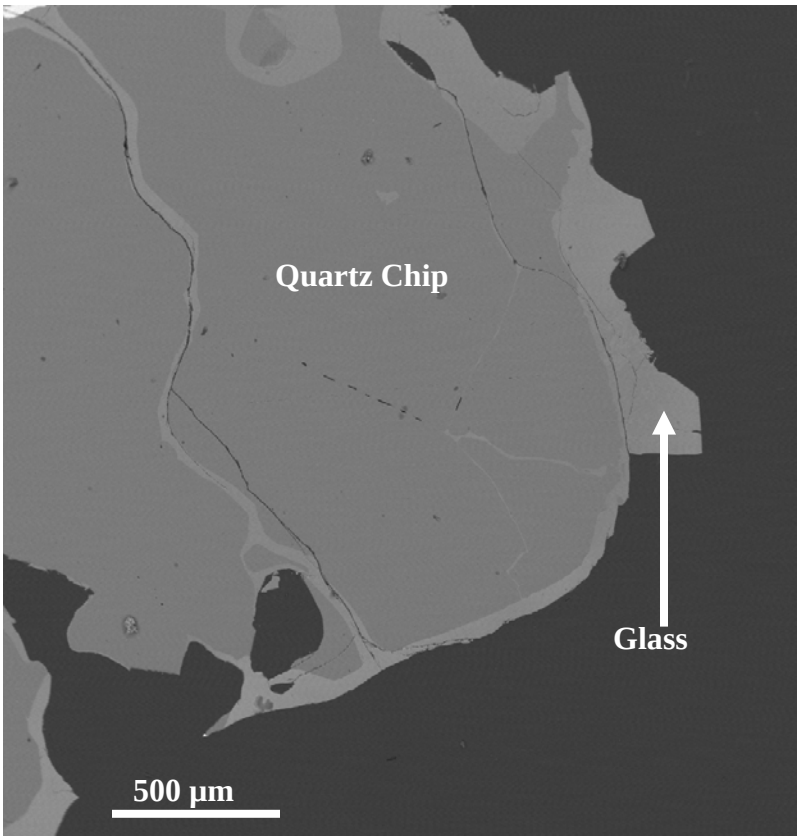

Figure 20: Fe (wt. %) vs. Cl (ppm) concentration in L1 and L2 glasses as determined by EPMA analysis. The ASIs for L1 and L2 are approximately 0.80 and 0.50 respectively.

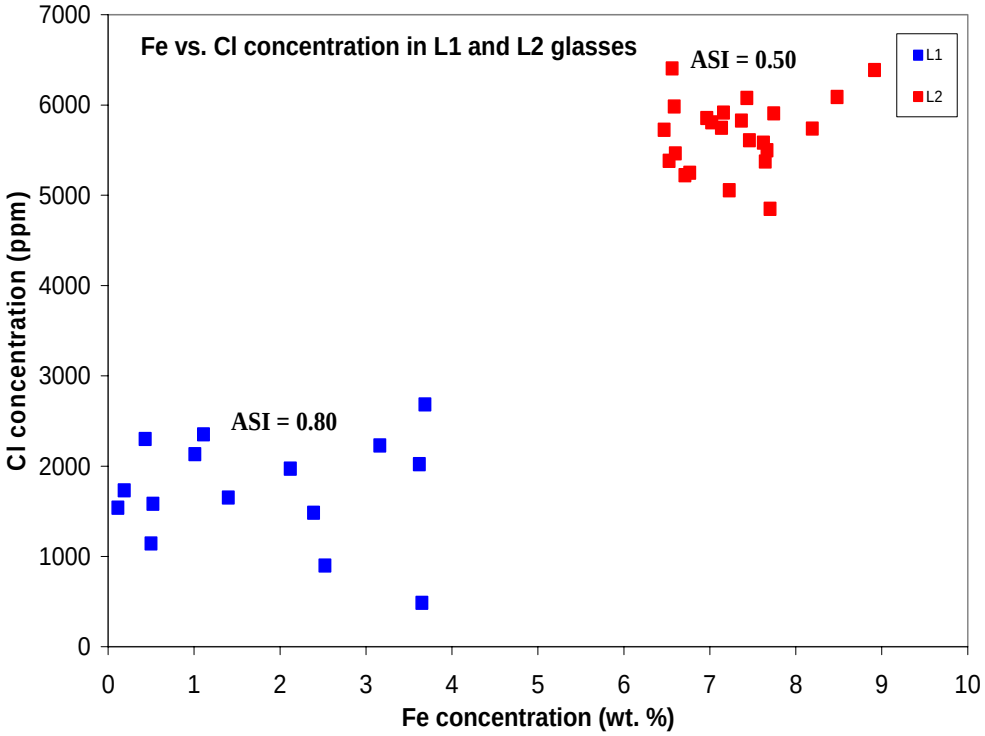

Experiments L1 and L2 were different with respect to oxygen fugacity as indicated by the formation of fayalite crystals in L1, and not in L2. In L1, iron was removed from the melt to form fayalite. Simon et al. (2004) states that iron concentration in experimental glasses is significantly higher in experiments performed at $fO_2 \sim$ QFM; the glass produced in L1 suggests the opposite. This is attributed to glass heterogeneity resulting from fayalite formation. The anomalously high concentrations of iron in L2 may be representative of the upper limits of iron solubility in melts at this oxygen fugacity and with an ASI of 0.50.

The activity of silver in the hydrothermal experiments was calculated by using the composition of the capsule. Silver concentrations were measured on the inside of the capsule walls that were used for experiments L1 and L2. The silver concentrations represent a range of values from 0-20 wt. %, where 3, 10, and 20 wt.% are representative of the gradation intervals of silver concentration across the capsule wall. The proportion of each region along the capsule wall was quantified by taking EDS analysis of individual points. It was estimated that 4/6 of the silver-bearing segment of the gold wall had the composition Ag_3Au_{97}, 1/6 of the wall had the composition $Ag_{10}Au_{90}$, and 1/6 of the wall had the composition $Ag_{20}Au_{80}$. The X_{Ag} for both L1 and L2 is 0.10, and, assuming Raoultian behavior (i.e. $X_{Ag}^{AgAu} = a(\mathrm{Ag})$), the a(Ag) in the hydrothermal experiments is approximated at 0.10.

Silver concentrations in the silicate glass run products from L1 and L2 were quantified by using LA-ICP-MS at ETH in Zurich. Silver concentrations are reported in Table 16. The average silver concentration for both glasses is on the order of 1.1 ± 0.2 ppm at an a(Ag) = 0.10. Differences in silver concentration throughout individual

glasses are most likely a consequence of glass heterogeneity. (Frank et al., (2002) suggested that metals present in the structures of melts occur as oxygenated species Silver is presumed to be present as the $AgO_{0.5}$ component in the melts discussed in this study. This occurs via the following equation

$$Ag^0 + ¼\ O_2 \rightarrow AgO_{0.5} \quad (10)$$

Table 16: Silver concentrations in run product glasses generated in hydrothermal experiments L1 and L2, concentrations are reported in ppm. Silver concentrations were determined by using LA-ICP-MS.

	L1 Glass	L2 Glass
	0.9	0.8
	0.5	1.1
	2.6	0.6
	2.3	1.3
Average (± 1σ)	1.3 ± 1.1	1.0 ± 0.3

Section 2: Vapor and brine inclusions from L1 and L2

Fluid inclusions were trapped in an inclusions-free quartz chip. These inclusions are interpreted as being representative samples of fluids present at run conditions. At 800°C and 140 MPa, the aqueous fluid was present as an immiscible vapor + brine pair in both experiments. The apparent salinities (wt. % NaCl equiv.) of the fluid inclusions as determined by microthermometry are reported in Table 17.

Table 17: Microthermometry data for fluid inclusions trapped in quartz chips in hydrothermal experiments L1 and L2; the starting composition of the aqueous solution was 15 wt. % NaCl equivalent.

L1			**L2**		
vapor	Tm_{ice}	wt. % NaCl eq.	**vapor**	Tm_{ice}	wt. % NaCl eq.
5	15.7	19.2	5	15.3	18.9
6	16.1	19.5	6	15.9	19.4
8	16.3	19.7	11	16.5	19.8
9	14.9	18.6	12	14.8	18.5
10	15.0	18.6	13	15.1	18.7
11	14.7	18.4	14	14.7	18.4
12	14.9	18.6	**brine**	Td_{NaCl}	wt. % NaCl eq.
13	15.5	19.0	1	285	37.2
brine	Td_{NaCl}	wt. % NaCl eq.	2	309	39.1
1	275	36.4	3	389	47.2
2	293	37.8	4	296	38.0
3	305	38.8	7	304	38.7
4	285	37.2	8	295	38.0
7	301	38.4	9	279	36.7
14	293	37.8	10	298	38.2
15	297	38.1			
16	284	37.1			

Section 3: Silver concentration and partition coefficients in fluid inclusions

Silver concentrations in the fluid inclusions as determined LA-ICPMS analysis are reported in Table 18. Frank et al., (2002) and Simon et al., (2002) indicate that metals are efficiently transported by high temperature vapor and brine phases, and that the extent of partitioning can be affected by several factors including pressure and HCl concentration. Simon (2003) determined that gold is more efficiently carried by the brine than the vapor phase. Data from this study indicates that silver behaves similarly to gold; concentrations of silver in the brine are an order of magnitude higher than those reported in the vapor phase. Silver is presumed to be transported as AgCl in the brine phase. It is unclear whether silver is complexed with chloride (AgCl) or hydroxide (AgOH) in the vapor phase. The partition coefficients for silver between brine and vapor ($D_{Ag}^{b/v}$) calculated for L1 and L2 are 9.0 ± 0.70, and 6.0 ± 0.60 respectively.

After MVP exsolution, metals partition between a melt, vapor and brine, and crystallizing phases. Partitioning of silver can be described by reactions that are occurring inside the experimental vessel. The exchange of silver between a melt and aqueous phase is described by the following reaction:

$$AgO_{0.5}{}^{m} + NaCl^{b,v} = AgCl^{b,v} + \tfrac{1}{2}\, Na_2O^{m} \quad (11)$$

$$K_{Ag,Na} = \frac{(a^{b,v}AgCl)\,(a^{m}Na_2O)^{1/2}}{(a^{m}AgO_{0.5})\,(a^{b,v}NaCl)} \quad (12)$$

Table 18: Silver concentrations (ppm) in vapor and brine inclusions from hydrothermal experiments L1 and L2 as determined by LA-ICPMS.

L1		
Brine	Laser Diameter (μm)	Ag (ppm)
my11a03	20	1920
my11a04	17	2105
my11a05	16	5895
my11a06	25	1770
my11a07	13	1392
my11a08	NA	2492
my11a09	NA	2164
AVERAGE		2534
STDEV		1521
Vapor		
my11a10	26	
my11a11	25	205
my11a12	25	271
my11a13	NA	398
AVERAGE		291
STDEV		98
L2		
Brine	Laser Diameter (μm)	Ag (ppm)
my11c10	22	2522
my11c11	20	4567
my11c12	20	2374
my11c13	15	2502
my11c14	NA	2159
AVERAGE		2825
STDEV		985
Vapor		
my11c03	18	NA
my11c04	16	251
my11c05	18	271
my11c06	20	469
my11c07	20	847
my11c08	20	637
AVERAGE		495
STDEV		252

Chapter 6: Discussion

The formation of porphyry and related ore deposits is a consequence of the magmatic, tectonic, chemical, and hydrologic processes that occur in the Earth's crust. Porphyry ore deposits are typically associated with both oxidized and reduced magmatic intrusions in volcanic arc settings, where the metals precipitated in the deposit are often a consequence of the degree of oxidation and the chemical composition of the related intrusion (Candela and Bouton, 1990, Candela, 1992, Hedenquist and Lowenstern, 1994, Barton, 1996, Blevin et al., 1996, Rowins, 2000, Thompson and Newberry, 2000, Titley, 2001). Ore metals present in silicic melts are inherited from the crust, mantle, and subducting slabs (Hedenquist and Lowenstern., 1994). A number of studies have suggested that the extent of processes such as crystallization of mineral phases and MVP exsolution play a determinant role in the potential for an ore deposit to form (Holland, 1972, Candela and Holland, 1984, Cygan and Candela, 1995, Candela and Piccoli, 1995, Williams et al., 1995, Jugo et al., 1999, Simon et al., 2003). The extent that metals will partition into mineral phases, prior to MVP exsolution can jeopardize the formation of a magmatic-hydrothermal deposit, because it is the total amount of the magmatic inventory of a metal available to the MVP that controls the potential for mineralization (Candela and Holland, 1986).

Pyrrhotite and magnetite can be found in intermediate to felsic igneous rocks. Experimentally determined mineral/melt partition coefficients from this study and Cygan and Candela, (1995), Jugo et al., (1999), Simon et al., (2003) indicate that magnetite and pyrrhotite have the ability to sequester gold, silver, and copper to

varying degrees. The crystallization of either magnetite or pyrrhotite from a magma can have a substantial impact on the potential for ore deposit formation; this effect will be amplified if MVP exsolution occurs late in the crystallization history of a magma.

The oxidation state of ore-generative magmas is ultimately a consequence of the inherited properties of a magma and magma evolution, which can encompass crystal fractionation and open system behavior such as C or Fe sulfide incorporation into magmas (Ishihara, 1981, Blevin and Chappell, 1992). Ore metal ratios in porphyry-type deposits have been shown to be a consequence of the oxidation state of the related magma, with Cu-Au deposits are commonly associated with more oxidized magmas and fO_2 ~ NNO, and W-Mo and Sn deposits associated with more reduced magmas (Ishihara, 1981, Hedenquist and Lowenstern, 1994, Blevin et al., 1996, Barton, 1996, Takagi, 2004).

Igneous intrusions related to Cu-Au porphyries are typically magnetite-bearing, whereas iron sulfides are present in small amounts (Ishihara, 1981). Because there is only a small percentage of iron sulfide crystallization in oxidized igneous intrusion, Cu-Au concentration in melts is the major source of ore metals for exsolved volatiles phases. Magnetite-bearing granites are often related to reduced, ilmenite-bearing rocks (fO_2 ~ QFM) suggesting that reduced granites are a progeny of a more oxidized counterpart or visa versa (Ishihara, 2000). K-Ar ages of magnetite-series and ilmenite-series granitoids and the associated mineralization in the Japanese island arc record an age progression from reduced to more oxidized granitoids (Ishihara, 1981). Isotope analyses indicate that the source of the Japanese magmas was the same, and

that variations in oxidation state could have been caused by an increase in sediment subduction along the convergent margin (Takagi, 2004). Ilmenite-series granites have less than 0.1 modal percent magnetite, pyrrhotite is more common, and to a large extent these intrusions are related to Sn, W, and Mo mineralization (Ishihara, 1981). Sulfur concentrations are relatively high in reduced intrusions because sulfur does not partition as strongly into an exsolved volatile phase but crystallizes to form sulfide minerals (Ishihara, 1981). This promotes the partitioning of Au and Cu into sulfide minerals, and in conjunction with low Cl content in hydrothermal fluids, precludes the formation of Au-Cu porphyries related to ilmenite-bearing granites (Ishihara, 1981). The extent to which magnetite and pyrrhotite crystallize in magmatic systems that generate both magnetite and ilmenite-bearing granites can have an affect on the formation of a porphyry deposit enriched in silver, because both minerals have the ability to sequester silver to some extent based on data generated in this study. Modeling the affects of magnetite and pyrrhotite fractionation in systems that can produce oxidized or reduced intrusions can provide some insight into extent of this affect.

Calculated $D_{Ag}^{Po/melt}$ ***and*** $D_{Ag}^{Mt/melt}$

This study was designed to investigate the extent to which silver partitions between magnetite, pyrrhotite, a melt, and vapor and brine phases at elevated temperatures and pressures. One goal of this project is to determine the degree to which magnetite and pyrrhotite can accommodate silver relative to the other system components. The two types of experiments presented in this study, silica tube and hydrothermal, can be used to calculate $D_{Ag}^{Po/melt}$, $D_{Ag}^{Mt/melt}$, which are a measure of the

extent of which silver concentrates in the crystalline phases magnetite and pyrrhotite relative to a melt.

LA-ICP-MS analysis of run product silicate glasses from hydrothermal experiments suggests that 1.1 ± 0.2 ppm silver at a(Ag) =0.10 ($X_{Ag}^{AgAu} = a(\mathrm{Ag})$) is soluble in peralkaline melts at a range of oxygen fugacities between QFM and NNO, 800°C and 140 MPa. In this range of oxygen fugacities both magnetite and pyrrhotite can precipitate as stable phases from a silicate melt based on data presented in Whitney (1984). To calculate $D_{Ag}^{Po/melt}$ and $D_{Ag}^{Mt/melt}$ the average concentration of silver in magnetite, 200 ppm, and pyrrhotite, 2800 ppm at an average a(Ag) = 0.13 ± 0.04 (1σ) were used to estimate silver solubility in these phases in magmatic-hydrothermal systems.

The silicate glasses from L1 and L2 were interpreted to be in equilibrium with silver metal at a(Ag) = 0.10. The concentration of silver in the silicate glasses has to be extrapolated to represent a system where the melt and silver metal were in equilibrium at a(Ag) = 0.13. This will make the data from the silica tube and hydrothermal experiments comparable; the systems had different a(Ag) at experimental conditions and this has to be corrected to generate accurate partition coefficients. The silver concentration in silicate glasses at an a(Ag) = 0.13 is approximated at 1.4 ppm. The approximate $D_{Ag}^{Mt/melt}$ and $D_{Ag}^{Po/melt}$ are:

$D_{Ag}^{Mt/melt} = 140$

$D_{Ag}^{Po/melt} = 2000$

The effects of crystallization of magnetite and pyrrhotite on silver concentrations in magmatic-hydrothermal systems are a function of the total amount of magnetite and pyrrhotite that crystallize prior to MVP exsolution and the partition coefficient for a metal between magmatic magnetite and pyrrhotite and a silicate melt. These factors are taken into account in bulk partition coefficients, $\overline{D}$. Modeling silver sequestration by magnetite and pyrrhotite from silicate melts takes into account these variables and is a useful tool for trying to predict the potential for silver accumulation in veins and stockwork structures or as trace constituents in ore minerals.

Modeling Cu, Ag, and Au sequestration by magnetite and pyrrhotite

Modeling sequestration of silver by magnetite and pyrrhotite in a silicate melt can be done by using the Rayleigh fractionation equation similar in the form used by Simon et al., 2003:

$$m_{Ag}^{melt} = m_{Ag}^{melt,initial} * F^{\overline{D}} \quad (13)$$

where m is the mass of Ag in a melt, F is the fraction of liquid remaining (0-1), and $\overline{D}$ is the bulk partition coefficient for Ag between magnetite and melt and pyrrhotite and melt. $\overline{D}$ is calculated using the following equation:

$$\overline{D}_{\mathrm{Ag}} = \mathrm{X_{Po}} * D_{Ag}^{Po/melt} + \mathrm{X_{Mt}} * D_{Ag}^{Mt/melt} \quad (14)$$

The $D_{Ag}^{Mt/melt}$, and $D_{Ag}^{Po/melt}$ are ~140 and ~2000 respectively at an a(Ag) = 0.13 ± 0.04 (1σ) at NNO > fO$_2$ > QFM and log$_{10}f$S$_2$ ranging from -3.74 to -0.18. The mass

fraction of magnetite (X_{Mt}) is approximated at 0.00 and 0.02 for rock types ranging from ilmenite-series to magnetite-series granites (Ishihara, 1981). The mass fraction of pyrrhotite (X_{Po}) is approximated at 0.00 and 0.02 for rock types ranging from magnetite-series to ilmenite-series granites (Luhr, 1990). Similar parameters can be used to model the effects of magnetite and pyrrhotite crystallization on Au and Cu budgets in evolving melts. $D_{Au}^{Mt/melt}$, $D_{Au}^{Po/melt}$, $D_{Cu}^{Mt/melt}$, and $D_{Cu}^{Po/melt}$ were calculated in Jugo et al., (1999), Simon et al., (2003), and Simon (2003) as 4, 140, 1, and 2600 respectively. Fractionation is modeled for the entire crystallization history of a melt. This model does not take into account MVP exsolution or changes in chemical composition of melt that can affect metal sequestration by magnetite and possibly pyrrhotite (Simon et al., 2003). Partition coefficients were evaluated as a function of the concentration of silver in the experimental charge to determine whether or not they follow Henry's Law. Henry's Law states the activity coefficient does not vary with respect to concentration. Partition coefficients calculated in this study, and in Jugo et al., (1999), Simon et al., (2003), and Simon (2003) follow Henry's Law.

The modeled effects of concurrent crystallization of pyrrhotite and magnetite on silver, gold and copper budgets in a silicate melt at QFM $\geq$ fO_2 $\geq$ NNO are presented in Figures 21, 22, and 23. The proportion of Ag, Au, and Cu remaining in the silicate melt with progressive crystallization is a function of the bulk partition coefficient ($\overline{D}$) for a metal with respect to magnetite and pyrrhotite. By isolating the proportion of Ag, Au and Cu that remain at 50% crystallization, the extent to which $\overline{D}$ controls ore metal budgets can be assessed (Table 19). The R notation (i.e. R_{Ag}) stands for the ratio of metal remaining in a melt with progressive crystallization.

Figure 21: Modeled effects of the crystallization of magnetite and pyrrhotite on silver budgets in a silicate melt at QFM ≥ fO_2 ≥ NNO. The bulk partition coefficients for silver at high, low, and moderate fO_2 are 2.8, 4, and 6.8 respectively. The mass fraction of magnetite is 0.00 - 0.02, and the mass fraction of pyrrhotite is 0.00- 0.002.

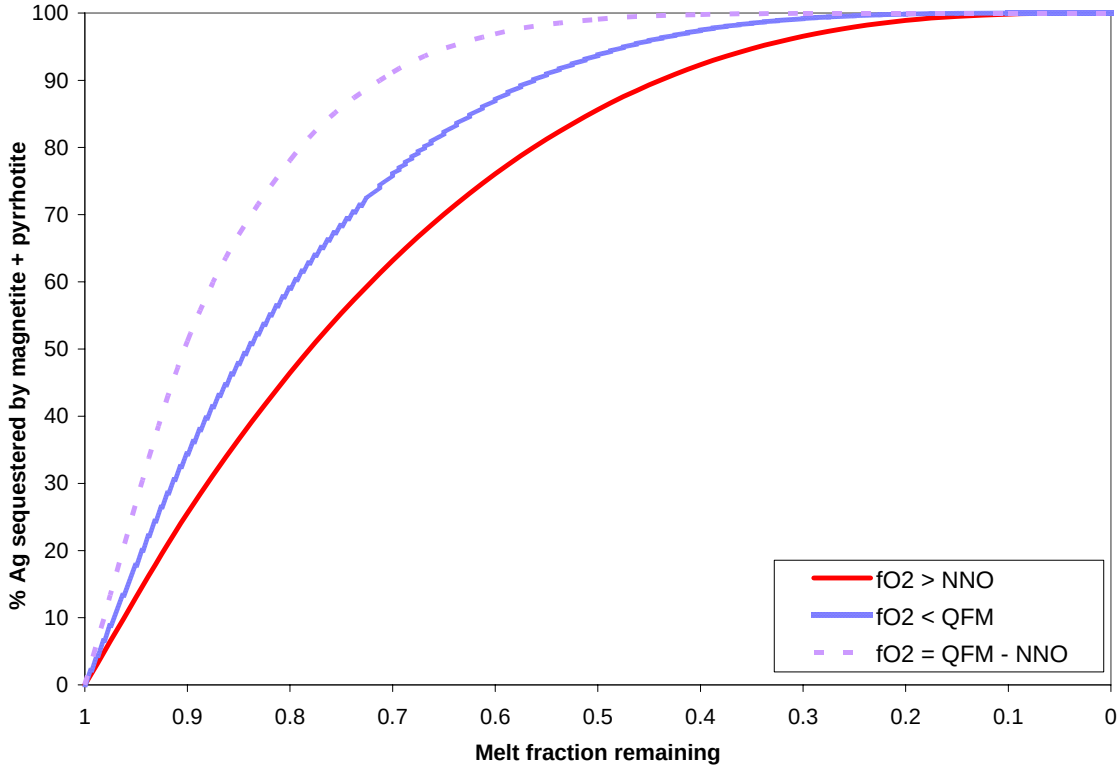

Figure 22: Modeled effects of the crystallization of magnetite and pyrrhotite on gold budgets in a silicate melt at QFM ≥ fO_2 ≥ NNO. Bulk partition coefficients for high, low, and moderate fO_2 are 0.08, 0.28, and 0.36 respectively. The mass fraction of magnetite is 0.00 - 0.02, and the mass fraction of pyrrhotite is 0.00- 0.002.

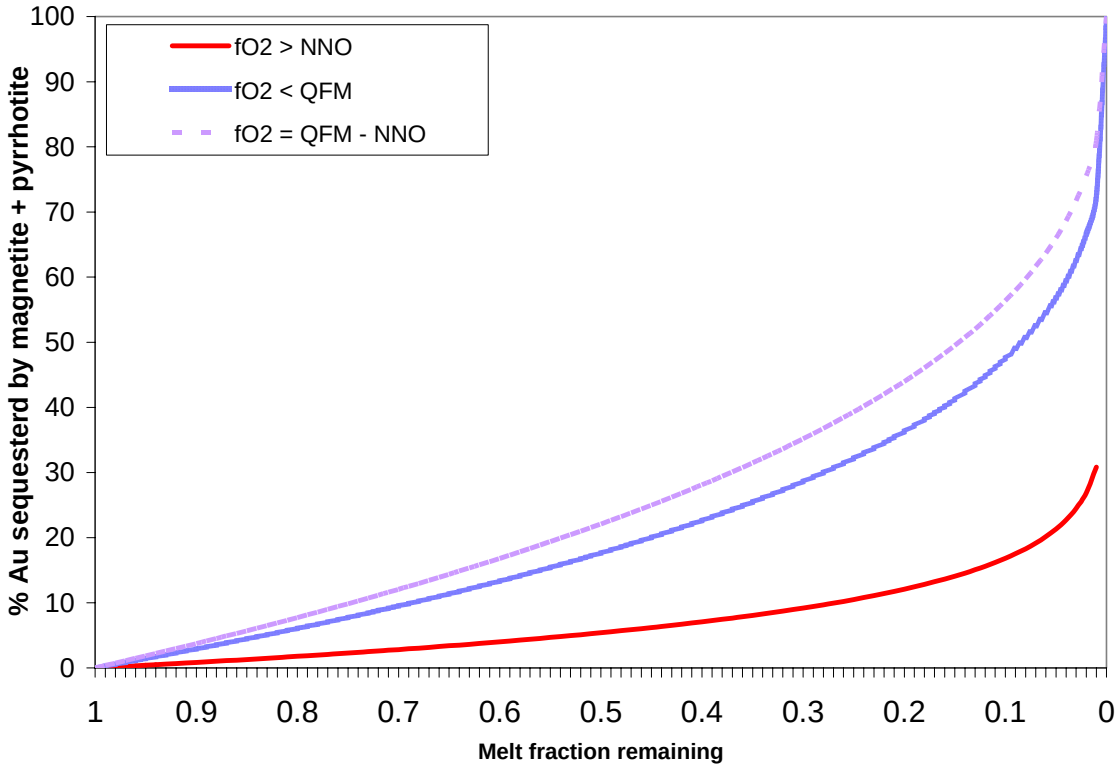

Figure 23: Modeled effects of the crystallization of magnetite and pyrrhotite on copper budgets in a silicate melt at QFM ≥ fO_2 ≥ NNO. Bulk partition coefficients for copper at high, low, and moderate fO_2 are 0.02, 5.2, and 5.22 respectively. The mass fraction of magnetite is 0.00 - 0.02, and the mass fraction of pyrrhotite is 0.00-0.002.

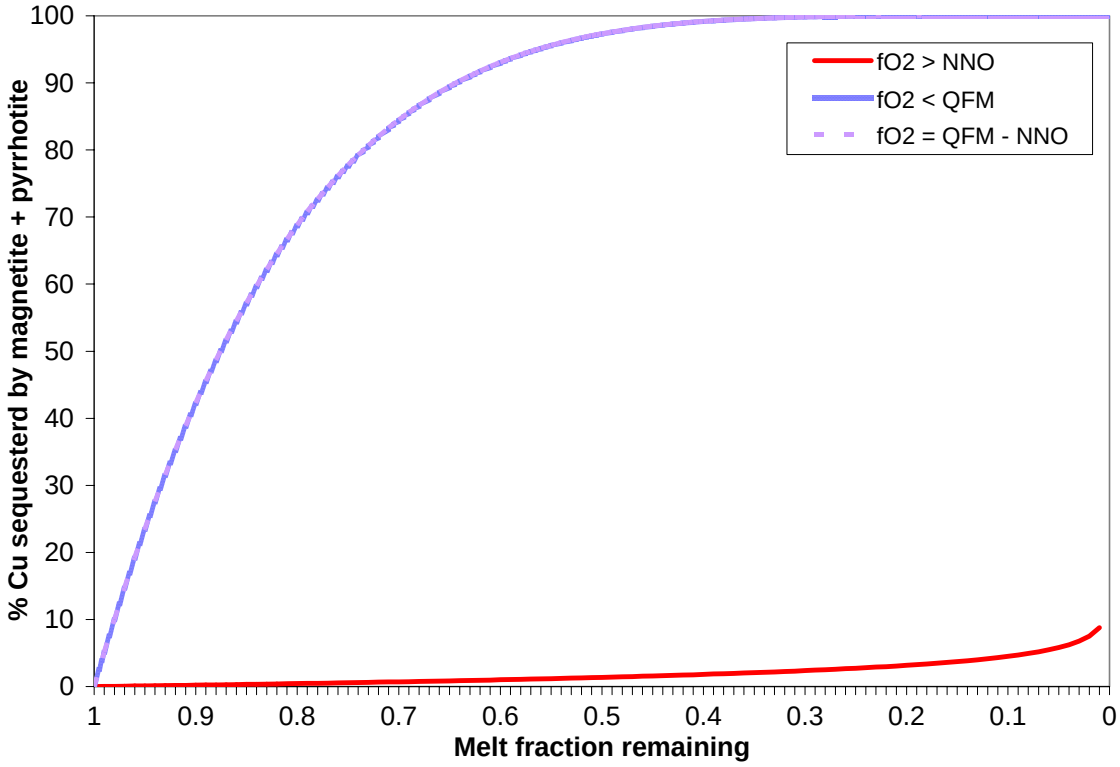

Table 19: The percent of Ag, Au and Cu remaining after 50% crystallization of a silicate melt at QFM ≥ fO_2 ≥ NNO; fO_2 > NNO was approximated using a mass fraction of Mt = 2.0% and Po = 0.0%, fO_2 < QFM was approximated using a mass fraction of Mt = 0.0% and Po = 0.2%, fO_2 = QFM – NNO was approximated using a mass fraction of Mt = 2.0% and Po = 0.2%.

	fO_2 > NNO	fO_2 < QFM	fO_2 = QFM - NNO
R_{Au}	95%	83%	78%
R_{Ag}	14%	6%	1%
R_{Cu}	99%	3%	3%

Based on these models, the fractionation of pyrrhotite (± magnetite) from a silicate melt, at fO_2 ranging from below QFM to NNO, where the mass fraction of pyrrhotite is estimated at 0.002, removes the largest percentage of Cu, Ag, and Au from a silicate melts. Melts crystallizing at fO_2 > NNO where just magnetite is present lose the smallest percentage of Cu, Ag, and Au at all degrees of crystallization. At 50% of melt crystallization, at fO_2 < QFM, approximately 97% of the copper present in a silicate melt is removed by pyrrhotite fractionation, 84% of the silver present is sequestered, and 17% of gold present is sequestered. At fO_2 < QFM, copper and silver are depleted in the melt to the larger extent by the fractionation of pyrrhotite as compared to gold, which is predicted by the experimentally determined $D_{Au}^{Po/melt}$, $D_{Ag}^{Po/melt}$, $D_{Cu}^{Po/melt}$. This is being attributed to large size of the gold cation as compared to copper and silver, where it is more difficult for gold to be efficiently incorporated into the structure of pyrrhotite without causing substantial lattice strain (Blundy and Wood, 2003). The extent of compatibility of Au, Ag, and Cu in pyrrhotite may be one of the primary processes controlling the regional variations in Au : Ag : Cu ratios present in porphyry deposits; similar conclusions were drawn in Jugo (1997); this will be discussed later in this section.

At intermediate fO_2 (QFM – NNO), 99% of the Ag and 97% of the Cu that is present in a silicate melt would be removed due to the concurrent fractionation of magnetite and pyrrhotite when 50% of a melt has crystallized. The gold content of a silicate melt at an intermediate oxygen fugacity is decreased by approximately 25% after 50% crystallization.

Magnetite incorporates the Group 1B metals to a lesser extent than does pyrrhotite. Model data indicate that at the highest reasonable mass fraction of magnetite 0.02, approximating fO_2 > NNO, a silicate melt can lose 75% of the total Ag present, 5% Au, and 1% Cu after 50% crystallization. The concentration of silver was measured in magnetites that were generated in a system where the total pressure amounted to no more than 1 bar. Simon (2003) showed, based on experimental data that metal solubility in mineral phases increases to some extent with decreasing pressure; this might have had a minor effect on the $D_{Ag}^{Mt/melt}$ calculated for this study. High concentrations of silver in magnetite may also be a consequence of Ag-Fe complexation. Silver may have a greater ability to bond with iron under these conditions as compared to copper or gold, making it easier for magnetite to incorporate larger amounts of silver. Copper and gold most likely enter the structure of magnetite as substitutions for iron; the extent of this is limited because on the large size of these ions. This may be the cause for the large $D_{Ag}^{Mt/melt}$ as compared to partition coefficients for copper and gold between silicate melts.

The model data presented above place a calculated upper limit on the affect that magnetite and pyrrhotite fractionation has on the silver, gold, and copper budgets of a crystallizing silicate melt, and demonstrate that pyrrhotite and magnetite fractionation can be significant. The models indicate that small variations in oxygen fugacity can significantly affect metal budgets a magmatic-hydrothermal system because of the partly overlapping stability fields of magnetite and pyrrhotite. The fractionation of both magnetite and pyrrhotite can affect the melt content of an ore

forming fluid, should it exsolve at any point during the crystallization history of a melt.

Cu, Ag, and Au constitute the Group 1B metals and are present at approximately 27 ppm, 56 ppb, and 1.3ppb, respectively in the continental crust (Rudnick and Gao, 2003). These values correspond to a Ag/Au ratio of 43, a Ag/Cu ratio of 0.002, and a Au/Cu ratio of 4.8E-5 in the continental crust. The primary control of ore metal ratios in porphyry deposits is their original crustal abundances. Ore metals inherited from crustal sources can concentrate in melts, fluids, and mineral phases via magmatic and chemical processes. Thus ore metal ratios evolve through time such that they no longer represent original crustal values. Modeling R_{Au}, $R_{Ag,}$ and R_{Cu} can provide insight into how pyrrhotite or magnetite crystallization can manipulate ore metal ratios throughout the crystallization history of a silicate melt. These models do not attempt to predict ore metal ratios and metal grades in natural ore generative systems.

For melt crystallizing at oxygen fugacities encompassing those between QFM and NNO, the amount of Ag removed relative to Au from the magma is maximized due to the fractionation of both magnetite and pyrrhotite. This is due to higher Mt/melt and Po/melt partition coefficients for silver than for gold and the high proportion of magnetite and pyrrhotite fractionating. For melts crystallizing below QFM or above NNO the proportion of silver and gold remaining in a melt over its entire crystallization history is higher as compared to melts fractionating at intermediate oxygen fugacity. The percentage of silver sequestered at high or low oxygen fugacity is greater than the percentage of gold sequestered.

Jugo et al. 1999 concluded that fractionation of an intermediate solid solution (Iss) with the composition $Cu_2Fe_3S_5$ can deplete a melt with respect to gold to a larger extent than pyrrhotite, where the $D_{Au}^{Iss/Po} = 42 \pm 9$ (1σ), and approximately 1.9 ± 0.4 (1σ) wt % Au was reported in the Iss (850°C,100MPa, fO_2 = NNO) . The degree to which silver would partition in an Iss has not been experimentally determined, although silver is mined from Cu-Fe sulfides in porphyry deposits, so some degree of solubility is inferred. Iss is stable over a wider range of oxygen fugacities than pyrrhotite, where Iss can fractionate at similar fO_2 as magnetite (Jugo et al., 1999). If Iss fractionation occurs, substantial amounts of gold and possibly silver could be sequestered, thus the proportion of silver remaining in a melt as compared to gold would evolve in response to this as well as magnetite and pyrrhotite fractionation.

The fractionation of pyrrhotite over the entire crystallization history of a silicate melt at fO_2 < QFM removes a larger proportion of copper as compared to silver; this is reasonable considering the difference in $D_{Cu}^{Po/melt}$ and $D_{Ag}^{Po/melt}$, where copper is more compatible in pyrrhotite as relative to silver. In more oxidized systems where fO_2 ranges between QFM to greater than NNO, the opposite is true; silver is removed to a larger extent than copper. The experimentally determined $D_{Cu}^{Mt/melt}$ is significantly lower than $D_{Ag}^{Mt/melt}$, where these values are 1 and 140 respectively. Because of this concurrent fractionation of magnetite and pyrrhotite or just magnetite fractionation removes a larger proportion of silver as compared to copper.

The models presented above were generated for silicate melts that are at different stages of oxidation, where the degree of oxidation was a function of the

mass fraction of the magnetite and pyrrhotite present. These models did not take into account the fractionation of ilmenite or an Iss, which are considered minerals responsible for sequestering copper and gold at the magmatic level (Ewert and Griffin, 1994, Jugo et al., 1999). Ilmenite-series granitoids contain a higher modal percent of pyrrhotite as compared to magnetite, and can contain up to 4 vol % ilmenite (Ishihara, 1981). The concurrent fractionation of ilmenite and pyrrhotite from a reduce melt may be akin to the effects of concurrent fractionation of magnetite and pyrrhotite in more oxidized melts. Ilmenite sequestration of ore metals may have a small affect of metal budgets available to the MVP. The effect of Iss fractionation was considered in reference to gold sequestration, Iss can also remove a substantial amount of copper from a melt should Iss fractionation occur (Jugo et al., 1999). Au, Ag, and Cu partition to a larger extent into pyrrhotite and Cu-Fe sulfides relative to magnetite, because of this fractionation of sulfide minerals has the largest effect on metal budgets in silicate melts. Because sulfides are sensitive to variations in fS_2/fO_2, the destabilization of pyrrhotite or Cu-Fe sulfides at any point during melt evolution, due to S-bearing MVP exsolution or sulfide mineral crystallization, may release previously sequestered metals, potential resetting the concentration of Au, Ag, and Cu in a silicate melt.

Ore metal concentrations in porphyries are often present in the following succession Cu > Ag > Au. This is largely controlled by the original abundance of these metals present in the continental crust. Fractionational crystallization and metal sequestration, controlled in part by the intensive parameters of a magmatic system,

and the timing of MVP exsolution from a silicate melt may account for regional variations in ore metal ratios seen in porphyry deposits around the world.

Chapter 7: Conclusions

The C_{Ag}^{Po} and C_{Ag}^{Mt} are approximated at 2800 ± 700 (1σ) ppm and 200 ± 100 ppm (1σ) respectively at 800°C, and at an a(Ag) = 0.13 ± 0.04 (1σ), and fO$_2$ = -14.90 to -11.62 and fS$_2$ = -4.06 to -0.18. $D_{Ag}^{Po/mt}$ is 14 ± 3 at 800°C and at an a(Ag) = 0.13 ± 0.4 (1σ) at fO$_2$ = -14.90 to -11.62 and fS$_2$ = -4.06 to -0.18. The concentration of silver in peralkaline melts is 1.1 ± 0.2 ppm at a(Ag) = 0.10 at a range of fO$_2$ from QFM to NNO. $D_{Ag}^{Mt/melt}$ and $D_{Ag}^{Po/melt}$ at 800°C and an a(Ag) = 0.13 ± 0.04 (1σ) and at the above mentioned fugacities are on the order of 140 and 2000 respectively. $D_{Ag}^{b/v}$ is ~ 7 at 800°C, 140 MPa, at fO$_2$ ranging between QFM and NNO and an a(Ag) = 0.10.

Au:Ag:Cu ratios present in porphyry deposits can be impacted by the fractionation of magnetite and sulfide minerals including pyrrhotite and Iss. Based on data generated in this study and from Jugo et al., 1999, Simon, 2003, and Simon et al., 2003, fractionation of sulfide minerals has the largest affect on ore metal budgets in silicate melts as compared to magnetite. With increasing fO$_2$, pyrrhotite and other sulfides will destabilize and possibly release their load of ore metals into the silicate melt. Because magnetite does not remove a significant quantity of ore metals compared to pyrrhotite, in high fO$_2$ melts the minimal effects of Au, Ag, and Cu sequestering should yield a high removal of these metals by the MVP.

Appendix I: Pyrrhotite Chemistry

Sample #	Fe	Ag	S	Mn	Si	Pb	Cu	Zn	Au	Total
17	60.1	0.330	37.48	0.021	b.d	NA	0.456	0.13	NA	98.6
17	60.4	0.499	37.27	0.021	b.d	NA	0.450	0.15	NA	98.8
17	59.9	0.341	37.15	0.022	b.d	NA	0.462	0.09	NA	98.0
17	59.9	0.342	36.79	0.019	b.d	NA	0.450	0.22	NA	97.8
17	59.8	0.295	37.20	0.025	b.d	NA	0.440	0.17	NA	97.9
17	59.8	0.332	36.72	0.025	b.d	NA	0.450	0.11	NA	97.5
17	59.9	0.282	36.94	0.032	b.d	NA	0.450	0.19	NA	97.8
17	59.3	0.246	37.61	0.022	b.d	NA	0.461	0.10	NA	97.8
17	57.5	0.319	36.34	0.024	b.d	NA	0.455	0.05	NA	94.7
AVG	**59.6**	**0.332**	**37.06**	**0.024**			**0.453**	**0.14**		**97.6**
STDEV	**0.8**	**0.070**	**0.40**	**0.004**			**0.007**	**0.06**		**1.2**
18	60.2	0.110	36.71	0.027	b.d	NA	0.478	0.12	NA	97.7
18	59.8	0.311	36.56	0.036	b.d	NA	0.474	0.13	NA	97.4
18	59.9	0.307	36.57	0.039	b.d	NA	0.486	0.06	NA	97.4
18	59.9	0.311	37.02	0.016	b.d	NA	0.489	0.17	NA	98.0
18	58.9	0.260	34.57	0.018	b.d	NA	0.455	0.23	NA	94.4
18	59.0	0.275	34.52	0.015	b.d	NA	0.459	0.26	NA	94.6
18	59.9	0.249	36.77	0.025	b.d	NA	0.331	0.13	NA	97.4
18	60.0	0.194	36.86	0.035	b.d	NA	0.314	0.14	NA	97.6
18	60.0	0.201	36.83	0.032	b.d	NA	0.319	0.03	NA	97.5
18	58.4	0.349	36.66	0.021	b.d	NA	0.319	0.11	NA	95.9
18	60.8	0.255	37.40	0.025	b.d	NA	0.413	0.20	NA	99.2
18	60.7	0.256	37.33	0.022	b.d	NA	0.416	0.28	NA	99.1
18	60.4	0.241	37.18	0.029	b.d	NA	0.423	0.27	NA	98.6
AVG	**59.8**	**0.255**	**36.54**	**0.026**			**0.414**	**0.17**		**97.3**
STDEV	**0.7**	**0.062**	**0.92**	**0.008**			**0.069**	**0.08**		**1.5**
19	59.6	0.328	39.39	0.081	b.d	NA	0.361	0.12	NA	99.9
19	59.8	0.203	38.42	0.088	b.d	NA	0.351	0.10	NA	99.0
19	60.4	0.430	38.86	0.075	b.d	NA	0.346	0.27	NA	100.4
19	59.8	0.316	38.42	0.077	b.d	NA	0.361	0.07	NA	99.1
19	60.6	0.302	38.20	0.083	b.d	NA	0.371	0.28	NA	99.9
19	59.8	0.637	38.09	0.087	b.d	NA	0.371	0.24	NA	99.3
19	60.2	0.194	37.41	0.073	b.d	NA	0.376	0.15	NA	98.5
19	59.9	0.307	37.38	0.104	b.d	NA	0.375	0.24	NA	98.4
19	60.4	0.299	39.14	0.095	b.d	NA	0.331	0.08	NA	100.3
19	59.6	0.324	37.43	0.101	b.d	NA	0.358	0.12	NA	98.0
19	59.7	0.281	38.04	0.089	b.d	NA	0.345	0.13	NA	98.6
19	59.9	0.365	37.89	0.103	b.d	NA	0.352	0.08	NA	98.7
19	60.5	0.323	38.82	0.085	b.d	NA	0.408	0.23	NA	100.5
19	57.4	0.123	40.91	0.059	b.d	NA	0.379	0.06	NA	99.1
AVG	**59.8**	**0.316**	**38.46**	**0.086**			**0.363**	**0.16**		**99.3**
STDEV	**0.7**	**0.119**	**0.95**	**0.013**			**0.019**	**0.08**		**0.8**

	Fe	Ag	S	Mn	Si	Pb	Cu	Zn	Au	Total
20	59.4	0.134	32.59	0.028	b.d	NA	0.269	0.13	NA	92.7
20	59.9	0.369	36.79	0.029	b.d	NA	0.335	0.16	NA	97.6
20	57.8	0.361	33.62	0.036	b.d	NA	0.405	0.07	NA	92.3
AVG	**59.0**	**0.288**	**34.33**	**0.031**			**0.336**	**0.12**		**94.2**
STDEV	**1.1**	**0.134**	**2.19**	**0.004**			**0.068**	**0.04**		**3.0**
21	59.6	0.243	37.77	0.015	b.d	NA	0.339	0.17	NA	98.2
21	59.2	0.414	37.31	0.031	b.d	NA	0.354	0.07	NA	97.4
21	60.4	0.314	37.67	0.026	b.d	NA	0.369	0.10	NA	98.9
21	60.6	0.348	39.42	0.030	b.d	NA	0.308	0.22	NA	101.0
21	60.2	0.280	38.19	0.039	b.d	NA	0.315	0.05	NA	99.2
21	60.6	0.321	38.50	0.024	b.d	NA	0.323	b.d	NA	99.8
21	60.6	0.307	38.16	0.034	b.d	NA	0.316	0.09	NA	99.6
21	60.7	0.272	38.46	0.026	b.d	NA	0.375	0.15	NA	100.1
21	60.2	0.326	38.08	0.031	b.d	NA	0.383	0.16	NA	99.2
21	59.9	0.330	38.67	0.023	b.d	NA	0.355	0.11	NA	99.5
21	60.4	0.328	37.81	0.024	b.d	NA	0.364	0.07	NA	99.0
21	60.8	0.174	37.71	0.028	b.d	NA	0.184	0.09	NA	99.1
21	60.5	0.230	38.05	0.018	b.d	NA	0.185	0.13	NA	99.2
21	60.8	0.225	38.03	0.026	b.d	NA	0.178	0.07	NA	99.4
21	59.4	0.151	39.61	0.029	b.d	NA	0.326	0.42	NA	100.0
21	57.8	0.286	37.47	0.030	b.d	NA	0.357	0.51	NA	96.5
AVG	**60.1**	**0.284**	**38.18**	**0.027**			**0.315**	**0.15**		**99.1**
STDEV	**0.8**	**0.067**	**0.64**	**0.006**			**0.069**	**0.13**		**1.1**
22	59.1	0.308	37.69	0.037	b.d	NA	0.369	0.36	NA	97.9
22	59.5	0.314	37.70	0.028	b.d	NA	0.360	0.50	NA	98.4
22	57.5	0.553	38.03	0.023	b.d	NA	0.397	0.42	NA	97.0
22	60.1	0.190	37.24	0.026	b.d	NA	0.363	0.55	NA	98.5
22	59.9	0.195	37.53	0.014	b.d	NA	0.381	0.43	NA	98.5
22	60.1	0.511	37.06	0.026	b.d	NA	0.390	0.45	NA	98.8
22	60.3	0.299	37.60	0.020	b.d	NA	0.400	0.52	NA	99.1
22	60.2	0.303	37.82	0.019	b.d	NA	0.401	0.57	NA	99.4
22	60.2	0.311	37.26	0.029	b.d	NA	0.397	0.41	NA	98.7
22	59.2	0.100	38.59	0.038	b.d	NA	0.185	0.52	NA	98.7
22	60.1	0.108	38.48	0.048	b.d	NA	0.192	0.50	NA	99.5
22	60.7	0.104	38.15	0.039	b.d	NA	0.199	0.51	NA	99.7
22	60.0	0.092	37.80	0.035	b.d	NA	0.185	0.44	NA	98.6
AVG	**59.8**	**0.261**	**37.77**	**0.029**			**0.324**	**0.47**		**98.7**
STDEV	**0.8**	**0.150**	**0.46**	**0.010**			**0.094**	**0.06**		**0.7**
24	60.3	0.343	37.29	0.019	b.d	NA	0.407	0.13	NA	98.6
24	60.5	0.343	37.15	0.008	b.d	NA	0.412	0.16	NA	98.7
24	60.2	0.349	37.25	0.011	b.d	NA	0.410	0.14	NA	98.4
24	60.3	0.328	38.09	0.014	b.d	NA	0.413	0.01	NA	99.2
24	60.4	0.411	37.59	0.026	b.d	NA	0.419	0.16	NA	99.1

	Fe	Ag	S	Mn	Si	Pb	Cu	Zn	Au	Total
24	60.3	0.328	37.23	0.027	b.d	NA	0.412	0.05	NA	98.4
24	60.7	0.410	37.26	0.012	b.d	NA	0.414	0.16	NA	99.0
24	60.5	0.286	37.17	0.015	b.d	NA	0.412	0.03	NA	98.4
24	60.4	0.315	37.72	0.013	b.d	NA	0.416	0.13	NA	99.1
AVG	**60.4**	**0.346**	**37.42**	**0.016**			**0.413**	**0.11**		**98.8**
STDEV	**0.1**	**0.039**	**0.30**	**0.006**			**0.003**	**0.05**		**0.3**
25	59.6	0.459	35.39	0.044	b.d	NA	0.359	0.15	NA	96.0
25	59.8	0.359	36.33	0.037	b.d	NA	0.378	0.01	NA	96.9
25	59.3	0.132	36.70	0.041	b.d	NA	0.369	0.11	NA	97.3
25	60.2	0.313	36.93	0.032	b.d	NA	0.360	0.10	NA	98.0
25	59.6	0.272	36.85	0.041	b.d	NA	0.374	0.09	NA	97.2
AVG	**59.8**	**0.307**	**36.44**	**0.039**			**0.368**	**0.09**		**97.1**
STDEV	**0.2**	**0.108**	**0.57**	**0.004**			**0.008**	**0.04**		**0.6**
27	59.5	0.416	39.99	0.046	b.d	0.08	0.203	0.09	b.d	100.4
27	59.8	0.392	40.06	0.030	b.d	0.10	0.188	0.02	b.d	100.6
27	59.4	0.255	39.96	0.050	b.d	0.09	0.200	0.19	b.d	100.1
27	60.1	0.166	40.48	0.040	b.d	0.08	0.200	0.02	b.d	101.1
27	57.2	0.408	36.11	0.028	b.d	0.09	0.207	0.05	b.d	94.1
27	59.9	0.174	40.75	0.030	b.d	0.11	0.213	0.03	b.d	101.2
27	59.2	0.261	41.10	0.043	b.d	0.07	0.203	b.d	b.d	100.9
27	60.5	0.456	40.10	0.034	b.d	0.10	0.345	b.d	b.d	101.5
27	59.7	0.201	38.75	0.036	b.d	0.07	0.334	0.06	b.d	99.1
27	60.8	0.311	40.26	0.022	b.d	0.14	0.339	0.13	b.d	102.0
27	59.8	0.214	39.81	0.029	b.d	0.08	0.322	0.02	b.d	100.3
27	59.4	0.309	38.16	0.024	b.d	NA	0.207	NA	NA	98.1
27	59.5	0.393	37.97	0.027	b.d	NA	0.199	NA	NA	98.1
27	59.7	0.305	38.20	0.035	b.d	NA	0.196	NA	NA	98.5
27	59.3	0.229	38.14	0.034	b.d	NA	0.246	NA	NA	98.0
AVG	**59.6**	**0.299**	**39.32**	**0.034**		**0.09**	**0.240**	**0.06**		**99.6**
STDEV	**0.7**	**0.095**	**1.37**	**0.008**		**0.02**	**0.061**	**0.06**		**2.0**
28	60.0	0.338	38.04	0.049	b.d	NA	0.303	0.09	NA	98.8
28	59.6	0.216	38.20	0.057	b.d	NA	0.304	0.09	NA	98.4
28	59.6	0.350	37.95	0.025	b.d	NA	0.307	0.17	NA	98.4
28	59.9	0.155	37.79	0.053	b.d	NA	0.296	0.25	NA	98.4
28	59.8	0.223	37.64	0.043	b.d	NA	0.305	b.d	NA	98.0
28	62.4	0.335	38.31	0.047	b.d	NA	0.337	NA	b.d	101.5
28	62.6	0.250	38.01	0.049	b.d	NA	0.315	NA	b.d	101.3
28	62.3	0.219	37.73	0.068	b.d	NA	0.322	NA	b.d	100.7

	Fe	Ag	S	Mn	Si	Pb	Cu	Zn	Au	Total
28	62.3	0.274	38.42	0.065	b.d	NA	0.321	NA	b.d	101.4
28	62.8	0.186	39.06	0.055	b.d	NA	0.394	NA	b.d	102.5
28	62.5	0.093	39.07	0.036	b.d	NA	0.387	NA	b.d	102.1
AVG	**61.3**	**0.240**	**38.20**	**0.050**			**0.326**	**0.12**		**100.2**
STDEV	**1.4**	**0.080**	**0.49**	**0.012**			**0.034**	**0.09**		**1.7**
29	60.0	0.141	38.43	0.032	b.d	0.05	0.439	0.06	b.d	99.2
29	59.6	0.145	38.54	0.024	b.d	0.10	0.447	0.16	b.d	99.0
29	60.8	0.241	40.22	0.037	b.d	0.12	0.446	0.05	b.d	102.0
29	60.7	0.363	39.91	0.024	b.d	0.12	0.467	0.04	b.d	101.7
29	60.5	0.429	39.97	0.018	b.d	0.07	0.453	0.25	b.d	101.8
29	60.6	0.175	39.65	0.019	b.d	0.09	0.443	0.14	b.d	101.1
29	60.8	0.169	39.91	0.024	b.d	0.06	0.447	0.17	b.d	101.6
29	58.8	0.303	39.13	0.043	b.d	0.12	0.453	0.07	b.d	99.0
29	59.1	0.275	38.88	0.036	b.d	0.10	0.456	0.06	b.d	99.0
29	58.6	0.335	39.44	0.050	b.d	0.09	0.459	0.14	b.d	99.1
AVG	**59.9**	**0.258**	**39.41**	**0.031**		**0.09**	**0.451**	**0.12**		**100.4**
STDEV	**0.8**	**0.100**	**0.63**	**0.011**		**0.02**	**0.008**	**0.07**		**1.4**
30	59.7	0.262	38.61	0.018	b.d	NA	0.520	NA	NA	99.1
30	59.5	0.346	38.10	0.032	b.d	NA	0.516	NA	NA	98.5
30	60.2	0.220	38.49	0.029	b.d	NA	0.510	NA	NA	99.6
30	60.2	0.264	38.39	0.020	b.d	NA	0.478	NA	NA	99.4
30	60.4	0.266	37.49	0.031	b.d	NA	0.474	NA	NA	98.7
30	56.6	0.362	37.39	0.034	b.d	0.07	0.500	0.15	b.d	95.2
30	59.7	0.404	39.39	0.019	b.d	0.09	0.497	0.17	b.d	100.3
30	60.0	0.313	38.80	0.030	b.d	0.11	0.475	0.07	b.d	99.9
30	59.8	0.323	39.46	0.045	b.d	0.09	0.471	0.11	b.d	100.3
30	60.4	0.246	40.88	0.018	b.d	0.08	0.456	b.d	b.d	102.1
30	59.3	0.230	39.41	0.012	b.d	0.07	0.471	0.10	b.d	99.6
30	59.8	0.432	38.63	0.013	b.d	0.07	0.486	0.18	b.d	99.7
30	60.1	0.571	38.47	0.020	b.d	0.08	0.482	0.11	b.d	99.9
30	60.2	0.187	38.37	0.020	b.d	0.09	0.471	0.05	b.d	99.5
30	59.9	0.286	39.57	0.031	b.d	0.12	0.456	0.06	b.d	100.5
30	60.0	0.445	38.21	0.018	b.d	0.10	0.462	b.d	b.d	99.3
AVG	**59.7**	**0.322**	**38.73**	**0.024**		**0.09**	**0.483**	**0.10**		**99.5**
STDEV	**0.8**	**0.101**	**0.86**	**0.009**		**0.02**	**0.020**	**0.06**		**1.4**
31	60.5	0.391	39.54	0.044	b.d	0.12	0.438	0.12	b.d	101.2
31	60.4	0.393	39.03	0.040	b.d	0.10	0.431	0.21	b.d	100.7
31	60.7	0.414	39.17	0.029	b.d	0.12	0.442	0.06	b.d	101.0
31	60.4	0.404	39.25	0.026	b.d	0.10	0.437	0.07	b.d	100.8
31	60.5	0.365	39.02	0.039	b.d	0.12	0.428	0.07	b.d	100.6
31	60.4	0.384	39.36	0.034	b.d	0.09	0.499	0.18	b.d	100.4

	Fe	Ag	S	Mn	Si	Pb	Cu	Zn	Au	101.0
31	60.3	0.190	39.05	0.019	b.d	0.13	0.489	0.07	b.d	100.3
31	60.6	0.239	39.60	0.020	b.d	0.11	0.496	0.06	b.d	101.2
31	60.1	0.292	38.64	0.027	b.d	NA	0.324	NA	NA	99.4
31	59.9	0.355	38.27	0.021	b.d	NA	0.323	NA	NA	98.9
31	60.0	0.265	38.45	0.027	b.d		0.323			99.1
AVG	**60.4**	**0.336**	**39.03**	**0.030**		**0.11**	**0.421**	**0.11**		**100.4**
STDEV	**0.26**	**0.076**	**0.43**	**0.009**		**0.01**	**0.068**	**0.06**		**0.8**
34	60.2	0.466	37.08	0.306	b.d	NA	0.160	0.09	NA	98.3
34	60.5	0.323	37.06	0.302	b.d	NA	0.153	0.14	NA	98.5
34	60.1	0.269	39.04	0.300	b.d	NA	0.154	0.18	NA	100.1
34	60.8	0.108	38.96	0.315	b.d	NA	0.154	0.01	NA	100.4
34	59.0	0.236	35.58	0.292	b.d	NA	0.147	0.17	NA	95.5
34	60.7	0.068	40.04	0.066	b.d	0.08	0.223	0.10	b.d	101.3
34	60.7	0.050	39.52	0.084	b.d	0.06	0.225	b.d	b.d	100.7
34	61.2	0.066	39.90	0.080	b.d	0.08	0.226	0.24	b.d	101.8
34	60.3	0.089	39.60	0.054	b.d	0.13	0.230	0.10	b.d	100.6
34	61.1	0.064	39.74	0.057	b.d	0.08	0.229	0.06	b.d	101.4
34	61.0	0.071	39.60	0.079	b.d	0.09	0.230	0.04	b.d	101.2
34	60.8	0.058	39.56	0.073	b.d	0.10	0.235	0.11	b.d	101.0
AVG	**60.5**	**0.156**	**38.81**	**0.167**		**0.09**	**0.197**	**0.11**		**100.1**
STDEV	**0.5**	**0.135**	**1.43**	**0.120**		**0.02**	**0.039**	**0.07**		**1.8**
35	59.4	0.619	39.85	0.434	b.d	NA	0.456	0.08	0.112	101.0
35	59.8	0.436	40.04	0.373	b.d	0.10	0.425	0.04	b.d	101.2
35	60.1	0.225	40.35	0.366	b.d	0.13	0.417	0.05	b.d	101.6
35	60.1	0.430	40.44	0.374	b.d	0.12	0.416	0.11	b.d	102.0
35	60.1	0.466	40.38	0.346	b.d	0.09	0.417	0.18	b.d	102.0
35	59.4	0.619	39.85	0.434	b.d	0.08	0.456	0.11	b.d	101.0
35	59.7	0.493	39.59	0.441	b.d	0.09	0.468	b.d	b.d	100.8
35	59.8	0.286	39.73	0.431	b.d	0.12	0.451	0.20	b.d	101.0
AVG	**59.8**	**0.447**	**40.03**	**0.400**		**0.11**	**0.438**	**0.11**		**101.3**
STDEV	**0.2**	**0.140**	**0.33**	**0.039**		**0.02**	**0.022**	**0.06**		**0.5**
36	60.2	0.270	40.19	0.300	b.d	0.08	0.410	0.14	b.d	101.6
36	60.1	0.355	40.16	0.282	b.d	0.08	0.403	0.05	b.d	101.5
36	59.5	0.422	40.28	0.310	b.d	0.10	0.410	0.09	b.d	101.1
36	60.2	0.332	40.39	0.308	b.d	0.07	0.401	0.13	b.d	101.9
36	59.9	0.425	40.48	0.298	b.d	0.09	0.410	0.13	b.d	101.8
AVG	**60.0**	**0.361**	**40.30**	**0.300**		**0.08**	**0.407**	**0.11**		**101.6**
STDEV	**0.3**	**0.065**	**0.14**	**0.011**		**0.01**	**0.005**	**0.04**		**0.3**
37	59.5	0.949	38.74	0.298	NA	NA	0.394	0.09	0.149	100.2
37	60.3	0.123	39.27	0.319	b.d	0.09	0.367	0.13	b.d	100.7
37	59.8	0.341	39.46	0.316	b.d	0.08	0.371	0.04	b.d	100.5
37	59.7	0.167	39.37	0.319	b.d	0.08	0.361	0.15	0.009	100.2
37	60.7	0.355	40.52	0.280	b.d	0.08	0.391	0.53	b.d	102.3
37	60.1	0.847	40.68	0.276	b.d	0.11	0.392	0.36	b.d	102.7

	Fe	Ag	S	Mn	Si	Pb	Cu	Zn	Au	Total
37	60.1	0.279	40.71	0.269	b.d	0.10	0.395	0.40	b.d	102.3
37	60.1	0.321	40.53	0.245	b.d	0.08	0.387	0.49	b.d	102.2
37	60.3	0.480	40.55	0.269	b.d	0.06	0.397	0.30	b.d	102.4
37	60.1	0.376	40.57	0.256	b.d	0.10	0.391	0.23	b.d	102.1
AVG	**60.1**	**0.365**	**40.18**	**0.283**		**0.09**	**0.384**	**0.30**		**101.7**
STDEV	**0.2**	**0.210**	**0.62**	**0.028**		**0.01**	**0.014**	**0.17**		**0.9**
38	59.6	0.437	38.21	0.278	b.d	0.07	0.443	0.03	b.d	99.17
38	60.6	0.419	39.27	0.264	b.d	0.06	0.451	0.16	b.d	101.3
38	60.6	0.276	39.38	0.279	b.d	0.13	0.439	0.15	b.d	101.3
38	60.6	0.296	39.29	0.285	b.d	0.14	0.439	0.20	b.d	101.2
38	60.5	0.296	40.03	0.291	b.d	0.12	0.409	0.17	b.d	101.8
38	61.2	0.176	39.66	0.325	b.d	0.09	0.393	b.d	0.036	101.9
38	60.8	0.138	39.88	0.294	b.d	0.11	0.408	0.13	b.d	101.7
38	60.9	0.267	39.51	0.315	b.d	0.13	0.394	0.18	b.d	101.7
38	60.7	0.142	39.20	0.361	b.d	0.10	0.395	0.15	b.d	101.1
38	60.7	0.238	39.35	0.366	b.d	0.08	0.399	0.05	b.d	101.2
38	60.9	0.379	38.58	0.371	b.d	0.08	0.397	0.07	0.003	100.7
38	61.1	0.257	39.19	0.383	b.d	0.09	0.385	0.16	b.d	101.6
38	59.9	0.195	38.88	0.272	b.d	0.10	0.837	0.11	b.d	100.3
38	60.0	0.181	38.79	0.280	b.d	0.09	0.831	0.10	0.026	100.3
38	60.1	0.187	38.57	0.288	b.d	0.07	0.826	0.09	b.d	100.1
38	60.3	0.140	39.06	0.269	b.d	0.09	0.785	0.10	b.d	100.8
AVG	**60.5**	**0.252**	**39.18**	**0.308**		**0.10**	**0.514**	**0.13**	**0.022**	**101.1**
STDEV	**0.4**	**0.096**	**0.49**	**0.041**		**0.02**	**0.184**	**0.05**	**0.017**	**0.7**
40	59.5	0.315	37.93	0.320	b.d	0.10	0.407	0.15	b.d	98.7
40	59.4	0.225	37.82	0.337	b.d	0.10	0.417	0.06	b.d	98.4
40	59.7	0.251	37.86	0.330	b.d	0.09	0.405	0.11	b.d	98.7
40	59.4	0.464	37.68	0.321	b.d	0.09	0.421	0.11	b.d	98.5
40	60.3	0.363	40.13	0.318	b.d	0.38	0.090	0.01	b.d	101.6
40	60.2	0.188	40.28	0.319	b.d	0.39	0.097	0.12	b.d	101.7
40	60.1	0.375	39.92	0.316	b.d	0.39	0.053	0.10	b.d	101.3
40	60.3	0.361	40.02	0.317	b.d	0.38	0.083	0.15	b.d	101.7
40	59.7	0.290	39.84	0.287	b.d	0.37	0.091	0.11	b.d	100.8
40	60.2	0.528	39.77	0.320	b.d	0.40	0.087	0.21	0.037	101.6
40	59.9	0.355	39.98	0.313	b.d	0.39	0.119	b.d	b.d	101.0
40	60.0	0.227	39.82	0.363	b.d	0.40	0.098	0.08	b.d	101.0
40	60.2	0.167	40.29	0.335	b.d	0.39	0.105	0.13	b.d	101.6
AVG	**59.9**	**0.316**	**39.33**	**0.323**		**0.30**	**0.190**	**0.12**	**0.014**	**100.5**
STDEV	**0.3**	**0.106**	**1.06**	**0.017**		**0.14**	**0.155**	**0.05**	**0.016**	**1.3**
44	59.5	0.151	38.61	0.566	b.d	0.06	0.582	0.00	0.196	99.8
44	58.6	0.359	37.50	0.583	b.d	0.12	0.589	0.10	0.198	98.1
44	59.9	0.113	38.98	0.229	b.d	0.08	0.510	0.11	b.d	100.0
44	59.6	0.058	37.83	0.158	b.d	0.09	0.490	b.d	b.d	98.2
44	60.2	0.127	38.24	0.071	b.d	0.13	0.441	0.08	b.d	99.30
44	59.7	0.045	37.65	0.069	b.d	0.12	0.422	0.00	b.d	98.0
44	59.8	0.115	36.66	0.040	b.d	0.09	0.132	0.10	b.d	97.0

	Fe	Ag	S	Mn	Si	Pb	Cu	Zn	Au	Total
44	59.6	0.147	38.92	0.252	b.d	0.09	0.467	0.20	b.d	99.7
44	59.8	0.142	39.00	0.251	b.d	0.09	0.448	0.09	b.d	99.9
44	60.2	0.189	38.79	0.277	b.d	0.07	0.457	0.16	b.d	100.2
44	59.2	0.295	38.62	0.262	b.d	0.10	0.457	0.22	b.d	99.2
44	59.8	0.189	38.38	0.267	b.d	0.16	0.457	0.06	b.d	99.3
44	59.8	0.234	38.30	0.265	b.d	0.08	0.457	0.11	b.d	99.3
44	60.3	0.172	38.84	0.249	b.d	0.12	0.434	0.11	b.d	100.2
44	60.1	0.166	38.72	0.251	b.d	0.08	0.445	0.08	b.d	99.9
44	60.1	0.210	38.72	0.227	b.d	0.09	0.443	0.06	b.d	99.9
44	60.2	0.155	38.84	0.238	b.d	0.12	0.437	0.10	0.062	100.2
44	60.3	0.127	38.84	0.254	b.d	0.12	0.438	0.11	b.d	100.3
44	59.8	0.080	38.43	0.245	b.d	0.11	0.436	0.14	b.d	99.3
44	60.2	0.172	38.75	0.256	b.d	0.06	0.436	0.14	b.d	100.0
44	60.0	0.134	38.54	0.268	b.d	0.09	0.436	0.10	b.d	99.6
44	60.1	0.173	38.79	0.244	b.d	0.09	0.451	0.14	b.d	100.1
44	59.8	0.194	38.39	0.280	b.d	0.11	0.454	0.19	b.d	99.5
44	58.9	0.186	38.50	0.265	b.d	0.10	0.457	0.16	0.037	98.7
44	59.9	0.146	38.76	0.272	b.d	0.08	0.455	0.12	b.d	99.8
44	60.4	0.183	38.97	0.282	b.d	0.06	0.451	0.17	b.d	100.6
44	59.4	0.185	39.01	0.266	b.d	0.06	0.453	0.16	b.d	99.6
44	59.8	0.173	38.51	0.364	b.d	0.07	0.423	b.d	b.d	99.4
44	59.5	0.332	38.34	0.376	b.d	0.10	0.418	0.16	b.d	99.3
44	59.6	0.141	38.36	0.383	b.d	0.10	0.431	0.06	b.d	99.2
44	59.7	0.464	38.31	0.397	b.d	0.08	0.428	0.12	b.d	99.5
44	59.9	0.272	38.26	0.338	b.d	0.09	0.426	0.08	b.d	99.5
44	59.7	0.177	38.25	0.331	b.d	0.10	0.429	0.12	b.d	99.2
44	59.1	0.232	39.14	0.351	b.d	0.06	0.420	0.16	b.d	99.5
44	59.7	0.459	38.15	0.363	b.d	0.08	0.410	0.15	b.d	99.4
AVG	**59.8**	**0.191**	**38.48**	**0.280**		**0.09**	**0.443**	**0.12**		**99.5**
STDEV	**0.4**	**0.095**	**0.49**	**0.110**		**0.02**	**0.066**	**0.05**		**0.7**
45	59.9	0.277	38.90	0.608	b.d	0.09	0.388	0.03	b.d	100.2
45	59.8	0.257	38.88	0.607	b.d	0.10	0.401	0.10	b.d	100.1
45	59.3	0.249	38.93	0.600	b.d	0.08	0.399	0.14	b.d	99.7
45	59.1	0.342	38.38	0.599	b.d	0.09	0.391	0.11	b.d	99.0
45	59.7	0.311	38.69	0.624	b.d	0.09	0.397	0.13	b.d	99.9
45	59.9	0.422	38.71	0.584	b.d	0.11	0.393	0.03	b.d	100.2
45	59.7	0.142	38.68	0.311	b.d	0.11	0.353	0.05	b.d	99.4
45	60.0	0.206	38.55	0.324	b.d	0.09	0.346	0.14	b.d	99.7
45	60.4	0.202	38.92	0.342	b.d	0.08	0.351	0.08	b.d	100.5
45	59.8	0.216	39.39	0.325	b.d	0.08	0.330	0.12	b.d	100.3
45	59.9	0.333	39.29	0.419	b.d	0.07	0.367	0.09	b.d	100.5
45	60.0	0.408	39.31	0.423	b.d	0.10	0.365	0.06	b.d	100.7
45	59.4	0.247	39.19	0.471	b.d	0.09	0.352	0.18	b.d	99.9
AVG	**59.8**	**0.278**	**38.91**	**0.480**		**0.09**	**0.372**	**0.10**		**100.0**
STDEV	**0.3**	**0.082**	**0.31**	**0.128**		**0.01**	**0.024**	**0.05**		**0.4**
46	60.0	0.243	38.77	0.369	b.d	0.10	0.353	0.04	b.d	99.9
46	60.5	0.218	38.92	0.358	b.d	0.04	0.359	0.11	b.d	100.6

	Fe	Ag	S	Mn	Si	Pb	Cu	Zn	Au	Total
46	60.2	0.241	38.61	0.386	b.d	0.08	0.370	0.13	b.d	100.0
46	60.4	0.284	37.43	0.219	b.d	0.08	0.399	0.03	b.d	98.8
46	60.6	0.168	37.59	0.256	b.d	0.10	0.384	0.15	b.d	99.
46	60.4	0.294	37.59	0.213	b.d	0.07	0.399	0.11	b.d	99.1
46	60.4	0.195	37.88	0.239	b.d	0.08	0.404	0.07	b.d	99.3
46	60.5	0.198	37.79	0.239	b.d	0.08	0.412	0.16	b.d	99.4
46	60.2	0.508	37.00	0.259	b.d	0.10	0.407	0.21	b.d	98.7
46	59.9	0.074	39.32	0.058	b.d	0.06	0.403	0.04	0.083	100.0
46	60.3	0.076	39.73	0.082	b.d	0.09	0.402	0.12	0.080	100.9
46	58.6	0.039	38.88	0.061	b.d	0.06	0.368	0.10	0.165	98.3
46	59.7	0.115	39.88	0.037	b.d	0.09	0.358	0.07	0.232	100.6
AVG	**60.1**	**0.204**	**38.41**	**0.214**		**0.09**	**0.386**	**0.10**	**0.140**	**99.6**
STDEV	**0.5**	**0.122**	**0.93**	**0.121**		**0.02**	**0.021**	**0.05**	**0.073**	**0.8**
47	59.3	0.218	37.78	0.687	b.d	0.06	0.515	0.10	b.d	98.7
47	59.4	0.343	37.54	0.639	b.d	0.05	0.539	0.11	b.d	98.6
47	59.5	0.375	37.74	0.656	b.d	0.09	0.544	0.08	0.023	99.1
AVG	**59.4**	**0.312**	**37.68**	**0.660**		**0.07**	**0.532**	**0.10**	**0.023**	**98.8**
STDEV	**0.11**	**0.083**	**0.12**	**0.025**		**0.02**	**0.016**	**0.01**		**0.2**
48	58.7	0.597	37.43	0.399	b.d	0.08	0.652	0.14	b.d	98.1
48	58.7	0.271	36.96	0.405	b.d	0.12	0.644	0.13	0.030	97.3
48	59.4	0.269	37.61	0.410	b.d	0.08	0.660	0.16	b.d	98.7
48	59.0	0.428	37.57	0.401	b.d	0.06	0.646	0.21	b.d	98.3
48	59.2	0.250	37.77	0.366	b.d	0.09	0.629	0.10	b.d	98.5
48	59.3	0.311	37.70	0.354	b.d	0.07	0.643	0.12	0.020	98.6
48	59.0	0.302	37.18	0.353	b.d	0.07	0.633	0.24	b.d	97.9
48	59.2	0.311	37.46	0.370	b.d	0.08	0.659	0.13	b.d	98.3
48	59.1	0.476	37.15	0.349	b.d	0.10	0.652	0.19	b.d	98.0
AVG	**59.1**	**0.357**	**37.43**	**0.379**		**0.09**	**0.646**	**0.16**	**0.025**	**98.2**
STDEV	**0.2**	**0.117**	**0.28**	**0.025**		**0.02**	**0.011**	**0.04**	**0.007**	**0.4**
49	56.4	0.141	37.54	0.328	b.d	b.d	0.594	0.08	1.918	97.0
49	56.9	0.078	38.00	0.332	b.d	b.d	0.608	0.11	1.380	97.4
49	57.8	0.084	36.74	0.373	b.d	0.07	0.621	0.08	0.439	96.3
49	59.5	0.057	38.09	0.337	b.d	0.13	0.413	0.13	b.d	98.7
49	59.2	0.068	37.96	0.333	b.d	0.10	0.404	0.12	b.d	98.2
49	59.6	0.062	38.31	0.325	b.d	0.09	0.402	0.15	b.d	99.0
49	59.8	0.062	37.79	0.338	b.d	0.10	0.426	0.16	b.d	98.8
AVG	**58.4**	**0.079**	**37.78**	**0.338**		**0.10**	**0.495**	**0.12**	**0.534**	**97.9**
STDEV	**1.4**	**0.029**	**0.52**	**0.016**		**0.02**	**0.105**	**0.03**	**0.794**	**1.0**
50	58.6	0.376	37.73	0.306	b.d	0.08	0.876	0.11	0.024	98.3
50	59.3	0.353	39.00	0.344	b.d	0.08	0.820	b.d	b.d	100.0
50	58.8	0.093	38.90	0.437	b.d	0.07	0.742	0.03	0.560	99.6
50	59.3	0.145	38.69	0.414	b.d	0.10	0.753	0.07	0.157	99.7
50	59.4	0.082	39.02	0.320	b.d	0.13	0.870	0.22	b.d	100.1
50	58.5	0.076	37.33	0.294	b.d	0.08	0.864	0.10	b.d	97.2

	Fe	Ag	S	Mn	Si	Pb	Cu	Zn	Au	Total
50	59.1	0.053	38.16	0.308	b.d	0.11	0.824	0.14	b.d	98.7
50	59.1	0.062	37.65	0.332	b.d	0.08	0.828	0.10	b.d	98.2
50	58.7	0.073	37.01	0.282	b.d	0.08	0.886	0.05	b.d	97.0
50	59.6	0.056	40.00	0.283	b.d	0.08	0.851	0.19	b.d	101.1
50	57.9	0.059	35.98	0.298	b.d	0.10	0.839	0.25	b.d	95.4
50	57.9	0.044	40.18	0.300	b.d	0.09	0.859	0.16	b.d	99.5
50	59.4	0.121	38.55	0.370	b.d	0.06	0.718	0.05	b.d	99.3
50	59.4	0.129	38.54	0.360	b.d	0.08	0.766	0.07	b.d	99.4
50	59.1	0.157	38.28	0.368	b.d	0.08	0.771	0.07	b.d	98.9
50	59.3	0.191	38.32	0.388	b.d	0.08	0.763	0.00	b.d	99.1
50	59.5	0.156	38.44	0.397	b.d	0.09	0.770	0.12	b.d	99.5
AVG	**59.0**	**0.131**	**38.34**	**0.341**		**0.09**	**0.812**	**0.11**		**98.9**
STDEV	**0.5**	**0.098**	**1.02**	**0.048**		**0.02**	**0.054**	**0.07**		**1.3**
51	59.8	0.137	38.05	0.283	b.d	0.08	1.383	b.d	b.d	99.7
51	59.7	0.397	38.16	0.285	b.d	0.09	1.432	0.17	b.d	100.2
51	59.5	0.224	38.18	0.286	b.d	0.13	1.389	0.06	b.d	99.8
51	59.3	0.321	38.19	0.296	b.d	0.09	1.429	0.02	b.d	99.8
51	60.2	0.239	38.33	0.272	b.d	0.07	1.411	0.02	b.d	100.6
51	58.1	0.322	37.26	0.387	b.d	0.09	2.747	0.08	b.d	99.0
51	58.3	0.254	37.53	0.357	b.d	0.11	2.586	0.02	b.d	99.2
51	58.2	0.259	37.51	0.379	b.d	0.08	2.746	0.12	b.d	99.4
51	59.9	0.165	37.90	0.142	b.d	0.09	1.019	0.04	b.d	99.3
51	60.2	0.406	37.86	0.133	b.d	0.06	1.069	b.d	b.d	99.8
51	59.7	0.236	37.82	0.139	b.d	0.11	1.056	0.13	b.d	99.2
51	59.1	0.099	38.18	0.472	b.d	0.07	2.196	0.07	0.022	100.2
51	58.8	0.161	38.08	0.440	b.d	0.08	2.582	0.02	0.042	100.3
51	58.5	0.159	37.82	0.430	b.d	0.07	2.496	0.10	0.095	99.7
51	59.8	0.124	38.68	0.435	b.d	0.13	2.132	0.14	0.162	101.2
51	58.5	0.203	38.10	0.435	b.d	0.08	2.704	0.15	0.267	100.5
51	58.4	0.146	37.49	0.428	b.d	0.09	2.668	0.15	0.743	100.1
51	58.7	0.161	37.89	0.437	b.d	0.13	2.456	0.11	0.174	100.1
51	58.5	0.303	38.06	0.401	b.d	0.10	2.665	0.06	0.233	100.3
51	58.6	0.203	38.00	0.430	b.d	0.08	2.746	0.12	0.069	100.3
AVG	**59.1**	**0.226**	**37.96**	**0.343**		**0.09**	**2.046**	**0.09**	**0.155**	**99.9**
STDEV	**0.7**	**0.088**	**0.33**	**0.109**		**0.02**	**0.676**	**0.05**	**0.205**	**0.5**
52	61.0	0.014	38.83	0.137	b.d	0.10	0.412	0.07	b.d	100.6
52	61.5	0.011	38.63	0.120	b.d	0.10	0.435	0.03	b.d	100.8
52	61.3	0.019	38.91	0.138	b.d	0.09	0.422	0.13	b.d	101.0
52	60.8	0.079	38.72	0.139	b.d	0.09	0.680	0.10	b.d	100.6
52	60.9	0.073	38.61	0.165	b.d	0.07	0.692	0.06	b.d	100.6
52	60.7	0.077	38.76	0.159	b.d	0.07	0.632	0.10	b.d	100.6
52	60.6	0.091	38.51	0.158	b.d	0.09	0.661	0.11	b.d	100.3
52	60.6	0.070	38.88	0.162	b.d	0.11	0.667	0.16	b.d	100.7
52	60.6	0.098	38.23	0.169	b.d	0.09	0.671	0.16	b.d	100.0
52	60.8	0.071	38.37	0.153	b.d	0.11	0.673	0.19	b.d	100.4
52	60.8	0.079	38.85	0.168	b.d	0.08	0.652	0.00	b.d	100.7
52	61.1	0.052	38.81	0.155	b.d	0.08	0.586	0.08	b.d	100.9

	Fe	Ag	S	Mn	Si	Pb	Cu	Zn	Au	Total
52	61.1	0.057	38.74	0.162	b.d	0.06	0.588	0.08	b.d	100.8
52	61.0	0.061	38.79	0.158	b.d	0.11	0.597	0.22	b.d	101.0
52	60.6	0.053	38.74	0.152	b.d	0.11	0.590	0.23	b.d	100.6
52	60.7	0.006	38.20	0.121	b.d	0.05	0.426	0.18	0.070	99.8
52	60.9	0.007	39.10	0.145	b.d	0.08	0.425	0.12	0.041	100.9
52	57.6	bd	39.91	0.103	b.d	0.06	0.423	0.05	b.d	98.2
52	60.7	0.007	38.04	0.116	b.d	0.09	0.421	0.09	b.d	99.5
52	60.3	0.009	39.26	0.113	b.d	0.10	0.432	0.20	b.d	100.5
52	59.0	0.005	39.89	0.119	b.d	0.05	0.413	0.03	b.d	100.3
AVG	**60.6**	**0.047**	**38.80**	**0.143**		**0.09**	**0.547**	**0.11**	**0.021**	**100.4**
STDEV	**0.7**	**0.033**	**0.47**	**0.021**		**0.02**	**0.114**	**0.07**	**0.025**	**0.6**
53	61.0	0.422	39.64	0.381	b.d	0.09	0.056	0.11	0.021	101.8
53	60.9	0.390	39.19	0.375	b.d	0.13	0.058	bd	b.d	101.1
53	61.0	0.397	39.25	0.406	b.d	0.07	0.051	0.09	b.d	101.3
53	60.6	0.331	38.42	0.111	b.d	0.10	0.469	0.13	0.013	100.4
53	60.9	0.214	39.05	0.144	b.d	0.08	0.466	0.09	b.d	101.0
53	60.9	0.306	38.87	0.125	b.d	0.10	0.448	0.09	b.d	100.9
53	60.0	0.398	38.63	0.112	b.d	0.08	0.454	0.09	b.d	100.2
53	61.3	0.387	39.51	0.372	b.d	0.09	0.058	0.16	b.d	101.9
53	60.8	0.577	39.23	0.402	b.d	0.09	0.053	0.01	b.d	101.2
53	60.5	0.406	39.20	0.402	b.d	0.09	0.052	0.00	b.d	100.6
53	61.1	0.005	39.51	0.154	b.d	0.07	0.515	0.21	b.d	101.7
53	61.1	0.012	39.07	0.126	b.d	0.07	0.512	0.14	b.d	101.1
53	60.9	0.008	39.40	0.128	b.d	0.11	0.507	0.09	b.d	101.2
AVG	**60.9**	**0.296**	**39.15**	**0.249**		**0.09**	**0.285**	**0.10**		**101.1**
STDEV	**0.2**	**0.183**	**0.35**	**0.136**		**0.02**	**0.223**	**0.06**		**0.4**
54	57.9	0.057	38.50	0.140	b.d	0.10	3.388	0.10	b.d	100.3
54	58.4	0.059	38.97	0.131	b.d	0.08	3.206	0.11	b.d	101.0
54	58.5	0.058	39.89	0.155	b.d	0.12	3.200	0.04	b.d	101.0
54	58.5	0.043	38.86	0.145	b.d	0.08	3.031	0.04	b.d	100.8
54	58.6	0.052	38.84	0.151	b.d	0.08	3.126	0.02	b.d	100.9
54	58.8	0.044	39.27	0.152	b.d	0.07	2.826	0.11	b.d	101.3
54	58.8	0.055	39.20	0.141	b.d	0.06	3.177	0.05	b.d	101.5
54	59.3	0.047	38.77	0.147	b.d	0.09	2.963	0.01	0.031	101.4
54	60.6	0.026	39.33	0.122	b.d	0.06	0.427	0.18	b.d	100.8
54	60.8	0.015	39.80	0.119	b.d	0.09	0.415	0.05	b.d	101.3
54	61.1	0.025	39.87	0.131	b.d	0.06	0.417	0.00	b.d	101.6
54	61.1	0.027	39.61	0.120	b.d	0.09	0.422	0.07	b.d	101.5
AVG	**59.4**	**0.042**	**39.24**	**0.138**		**0.08**	**2.217**	**0.07**		**101.2**
STDEV	**1.2**	**0.015**	**0.47**	**0.013**		**0.02**	**1.334**	**0.05**		**0.4**
55	60.7	0.184	37.03	0.077	b.d	0.07	0.161	0.11	b.d	98.4
55	60.4	0.371	36.87	0.069	b.d	0.09	0.162	0.13	b.d	98.2
55	60.6	0.192	36.60	0.049	b.d	0.10	0.155	0.08	b.d	97.8
55	60.0	0.317	36.47	0.054	b.d	0.09	0.145	0.17	b.d	97.2
55	60.9	0.309	36.70	0.073	b.d	0.07	0.148	0.03	b.d	98.3
55	60.9	0.116	36.68	0.063	b.d	0.08	0.160	0.06	b.d	98.1

	Fe	Ag	S	Mn	Si	Pb	Cu	Zn	Au	Total
55	60.0	0.166	36.44	0.311	b.d	0.12	0.576	0.25	b.d	97.9
55	59.8	0.182	36.43	0.356	b.d	0.11	0.578	0.13	b.d	97.7
55	60.1	0.121	36.01	0.308	b.d	0.09	0.568	0.16	b.d	97.4
55	60.1	0.301	37.91	0.277	b.d	0.05	0.255	0.12	b.d	99.1
55	60.0	0.289	38.01	0.286	b.d	0.13	0.268	0.08	b.d	99.1
55	60.4	0.215	37.93	0.288	b.d	0.10	0.255	0.14	b.d	99.4
55	59.9	0.352	37.96	0.281	b.d	0.11	0.261	0.11	b.d	99.1
55	60.3	0.344	37.97	0.288	b.d	0.10	0.261	0.07	b.d	99.4
55	59.6	0.151	37.31	0.342	b.d	0.09	0.276	0.10	1.125	99.0
55	59.9	0.193	37.25	0.306	b.d	0.07	0.270	0.18	0.617	98.8
55	59.6	0.258	37.15	0.311	b.d	0.11	0.248	0.05	0.597	98.3
55	60.0	0.159	37.27	0.333	b.d	0.11	0.269	0.17	0.249	98.6
55	59.3	0.122	37.46	0.281	b.d	0.11	0.520	0.09	0.796	98.8
55	59.4	0.211	37.40	0.288	b.d	0.09	0.513	0.00	0.513	98.5
55	59.2	0.203	37.32	0.275	b.d	0.06	0.512	0.14	0.508	98.3
55	60.2	0.190	37.32	0.292	b.d	0.11	0.520	0.07	b.d	98.7
AVG	**60.1**	**0.225**	**37.16**	**0.237**		**0.09**	**0.322**	**0.11**	**0.370**	**98.5**
STDEV	**0.5**	**0.079**	**0.58**	**0.110**		**0.02**	**0.160**	**0.06**	**0.379**	**0.6**
56	59.4	0.358	36.63	0.381	b.d	0.08	0.469	0.19	b.d	97.6
56	59.5	0.313	36.77	0.380	b.d	0.09	0.485	0.15	b.d	97.7
56	59.7	0.278	36.99	0.385	b.d	0.09	0.497	0.08	b.d	98.1
56	59.8	0.192	36.61	0.416	b.d	0.12	0.505	0.08	b.d	97.8
56	59.6	0.449	36.65	0.406	b.d	0.08	0.505	0.12	b.d	97.8
56	60.1	0.118	37.57	0.222	b.d	0.08	0.307	0.02	b.d	98.5
56	60.1	0.115	37.40	0.189	b.d	0.09	0.297	0.07	b.d	98.3
56	60.5	0.099	37.26	0.207	b.d	0.07	0.299	0.07	b.d	98.6
56	59.6	0.361	36.96	0.589	b.d	0.08	0.486	0.15	b.d	98.3
56	59.3	0.204	36.95	0.607	b.d	0.06	0.479	0.24	b.d	97.9
56	59.2	0.305	36.99	0.595	b.d	0.08	0.476	0.10	b.d	97.8
56	59.3	0.434	36.79	0.588	b.d	0.10	0.470	0.19	b.d	97.9
56	59.3	0.333	36.44	0.358	b.d	0.06	0.195	0.03	0.134	96.9
56	59.6	0.269	37.23	0.358	b.d	0.09	0.195	0.22	0.163	98.2
56	59.5	0.287	36.81	0.363	b.d	0.11	0.195	0.09	0.121	97.5
56	60.3	0.103	37.12	0.396	b.d	0.09	0.481	0.07	b.d	98.6
56	60.2	0.098	37.07	0.392	b.d	0.08	0.483	0.06	b.d	98.4
56	60.1	0.367	37.03	0.388	b.d	0.11	0.487	0.12	b.d	98.6
56	59.6	0.426	36.92	0.408	b.d	0.08	0.490	0.12	b.d	98.1
AVG	**59.7**	**0.269**	**36.96**	**0.401**		**0.09**	**0.411**	**0.12**	**0.087**	**98.0**
STDEV	**0.3**	**0.120**	**0.28**	**0.123**		**0.02**	**0.118**	**0.06**	**0.073**	**0.4**
57	59.9	0.153	37.12	0.344	b.d	0.10	0.540	0.18	b.d	98.4
57	59.2	0.305	37.18	0.369	b.d	0.07	0.551	0.07	b.d	97.8
57	60.1	0.313	37.01	0.356	b.d	0.10	0.535	0.09	b.d	98.6
57	59.7	0.335	37.09	0.374	b.d	0.08	0.506	0.29	b.d	98.5
57	60.1	0.104	37.21	0.351	b.d	0.07	0.484	0.14	b.d	98.5
57	60.3	0.164	36.74	0.343	b.d	0.10	0.498	0.17	b.d	98.4
57	59.9	0.476	36.75	0.340	b.d	0.08	0.503	0.14	b.d	98.2
57	60.1	0.329	36.87	0.337	b.d	0.09	0.536	0.15	b.d	98.4

	Fe	Ag	S	Mn	Si	Pb	Cu	Zn	Au	Total
57	59.9	0.259	36.85	0.346	b.d	0.12	0.540	0.20	b.d	98.3
57	60.0	0.169	36.92	0.341	b.d	0.11	0.521	0.15	b.d	98.3
57	60.1	0.163	39.26	0.403	b.d	0.10	0.498	0.11	0.049	100.8
57	59.3	0.219	37.70	0.402	b.d	0.11	0.481	0.27	0.074	99.1
57	59.4	0.218	35.28	0.384	b.d	0.07	0.472	0.13	0.055	96.0
57	59.1	0.121	38.18	0.379	b.d	0.07	0.382	0.05	0.275	98.7
57	60.3	0.180	38.33	0.398	b.d	0.08	0.363	0.13	0.053	99.9
57	60.7	0.348	37.65	0.390	b.d	0.06	0.368	0.02	0.042	99.5
57	60.2	0.257	38.75	0.388	b.d	0.06	0.356	0.13	0.007	100.3
57	60.0	0.198	37.54	0.374	b.d	0.10	0.375	0.12	0.450	99.3
57	60.1	0.399	39.68	0.346	b.d	0.06	0.470	0.04	b.d	101.1
57	60.6	0.339	38.40	0.382	b.d	0.07	0.456	0.18	b.d	100.4
57	60.2	0.270	38.50	0.356	b.d	0.08	0.477	0.06	b.d	100.0
57	60.6	0.232	37.11	0.411	b.d	0.09	0.492	b.d	b.d	99.0
57	60.4	0.254	37.26	0.354	b.d	0.07	0.484	Bbd	b.d	98.9
57	60.2	0.411	36.82	0.389	b.d	0.07	0.502	0.09	b.d	98.6
57	60.3	0.260	37.00	0.381	b.d	0.08	0.491	0.10	b.d	98.7
57	59.9	0.362	36.85	0.345	b.d	0.11	0.500	0.20	b.d	98.3
57	61.5	b.d	37.52	b.d	b.d	0.11	0.004	bd	b.d	99.2
57	61.6	bd	37.39	0.004	b.d	0.08	b.d	bd	b.d	99.1
57	61.5	0.005	37.51	b.d	b.d	0.10	b.d	0.16	b.d	99.3
57	61.0	bd	37.31	0.003	b.d	0.10	b.d	0.04	b.d	98.5
57	60.1	0.126	39.26	0.403	b.d	0.10	0.498	0.11	0.047	100.7
57	59.4	0.169	35.28	0.384	b.d	0.07	0.472	0.13	0.053	96.0
AVG	**60.2**	**0.238**	**37.45**	**0.324**		**0.09**	**0.417**	**0.14**	**0.110**	**98.9**
STDEV	**0.6**	**0.113**	**0.98**	**0.126**		**0.02**	**0.168**	**0.06**	**0.140**	**1.1**
58	60.0	0.010	38.40	0.329	b.d	0.09	0.707	0.14	b.d	99.7
58	60.3	0.006	38.40	0.349	b.d	0.08	0.652	0.00	b.d	99.9
58	59.8	0.009	38.40	0.347	b.d	0.08	0.697	0.15	b.d	99.6
58	59.9	0.005	38.35	0.337	b.d	0.09	0.694	0.12	b.d	99.6
58	59.7	0.005	38.51	0.327	b.d	0.13	0.680	0.14	b.d	99.6
58	59.6	bd	38.53	0.352	b.d	0.10	0.701	0.18	b.d	99.5
58	59.9	0.012	38.80	0.268	b.d	0.08	0.655	0.15	b.d	100.0
58	59.8	bd	38.67	0.255	b.d	0.10	0.658	b.d	b.d	99.5
58	59.7	0.004	38.84	0.276	b.d	0.08	0.661	0.17	b.d	99.8
58	59.8	0.009	38.96	0.279	b.d	0.07	0.653	0.13	b.d	100.0
58	59.9	0.011	38.81	0.267	b.d	0.10	0.645	0.19	b.d	99.9
58	59.8	0.009	38.57	0.274	b.d	0.10	0.668	b.d	b.d	99.4
58	59.8	0.009	38.77	0.288	b.d	0.09	0.575	0.17	b.d	99.7
58	59.8	0.070	38.68	0.261	b.d	0.10	0.593	0.08	b.d	99.6
58	60.2	0.004	38.84	0.277	b.d	0.08	0.592	0.06	b.d	99.9
58	60.0	bd	38.87	0.270	b.d	0.09	0.589	0.05	b.d	99.9
58	59.8	bd	39.03	0.270	b.d	0.09	0.594	0.14	b.d	99.9
58	60.4	bd	39.16	0.280	b.d	0.11	0.623	0.21	b.d	100.8
AVG	**59.9**	**0.013**	**38.70**	**0.295**		**0.09**	**0.646**	**0.12**		**99.8**
STDEV	**0.2**	**0.017**	**0.24**	**0.034**		**0.01**	**0.043**	**0.07**		**0.3**

	Fe	Ag	S	Mn	Si	Pb	Cu	Zn	Au	Total
59	60.2	0.005	38.46	0.322	b.d	0.12	0.421	0.07	0.054	99.1
59	60.0	0.011	37.90	0.305	b.d	0.09	0.417	0.12	0.073	99.7
59	60.0	0.005	38.25	0.315	b.d	0.12	0.420	0.02	0.029	99.0
59	60.4	0.006	38.27	0.319	b.d	0.10	0.423	bd	b.d	99.2
59	59.8	0.011	38.49	0.334	b.d	0.08	0.415	0.10	b.d	99.6
59	59.9	0.010	37.86	0.163	b.d	0.08	0.632	0.12	b.d	99.3
59	59.9	0.009	38.25	0.132	b.d	0.09	0.626	0.00	b.d	98.9
59	59.6	0.004	38.14	0.145	b.d	0.07	0.637	0.06	0.055	99.0
59	59.3	bd	38.52	0.149	b.d	0.11	0.588	0.16	0.634	99.0
59	59.2	0.009	38.93	0.169	b.d	0.09	0.580	0.14	0.509	99.5
59	60.3	0.433	38.75	0.309	b.d	0.13	0.129	0.06	b.d	99.7
59	59.8	0.401	38.80	0.292	b.d	0.06	0.131	0.14	b.d	100.2
59	60.0	0.402	39.04	0.264	b.d	0.08	0.129	0.05	b.d	99.7
59	60.1	0.265	38.63	0.302	b.d	0.10	0.123	bd	b.d	100.0
59	59.7	0.434	38.92	0.287	b.d	0.06	0.123	0.05	b.d	99.6
59	60.3	0.023	38.37	0.186	b.d	0.07	0.329	0.21	b.d	99.7
59	60.8	0.018	38.64	0.213	b.d	0.06	0.328	0.08	b.d	99.5
59	60.5	0.016	38.40	0.207	b.d	0.09	0.323	0.02	b.d	99.6
59	60.6	0.023	38.01	0.197	b.d	0.11	0.315	0.10	b.d	99.6
59	59.6	0.070	38.74	0.059	b.d	0.08	1.463	0.15	b.d	99.5
59	59.6	0.065	39.07	0.050	b.d	0.09	1.468	0.13	b.d	100.2
59	59.3	0.077	38.84	0.058	b.d	0.08	1.392	0.06	b.d	100.5
59	59.6	0.065	38.84	0.053	b.d	0.07	1.456	bd	b.d	99.9
59	59.3	0.070	38.80	0.055	b.d	0.11	1.479	0.13	b.d	100.1
59	60.1	0.340	38.84	0.253	b.d	0.10	0.349	0.08	b.d	99.9
59	60.7	0.330	38.99	0.252	b.d	0.08	0.368	0.00	b.d	100.2
59	60.1	0.353	38.86	0.249	b.d	0.09	0.362	0.17	b.d	100.8
59	60.2	0.246	38.93	0.287	b.d	0.09	0.368	0.00	b.d	100.3
59	59.8	0.212	38.84	0.260	b.d	0.09	0.369	0.03	b.d	100.1
59	60.1	0.314	38.90	0.262	b.d	0.09	0.360	0.03	b.d	99.7
59	60.2	0.034	38.52	0.200	b.d	0.08	0.385	bd	b.d	100.1
59	60.3	0.033	38.93	0.198	b.d	0.10	0.395	0.13	b.d	99.5
59	60.5	0.032	38.83	0.216	b.d	0.08	0.385	0.00	b.d	100.1
59	59.9	0.027	38.91	0.238	b.d	0.08	0.392	0.11	b.d	100.1
59	60.1	0.030	39.01	0.212	b.d	0.10	0.380	0.05	b.d	99.8
59	59.9	0.031	39.23	0.210	b.d	0.08	0.390	0.14	b.d	99.9
AVG	**60.0**	**0.123**	**38.65**	**0.217**		**0.09**	**0.520**	**0.09**	**0.102**	**99.7**
STDEV	**0.3**	**0.152**	**0.35**	**0.085**		**0.02**	**0.396**	**0.06**	**0.195**	**0.4**
60	59.6	0.190	39.18	0.583	b.d	0.07	0.427	0.16	b.d	100.2
60	59.3	0.438	38.86	0.551	b.d	0.06	0.440	0.03	b.d	99.7
60	59.3	0.156	38.87	0.586	b.d	0.09	0.439	0.06	b.d	99.5
60	59.7	0.110	39.04	0.583	b.d	0.10	0.428	0.01	b.d	100.0
60	59.7	0.356	38.96	0.598	b.d	0.10	0.423	0.13	b.d	100.3
60	59.3	0.678	39.61	0.438	b.d	0.09	0.445	0.14	b.d	100.9
60	59.4	0.464	39.29	0.437	b.d	0.07	0.433	0.16	b.d	100.2
60	59.8	0.515	39.47	0.448	b.d	0.11	0.431	0.09	b.d	100.9
60	59.5	0.292	38.77	0.436	b.d	0.09	0.440	0.13	b.d	99.7
60	59.7	0.440	38.85	0.435	b.d	0.09	0.441	0.02	b.d	99.9

	Fe	Ag	S	Mn	Si	Pb	Cu	Zn	Au	Total
60	60.0	0.628	39.47	0.451	b.d	0.09	0.440	0.11	b.d	101.3
60	59.6	0.547	38.98	0.426	b.d	0.10	0.429	0.04	b.d	100.1
60	59.4	0.127	39.11	0.429	b.d	0.06	0.419	0.09	b.d	99.7
60	60.4	0.107	39.26	0.090	b.d	0.11	0.155	0.12	b.d	100.3
60	60.2	0.101	38.38	0.097	b.d	0.08	0.156	0.05	b.d	99.1
60	60.2	0.095	38.91	0.099	b.d	0.10	0.165	0.16	b.d	99.8
60	60.2	0.089	38.87	0.104	b.d	0.08	0.163	0.02	b.d	99.6
60	59.9	0.114	38.92	0.089	b.d	0.05	0.161	0.07	b.d	99.3
60	59.6	0.378	38.52	0.402	b.d	0.08	0.427	0.06	b.d	99.5
60	59.5	0.520	38.57	0.397	b.d	0.09	0.430	0.10	b.d	99.6
60	59.5	0.384	38.81	0.403	b.d	0.07	0.432	0.12	b.d	99.8
60	59.1	0.533	38.55	0.391	b.d	0.12	0.439	0.14	b.d	99.3
60	59.2	0.336	38.68	0.405	b.d	0.10	0.426	0.01	b.d	99.2
60	59.9	0.161	38.01	0.444	b.d	0.12	0.430	0.03	b.d	99.2
60	59.5	0.232	38.12	0.442	b.d	0.12	0.426	0.01	b.d	98.9
60	59.6	0.372	37.96	0.428	b.d	0.07	0.440	0.12	b.d	99.0
60	59.7	0.313	38.29	0.437	b.d	0.07	0.431	bd	b.d	99.3
60	59.2	0.635	38.03	0.409	b.d	0.10	0.442	bd	b.d	99.0
60	59.3	0.560	38.26	0.459	b.d	0.09	0.434	0.09	b.d	99.3
AVG	**59.7**	**0.340**	**38.78**	**0.396**		**0.09**	**0.386**	**0.09**		**99.8**
STDEV	**0.3**	**0.189**	**0.45**	**0.152**		**0.02**	**0.105**	**0.05**		**0.6**

Appendix II: Magnetite Chemistry

Sample #	FeO	Ag	S	Mn	Si	Pb	Cu	Zn	Au	Total
18	91.4	0.029	0.009	0.018	b.d	NA	b.d	0.11	b.d	91.6
18	91.3	0.025	0.013	0.037	b.d	NA	b.d	0.12	b.d	91.5
18	90.7	0.015	0.019	0.022	b.d	0.03	b.d	b.d	b.d	90.8
18	90.8	0.005	b.d	0.032	b.d	0.03	0.009	0.11	b.d	91.0
18	89.1	0.009	0.023	0.051	b.d	0.05	0.008	0.20	b.d	89.5
18	89.8	0.028	0.017	0.064	b.d	0.03	0.011	0.39	b.d	90.4
18	89.0	0.020	0.022	0.081	b.d	0.03	b.d	0.39	b.d	89.6
AVG	**90.3**	**0.019**	**0.015**	**0.044**		**0.04**	**0.004**	**0.19**		**90.6**
STDEV	**1.0**	**0.009**	**0.008**	**0.023**		**0.01**	**0.005**	**0.15**		**0.8**
19	88.9	0.009	0.023	0.261	b.d	0.04	0.007	0.46	b.d	89.8
AVG	**88.9**	**0.009**	**0.023**	**0.261**		**0.04**	**0.007**	**0.46**		**89.8**
STDEV										
21	90.0	0.008	b.d	0.075	b.d	NA	b.d	0.40	NA	90.5
21	90.3	0.025	0.014	0.075	b.d	NA	0.008	0.45	NA	90.9
21	91.6	b.d	0.009	0.092	b.d	NA	b.d	b.d	NA	91.7
21	91.9	0.017	b.d	0.034	b.d	NA	b.d	0.13	NA	92.2
21	92.9	0.014	0.019	0.026	b.d	NA	b.d	0.07	NA	93.1
21	91.3	0.012	0.008	0.018	b.d	NA	b.d	b.d	NA	91.4
21	90.9	0.021	0.014	0.056	b.d	NA	b.d	0.13	NA	91.2
21	91.3	0.004	0.015	0.057	b.d	NA	0.006	b.d	NA	91.5
21	92.0	0.005	0.014	0.026	b.d	NA	0.005	b.d	NA	92.1
AVG	**91.4**	**0.012**	**0.010**	**0.051**			**0.002**	**0.13**		**91.6**
STDEV	**0.9**	**0.008**	**0.007**	**0.026**			**0.003**	**0.17**		**0.8**
22	89.4	0.009	0.023	0.070	b.d	0.05	b.d	0.37	b.d	90.0
22	90.2	0.014	0.025	0.083	b.d	0.04	b.d	0.39	b.d	90.8
22	91.4	0.006	0.011	0.048	b.d	0.04	b.d	0.06	b.d	91.6
22	89.7	0.003	0.014	0.057	b.d	0.05	b.d	0.20	b.d	90.0
22	89.8	b.d	0.012	0.049	b.d	0.05	0.011	0.16	b.d	90.1
AVG	**90.1**	**0.006**	**0.017**	**0.061**		**0.04**	**0.002**	**0.23**		**90.5**
STDEV	**0.8**	**0.005**	**0.006**	**0.015**		**0.01**	**0.005**	**0.14**		**0.7**
24	92.5	0.015	0.008	0.061	b.d	NA	b.d	0.000	NA	92.8
24	90.5	0.072	b.d	0.074	b.d	NA	0.011	0.011	NA	91.0
24	91.2	0.068	0.013	0.072	b.d	NA	0.015	0.015	NA	91.9
24	90.8	0.082	0.016	0.056	b.d	NA	0.010	0.010	NA	91.4

	FeO	Ag	S	Mn	Si	Pb	Cu	Zn	Au	Total
24	90.2	0.006	b.d	0.060	b.d	NA	0.007	0.24	NA	90.5
24	90.5	0.017	0.023	0.072	b.d	NA	0.011	0.43	NA	91.2
24	89.8	0.033	0.020	0.071	b.d	NA	b.d	0.33	NA	90.4
AVG	**90.8**	**0.042**	**0.012**	**0.066**			**0.008**	**0.34**		**91.3**
STDEV	**0.9**	**0.031**	**0.009**	**0.007**			**0.006**	**0.09**		**0.8**
25	91.4	0.014	0.014	0.062	b.d	NA	b.d	0.14	NA	91.7
25	91.2	0.007	0.001	0.027	b.d	NA	b.d	b.d	NA	91.3
25	91.3	0.007	b.d	0.042	b.d	NA	b.d	0.05	NA	91.5
AVG	**91.3**	**0.009**	**0.005**	**0.044**				**0.06**		**91.5**
STDEV	**0.1**	**0.004**	**0.008**	**0.018**				**0.07**		**0.2**
27	90.2	0.016	0.008	0.052	b.d	0.04	0.006	0.10	b.d	90.4
27	91.1	0.012	0.009	0.038	b.d	0.02	b.d	b.d	b.d	91.2
AVG	**90.6**	**0.014**	**0.009**	**0.045**		**0.03**	**0.003**	**0.10**		**90.8**
STDEV	**0.6**	**0.003**	**0.001**	**0.010**		**0.01**	**0.004**			**0.6**
28	89.3	0.098	0.001	0.157	b.d	NA	0.011	0.57	NA	90.2
28	90.1	0.014	0.001	0.118	b.d	NA	b.d	0.24	NA	90.5
28	89.5	0.081	0.009	0.151	b.d	NA	0.006	0.44	NA	90.2
28	89.9	0.059	0.008	0.120	b.d	NA	0.010	0.38	NA	90.6
28	90.5	0.049	b.d	0.078	b.d	NA	b.d	0.12	NA	90.7
28	90.2	0.080	0.020	0.100	b.d	NA	0.012	0.28	NA	90.5
28	90.4	0.030	0.018	0.093	b.d	NA	0.014	0.19	NA	90.8
28	91.1	0.004	b.d	0.086	b.d	NA	b.d	0.20	NA	91.5
28	90.1	b.d	b.d	0.164	b.d	NA	b.d	b.d	NA	90.3
28	90.0	0.003	b.d	0.159	b.d	NA	b.d	b.d	NA	90.2
28	91.4	b.d	b.d	0.038	b.d	NA	0.004	b.d	NA	91.5
28	89.7	0.003	b.d	0.136	b.d	NA	0.005	b.d	NA	90.0
28	91.1	0.005	0.008	0.068	b.d	NA	b.d	b.d	NA	91.2
28	91.1	0.016	0.020	0.100	b.d	NA	0.004	b.d	NA	91.2
AVG	**90.3**	**0.032**	**0.006**	**0.112**			**0.005**	**0.30**		**90.7**
STDEV	**0.6**	**0.035**	**0.008**	**0.038**			**0.005**	**0.16**		**0.5**
29	91.6	b.d	0.005	0.072	b.d	0.04	b.d	0.41	b.d	92.2
29	92.8	b.d	0.010	0.054	b.d	0.05	b.d	0.11	b.d	93.0
29	92.2	0.006	b.d	0.054	b.d	0.03	b.d	0.21	b.d	92.5
29	92.5	0.005	0.023	0.054	b.d	0.02	b.d	b.d.	b.d	92.6
29	91.4	0.008	b.d	0.057	b.d	0.02	b.d	0.19	b.d	91.8
29	91.5	0.003	b.d	0.073	b.d	0.02	b.d	0.29	b.d	91.9
AVG	**92.0**	**0.004**	**0.006**	**0.061**		**0.03**		**0.20**		**92.3**
STDEV	**0.5**	**0.003**	**0.009**	**0.009**		**0.01**		**0.14**		**0.5**

	FeO	Ag	S	Mn	Si	Pb	Cu	Zn	Au	Total
30	91.3	0.006	0.012	0.042	b.d	NA	b.d	b.d	NA	91.4
30	91.8	0.012	0.014	0.038	b.d	NA	b.d	b.d	NA	91.9
30	91.5	0.015	0.015	0.034	b.d	NA	b.d	b.d	NA	91.6
30	90.8	0.033	0.019	0.050	b.d	NA	0.005	b.d	NA	91.0
30	90.6	0.004	b.d	0.057	b.d	NA	b.d	b.d	NA	90.7
30	89.6	0.039	0.025	0.025	b.d	0.05	0.007	0.37	b.d	90.2
30	91.0	0.024	b.d	0.035	b.d	0.03	b.d	0.25	b.d	91.4
30	90.1	0.045	0.018	0.043	b.d	0.04	0.010	0.57	b.d	90.9
30	90.6	0.036	0.018	0.028	b.d	0.04	0.009	0.35	b.d	91.2
30	90.7	0.018	0.011	0.033	b.d	0.02	b.d	0.44	b.d	91.3
30	91.2	0.013	b.d	0.019	b.d	0.04	0.005	0.33	b.d	91.6
30	88.6	0.021	0.013	0.028	b.d	0.04	b.d	0.34	b.d	89.0
30	88.1	0.023	0.015	0.024	b.d	0.02	0.004	0.27	b.d	88.5
30	90.7	0.012	0.010	0.024	b.d	0.03	b.d	0.31	b.d	91.1
AVG	**90.5**	**0.021**	**0.012**	**0.034**		**0.04**	**0.003**	**0.36**		**90.9**
STDEV	**1.1**	**0.013**	**0.008**	**0.011**		**0.01**	**0.004**	**0.10**		**1.0**
31	90.5	0.037	0.019	0.072	b.d	0.04	0.005	0.49	b.d	91.3
31	91.4	0.040	b.d	0.080	b.d	0.02	b.d	0.33	b.d	91.9
31	92.5	0.067	b.d	0.081	b.d	0.05	b.d	0.40	b.d	93.1
31	90.7	0.098	0.020	0.063	b.d	0.03	0.009	0.33	b.d	91.3
31	91.4	0.037	0.007	0.085	b.d	0.03	0.006	0.39	b.d	92.0
31	90.5	0.050	b.d	0.094	b.d	0.03	0.006	0.40	b.d	91.2
31	92.4	0.011	b.d	0.051	b.d	0.05	b.d	0.07	b.d	92.7
31	92.3	0.005	b.d	0.045	b.d	0.05	b.d	0.06	b.d	92.5
31	91.4	0.008	0.010	0.035	b.d	0.02	b.d	0.16	b.d	91.8
31	92.9	b.d	b.d	0.037	b.d	0.04	b.d	0.06	b.d	93.1
31	92.7	0.009	0.008	0.076	b.d	0.03	b.d	0.14	b.d	93.0
31	92.4	0.003	b.d	0.051	b.d	0.02	b.d	0.05	b.d	92.6
31	92.3	0.004	b.d	0.044	b.d	0.02	0.005	0.13	b.d	92.5
31	92.7	0.003	b.d	0.057	b.d	0.02	0.008	0.13	b.d	93.0
31	92.3	0.003	b.d	0.070	b.d	0.01	b.d	0.07	b.d	92.5
AVG	**91.9**	**0.025**	**0.004**	**0.063**		**0.03**	**0.003**	**0.21**		**92.3**
STDEV	**0.8**	**0.029**	**0.007**	**0.018**		**0.01**	**0.004**	**0.16**		**0.7**
34	87.3	0.050	0.016	1.568	0.018	b.d	b.d	0.52	b.d	89.4
34	89.0	0.020	0.015	1.790	0.017	0.03	0.011	0.44	b.d	91.4
34	89.6	0.048	0.016	1.343	0.016	0.02	b.d	0.17	b.d	91.3
34	89.5	0.023	b.d	1.585	0.018	0.02	b.d	0.33	b.d	91.6
34	89.1	0.037	0.017	1.759	0.034	0.07	0.004	0.42	b.d	91.4
34	86.6	0.009	0.015	2.263	0.026	0.04	b.d	0.33	b.d	89.3
AVG	**88.5**	**0.031**	**0.013**	**1.718**	**0.021**	**0.03**	**0.002**	**0.37**		**90.7**
STDEV	**1.3**	**0.016**	**0.006**	**0.311**	**0.007**	**0.02**	**0.004**	**0.12**		**1.1**

	FeO	Ag	S	Mn	Si	Pb	Cu	Zn	Au	Total
35	90.1	0.019	b.d	0.469	b.d	0.02	0.006	0.03	b.d	90.7
35	88.9	0.046	0.018	1.157	b.d	0.03	0.006	0.39	b.d	90.6
35	88.4	0.027	0.007	1.214	b.d	0.02	0.004	0.36	b.d	90.1
35	90.0	0.030	0.015	0.784	b.d	0.03	0.006	0.26	b.d	91.3
35	89.5	0.011	0.009	0.704	b.d	0.03	b.d	0.06	b.d	90.3
35	88.0	0.034	0.010	1.119	b.d	0.02	b.d	0.35	b.d	89.6
AVG	**89.1**	**0.028**	**0.010**	**0.908**		**0.02**	**0.004**	**0.24**	**b.d**	**90.4**
STDEV	**0.8**	**0.012**	**0.006**	**0.300**		**0.01**	**0.003**	**0.16**		**0.6**
36	89.0	0.017	b.d	1.298	b.d	0.04	b.d	0.39	b.d	90.8
36	88.5	0.016	0.011	1.384	b.d	0.02	0.010	0.34	b.d	90.3
36	89.6	0.018	0.016	0.935	b.d	0.03	0.005	0.09	b.d	90.7
36	89.9	0.010	0.021	0.885	b.d	0.03	0.008	0.17	b.d	91.0
36	90.2	0.004	0.015	0.686	b.d	0.03	0.006	0.21	b.d	91.2
36	91.2	0.005	0.007	0.226	b.d	0.05	b.d	0.06	b.d	91.6
36	91.2	b.d	b.d	0.185	b.d	0.04	b.d	0.03	b.d	91.5
36	91.0	b.d	b.d	0.271	b.d	0.04	b.d	0.13	b.d	91.5
AVG	**90.1**	**0.009**	**0.009**	**0.734**		**0.03**	**0.004**	**0.18**		**91.1**
STDEV	**1.0**	**0.008**	**0.008**	**0.475**		**0.01**	**0.004**	**0.13**		**0.5**
37	89.2	0.012	0.017	0.871	b.d	0.03	b.d	0.38	b.d	90.6
37	90.3	0.022	0.013	0.726	b.d	0.04	b.d	0.28	b.d	91.5
37	89.5	0.066	0.011	0.796	b.d	0.04	0.012	0.42	b.d	90.9
37	89.6	0.029	0.007	0.503	b.d	0.02	0.004	0.19	b.d	90.4
37	90.6	0.010	b.d	0.511	b.d	0.05	0.006	1.04	b.d	92.3
37	89.6	0.011	0.017	0.840	b.d	0.04	0.004	1.36	b.d	91.9
37	89.8	0.003	0.012	0.635	b.d	0.04	b.d	1.32	b.d	92.0
37	91.2	0.006	0.008	0.365	b.d	0.03	b.d	0.50	b.d	92.1
AVG	**90.0**	**0.020**	**0.011**	**0.656**		**0.04**	**0.003**	**0.69**		**91.5**
STDEV	**0.7**	**0.020**	**0.006**	**0.183**		**0.01**	**0.004**	**0.48**		**0.7**
38	88.7	0.036	b.d	0.840	0.045	0.04	0.006	0.53	b.d	90.2
38	88.8	0.064	0.017	0.850	0.040	0.01	b.d	0.55	b.d	90.4
38	89.2	0.011	b.d	0.856	0.033	0.05	0.004	0.50	b.d	90.7
38	88.9	0.012	0.012	0.877	0.042	0.04	b.d	0.50	b.d	90.4
38	90.7	b.d	0.025	0.522	b.d	0.02	b.d	0.08	b.d	91.3
38	88.5	0.060	b.d	0.699	b.d	0.03	0.009	0.32	b.d	89.7
AVG	**89.1**	**0.031**	**0.009**	**0.774**	**0.027**	**0.03**	**0.003**	**0.41**	**b.d**	**90.5**
STDEV	**0.7**	**0.027**	**0.011**	**0.139**	**0.021**	**0.01**	**0.004**	**0.18**		**0.6**

	FeO	Ag	S	Mn	Si	Pb	Cu	Zn	Au	Total
44	92.3	b.d	0.017	0.086	b.d	0.01	b.d	0.24	b.d	92.7
44	92.0	b.d	0.023	0.072	b.d	0.06	b.d	0.11	b.d	92.4
44	92.0	b.d	0.007	0.175	b.d	0.04	b.d	0.14	b.d	92.4
44	92.0	b.d	0.019	0.129	b.d	0.01	b.d	0.18	b.d	92.4
44	92.1	b.d	0.024	0.085	b.d	0.05	b.d	0.17	b.d	92.5
44	91.9	b.d	b.d	0.053	b.d	0.01	b.d	0.08	b.d	92.1
44	91.8	b.d	0.026	0.069	b.d	0.01	b.d	0.17	b.d	92.1
44	92.1	b.d	0.017	0.066	b.d	0.02	b.d	0.10	b.d	92.3
44	89.4	0.014	b.d	1.346	b.d	0.03	0.017	0.31	b.d	91.1
44	90.2	0.025	b.d	0.678	b.d	0.03	0.007	0.02	b.d	91.0
44	90.4	0.018	b.d	0.728	b.d	0.03	b.d	0.08	b.d	91.4
44	91.06	0.029	b.d	0.691	b.d	0.02	0.010	0.03	b.d	91.9
44	89.5	0.026	b.d	1.276	b.d	0.05	0.002	0.28	b.d	91.1
AVG	**91.3**	**0.009**	**0.010**	**0.420**		**0.03**	**0.003**	**0.15**		**92.0**
STDEV	**1.0**	**0.012**	**0.011**	**0.474**		**0.02**	**0.005**	**0.09**		**0.6**
45	91.6	0.039	b.d	0.164	b.d	0.06	0.006	b.d	b.d	91.9
45	91.0	0.055	0.013	0.396	b.d	0.04	0.009	0.10	b.d	91.6
45	91.1	0.038	0.018	0.639	b.d	0.04	0.004	0.16	b.d	92.1
45	90.8	0.079	b.d	0.382	b.d	0.03	0.013	0.16	b.d	91.5
45	90.6	0.087	b.d	0.625	b.d	0.04	0.007	0.15	b.d	91.6
45	91.2	0.003	0.023	0.570	b.d	0.04	b.d	0.13	b.d	92.1
AVG	**91.1**	**0.050**	**0.009**	**0.463**		**0.04**	**0.006**	**0.12**		**91.8**
STDEV	**0.3**	**0.031**	**0.010**	**0.184**		**0.01**	**0.004**	**0.06**		**0.2**
46	91.3	0.017	0.025	0.376	b.d	0.00	b.d	0.07	b.d	91.8
46	91.5	0.013	0.017	0.441	b.d	0.04	b.d	0.10	b.d	92.2
46	91.6	0.038	0.015	0.272	b.d	0.04	0.007	0.08	b.d	92.1
46	92.0	0.041	b.d	0.216	b.d	0.04	0.007	b.d	b.d	92.4
46	91.0	0.019	0.011	0.373	b.d	0.05	b.d	0.15	b.d	91.7
46	90.79	0.021	0.008	0.308	b.d	0.03	0.008	0.11	b.d	91.3
AVG	**91.4**	**0.025**	**0.013**	**0.331**		**0.04**	**0.004**	**0.08**		**91.9**
STDEV	**0.5**	**0.012**	**0.009**	**0.081**		**0.02**	**0.004**	**0.05**		**0.4**
47	86.8	0.009	0.015	1.684	0.021	0.03	0.005	0.56	b.d	89.2
47	87.6	b.d	0.024	1.986	0.023	0.03	b.d	0.37	b.d	90.1
47	87.7	0.004	b.d	1.994	0.026	0.02	b.d	0.34	b.d	90.1
47	86.4	0.033	0.006	2.846	0.045	0.05	0.013	0.54	b.d	90.0
AVG	**87.1**	**0.011**	**0.011**	**2.127**	**0.029**	**0.03**	**0.004**	**0.45**		**89.8**
STDEV	**0.6**	**0.015**	**0.010**	**0.500**	**0.011**	**0.01**	**0.006**	**0.12**		**0.4**

	FeO	Ag	S	Mn	Si	Pb	Cu	Zn	Au	Total
48	88.2	0.042	0.023	0.827	b.d	0.02	b.d	1.46	b.d	90.7
48	88.3	0.042	0.011	0.871	b.d	0.03	0.004	1.50	b.d	90.9
AVG	**88.3**	**0.042**	**0.017**	**0.849**		**0.02**	**0.002**	**1.48**		**90.8**
STDEV	**0.1**	**b.d**	**0.008**	**0.031**		**0.01**	**0.003**	**0.03**		**0.3**
49	90.2	0.018	0.016	0.346	b.d	0.03	b.d	0.21	b.d	90.9
49	90.7	b.d	0.010	0.296	b.d	0.02	0.004	0.15	b.d	91.2
49	89.7	b.d	0.019	0.303	b.d	0.02	0.006	0.24	b.d	90.3
AVG	**90.2**	**0.006**	**0.015**	**0.315**		**0.02**	**0.003**	**0.20**		**90.8**
STDEV	**0.5**	**0.010**	**0.004**	**0.027**		**0.01**	**0.003**	**0.04**		**0.5**
50	91.7	b.d	0.019	0.061	b.d	0.03	b.d	0.10	b.d	92.0
50	91.3	b.d	0.014	0.107	b.d	0.03	b.d	0.07	b.d	91.5
50	91.8	b.d	0.016	0.110	b.d	0.04	0.008	0.18	b.d	92.2
50	87.6	0.006	0.011	0.711	b.d	0.04	b.d	0.22	b.d	88.7
50	90.0	0.013	b.d	0.785	b.d	0.04	b.d	0.25	b.d	91.1
50	91.1	0.005	b.d	0.550	b.d	0.05	0.013	0.09	b.d	92.6
AVG	**90.4**	**0.004**	**0.010**	**0.387**		**0.04**	**0.003**	**0.15**		**91.4**
STDEV	**1.7**	**0.005**	**0.008**	**0.332**		**0.01**	**0.005**	**0.07**		**1.4**
51	89.2	0.009	0.015	1.000	b.d	0.06	0.028	0.34	b.d	90.7
51	91.0	0.005	0.018	0.304	b.d	0.03	0.009	0.07	b.d	91.5
51	90.2	0.002	0.015	0.524	b.d	0.02	0.016	0.40	b.d	91.2
51	89.6	0.009	0.023	0.971	b.d	0.03	0.034	0.12	b.d	90.9
51	90.4	0.005	0.023	0.528	b.d	0.07	0.015	0.12	b.d	91.2
AVG	**90.1**	**0.006**	**0.019**	**0.666**		**0.04**	**0.020**	**0.21**		**91.1**
STDEV	**0.7**	**0.003**	**0.004**	**0.306**		**0.02**	**0.010**	**0.15**		**0.3**
52	89.5	b.d	0.023	0.369	b.d	0.04	b.d	0.47	b.d	90.5
52	90.0	b.d	0.021	0.385	b.d	0.04	b.d	0.30	b.d	90.9
52	90.3	b.d	0.023	0.271	b.d	0.03	b.d	0.24	b.d	90.9
52	90.0	0.037	0.015	0.735	b.d	0.05	b.d	0.19	b.d	91.1
52	90.3	0.037	b.d	0.807	b.d	0.03	b.d	0.25	b.d	91.5
52	91.1	0.079	0.010	0.802	b.d	0.02	0.006	0.36	b.d	92.4
52	91.7	0.026	b.d	0.406	b.d	0.02	b.d	b.d	b.d	92.4
52	82.9	0.070	0.015	0.715	b.d	0.02	0.008	0.27	b.d	83.8
52	90.3	0.037	0.007	0.742	b.d	0.05	0.009	0.26	b.d	91.7
52	89.5	0.093	b.d	0.739	b.d	0.01	0.004	0.31	b.d	90.7
52	89.3	0.092	b.d	0.661	b.d	0.02	0.004	0.21	b.d	90.4
AVG	**89.6**	**0.043**	**0.010**	**0.603**		**0.03**	**0.003**	**0.26**	**b.d**	**90.6**
STDEV	**2.4**	**0.036**	**0.009**	**0.201**		**0.01**	**0.003**	**0.12**	**b.d**	**2.3**

	FeO	Ag	S	Mn	Si	Pb	Cu	Zn	Au	Total
53	88.9	0.085	0.024	1.258	b.d	b.d	b.d	0.12	b.d	90.5
AVG	**88.9**	**0.085**	**0.024**	**1.258**				**0.12**		**90.5**
54	90.2	0.083	0.014	0.719	b.d	0.04	b.d	0.10	b.d	91.2
54	91.1	0.054	0.020	0.664	b.d	0.01	0.004	0.19	b.d	92.1
54	90.0	0.073	b.d	0.776	b.d	0.04	0.005	0.24	b.d	91.2
54	90.0	0.099	0.015	0.540	b.d	0.02	0.009	0.17	b.d	90.9
54	89.6	0.057	0.010	0.751	b.d	0.02	b.d	0.43	b.d	90.9
54	89.6	0.060	0.024	0.788	b.d	0.05	0.005	0.20	b.d	90.8
54	90.4	0.026	0.017	0.656	b.d	0.02	b.d	0.22	b.d	91.4
54	89.1	0.053	0.010	0.816	b.d	0.02	0.007	0.36	b.d	90.4
AVG	**90.0**	**0.063**	**0.014**	**0.714**		**0.03**	**0.004**	**0.24**		**91.1**
STDEV	**0.60**	**0.022**	**0.007**	**0.090**		**0.01**	**0.003**	**0.11**		**0.5**
55	88.6	b.d	0.017	0.744	b.d	0.05	0.007	0.48	b.d	90.2
55	88.7	0.003	0.021	0.771	b.d	0.04	0.008	0.57	b.d	90.5
55	89.2	b.d	0.020	0.908	b.d	0.02	b.d	0.50	b.d	90.7
55	88.7	0.045	0.011	1.019	b.d	0.04	0.010	0.39	b.d	90.4
55	89.7	0.021	0.010	1.141	b.d	0.02	b.d	0.42	b.d	91.4
55	89.0	0.053	b.d	1.041	b.d	0.02	0.005	0.51	b.d	90.7
55	90.0	0.010	0.021	0.898	b.d	0.02	b.d	0.41	b.d	91.4
55	89.4	0.058	0.019	1.060	b.d	0.04	0.008	0.54	b.d	90.9
AVG	**89.6**	**0.024**	**0.015**	**0.948**		**0.03**	**0.005**	**0.48**		**90.8**
STDEV	**0.5**	**0.025**	**0.007**	**0.142**		**0.01**	**0.004**	**0.06**		**0.4**
56	89.6	0.024	0.013	0.868	b.d	0.05	b.d	0.22	b.d	90.9
56	89.2	0.031	b.d	1.210	b.d	0.04	b.d	0.33	b.d	90.9
56	88.7	0.072	0.011	1.187	b.d	0.03	0.010	0.25	b.d	90.5
56	87.8	0.049	b.d	1.242	b.d	0.02	0.004	0.34	b.d	89.6
56	88.6	0.022	b.d	1.192	b.d	0.03	b.d	0.37	b.d	90.3
56	88.8	0.004	0.021	1.143	b.d	0.04	b.d	0.42	b.d	90.5
56	87.7	b.d	0.014	1.033	b.d	0.05	0.010	0.33	b.d	89.2
56	87.9	0.017	0.014	1.024	b.d	0.03	b.d	0.30	b.d	89.4
56	88.0	0.091	0.025	1.174	b.d	0.02	0.007	0.48	b.d	90.0
56	88.6	0.004	0.007	0.948	b.d	0.04	b.d	0.37	b.d	89.6
56	89.9	0.005	0.013	0.748	b.d	0.04	b.d	0.09	b.d	90.7
56	89.7	0.004	b.d	0.637	b.d	0.06	b.d	0.19	b.d	90.8
56	90.8	0.007	b.d	0.617	b.d	0.04	b.d	0.02	b.d	91.4
56	90.7	b.d	b.d	0.739	b.d	0.01	b.d	0.13	b.d	91.3
56	90.0	0.009	0.007	0.865	b.d	0.03	b.d	0.13	b.d	91.4
56	89.8	0.018	0.013	1.026	b.d	0.05	b.d	0.38	b.d	91.3
56	88.0	0.007	0.037	1.121	b.d	0.04	0.016	0.36	b.d	90.5
56	88.2	0.015	b.d	1.209	b.d	0.02	0.010	0.38	b.d	90.6
56	88.9	0.012	0.020	1.237	b.d	0.02	0.014	0.42	b.d	90.4
56	89.4	0.010	0.015	0.927	b.d	0.04	0.007	0.18	b.d	90.8
AVG	**89.0**	**0.020**	**0.011**	**1.007**		**0.04**	**0.004**	**0.29**		**90.5**
STDEV	**0.8**	**0.024**	**0.010**	**0.205**		**0.01**	**0.005**	**0.13**		**0.7**

	FeO	Ag	S	Mn	Si	Pb	Cu	Zn	Au	Total
57	89.5	0.010	0.023	1.046	b.d	0.05	b.d	0.52	b.d	91.2
57	90.4	0.005	0.025	0.776	b.d	0.04	b.d	0.42	b.d	91.7
57	91.0	0.004	0.023	0.647	b.d	0.05	0.007	0.34	b.d	92.1
57	90.7	0.005	b.d	0.720	b.d	0.03	0.005	0.36	b.d	91.9
57	88.9	0.035	0.019	1.152	b.d	0.05	b.d	0.48	b.d	90.7
57	90.2	0.026	b.d	0.733	b.d	0.03	0.005	0.09	b.d	91.1
57	89.5	0.047	b.d	1.126	b.d	0.02	0.012	0.60	b.d	91.3
57	89.6	0.074	0.010	1.030	b.d	0.03	0.019	0.30	b.d	91.1
57	90.6	0.009	0.009	0.910	b.d	0.04	0.009	0.46	b.d	92.1
57	88.4	0.010	0.010	1.140	b.d	0.02	0.005	0.56	b.d	90.2
57	91.3	b.d	b.d	0.066	b.d	0.01	b.d	0.03	b.d	91.4
57	89.1	b.d	b.d	0.344	b.d	0.04	0.006	0.09	b.d	89.6
57	91.3	b.d	b.d	0.062	b.d	0.03	b.d	b.d	b.d	91.5
AVG	**90.0**	**0.017**	**0.009**	**0.750**	**b.d**	**0.03**	**0.005**	**0.33**		**91.2**
STDEV	**0.9**	**0.022**	**0.010**	**0.384**	**b.d**	**0.01**	**0.006**	**0.21**		**0.7**
59	89.8	0.029	0.022	0.953	b.d	0.04	b.d	0.20	b.d	91.1
59	89.6	0.019	0.013	0.974	b.d	0.02	b.d	0.29	b.d	91.0
59	88.9	0.023	b.d	0.912	b.d	0.03	b.d	0.24	b.d	90.2
59	88.8	0.036	b.d	0.926	b.d	0.06	b.d	0.31	b.d	90.2
59	89.1	0.005	0.023	0.909	b.d	0.01	b.d	0.25	b.d	90.3
59	89.7	0.008	0.013	0.934	b.d	0.00	b.d	0.22	b.d	90.9
AVG	**89.3**	**0.020**	**0.012**	**0.935**		**0.03**		**0.25**		**90.6**
STDEV	**0.4**	**0.012**	**0.010**	**0.025**		**0.02**		**0.04**		**0.4**
60	88.2	0.028	0.010	1.258	b.d	0.03	b.d	0.26	b.d	89.8
60	88.1	0.021	b.d	1.223	b.d	0.06	0.010	0.27	b.d	89.7
60	87.9	0.030	0.007	1.269	b.d	0.02	0.004	0.35	b.d	89.6
60	89.7	0.016	b.d	1.100	b.d	0.02	b.d	0.20	b.d	91.1
AVG	**88.5**	**0.024**	**0.004**	**1.212**		**0.03**	**0.004**	**0.27**		**90.1**
STDEV	**0.9**	**0.007**	**0.005**	**0.078**		**0.02**	**0.005**	**0.06**		**0.7**

Appendix III: Silver-iron sulfide Chemistry

	Fe	Ag	S	Mn	Si	Pb	Cu	Zn	Au	Total
Sample 17										
Avg	25.3	44.4	14.9	0.03	b.d		4.8	0.49	NA	90.0
COUNT	1									
Sample 18										
Avg	12.0	58.9	19.0	0.03	b.d		3.3	2.0	NA	95.4
Std	6.7	9.9	3.2	0.01	b.d		0.8	2.8		1.9
COUNT	8									
Sample 19										
Avg	10.5	63.0	18.3	0.07	b.d		1.4	0.9	NA	94.2
Std	5.9	12.3	2.6	0.06	b.d		0.4	1.1		3.1
COUNT	2									
Sample 21										
Avg	4.4	75.7	14.1	0.01	b.d		0.5	0.6	NA	95.4
Std	3	4	2	0	b.d		0.0	1.0		3.0
COUNT	10									
Sample 22										
Avg	14.4	59.5	15.0	0.05	b.d		1.8	6.2	NA	97.1
Std	8.0	12.9	1.4	0.01	b.d		0.7	8.5		3.1
COUNT										
Sample 24										
Avg	7.5	69.5	17.5	0.02	b.d		1.4	0.5	NA	96.5
Std	1.4	3.2	1.0	0.01	b.d		0.3	0.4		1.3
COUNT	6									
Sample 25										
Avg	2.5	80.6	14.1	0.02	b.d		1.0	0.1	NA	98.3
Std	1.1	1.2	0.7	0.02	b.d		0.7	0.0		1.4
COUNT	2									
Sample 27										
Avg	3.9	73.3	15.4	0.04	b.d	0.4	1.6	0.60	NA	95.4
Std										
COUNT	1									
Sample 28										
Avg	7.7	66.4	17.8	0.04	b.d		2.8	1.3	NA	96.1
Std	2.2	6.2	1.7	0.02	b.d		1.0	1.8		0.5
COUNT	3									
Sample 29										
Avg	4.0	73.7	14.6	0.01	b.d	1.0	1.9	0.5	NA	95.8
Std	2.1	4.9	1.4	0.01	b.d	0.3	0.7	0.7		2.2
COUNT	6									

Sample 31	Fe	Ag	S	Mn	Si	Pb	Cu	Zn	Au	Total
Avg	3.4	79.2	14.5	0.04	b.d	0.4	0.5	0.3	NA	98.6
Std	1.4	2.5	0.6	0.02	b.d	0.1	0.2	0.5		0.4
COUNT	5									
Sample 34										
Avg	9.4	61.9	19.0	0.36	b.d	0.5	1.6	1.4	NA	94.1
Std	4.3	8.1	2.3	0.42		0.3	0.5	2.1		3.1
COUNT										
Sample 35										
Avg	4.5	72.4	16.1	0.27	b.d	1.6	2.6	0.2	NA	97.7
Std	0.8	2.2	0.3	0.06		1.4	0.3	0.1		1.2
COUNT	5									
Sample 36										
Avg	5.6	68.9	16.3	0.28	b.d	1.0	2.0	1.9	NA	96.1
Std	3.0	5.6	1.8	0.25		0.6	0.7	1.5		4.4
COUNT	3									
Sample 37										
Avg	4.2	72.3	15.1	0.10	b.d	3.8	2.1	0.1	NA	97.9
Std	1.1	4.20	0.8	0.04		2.7	0.7	0.1		1.7
COUNT	3									
Sample 40										
Avg	5.1	67.7	14.7	0.21	b.d	4.7	1.9	0.6	NA	95.2
Std	2.4	5.3	2.5	0.18		5.2	0.7	0.9		0.8
COUNT	5									
Sample 44										
Avg	4.7	67.1	14.0	0.20	b.d	3.9	2.2	0.5	2.1	94.8
Std	1.	7.2	1.4	0.10		2.9	0.8	0.6	0.7	2.2
COUNT	5									
Sample 45										
Avg	3.4	75.9	13.0	0.06	b.d	0.4	2.3	0.03	NA	95.3
Std	1.7	3.1	3.1	0.05		0.2	0.4	0.02		3.0
COUNT	5									
Sample 46										
Avg	3.72	72.3	14.1	0.14	b.d	2.4	2.7	0.3	b.d	95.6
Std	0.70	0.6	0.6	0.08		0.6	0.1	0.1		1.3
COUNT	3									
Sample 49										
Avg	13.9	50.6	17.2	0.05	b.d	3.1	1.9	b.d	5.3	92.2
Std	2.7	3.3	1.1	0.02		1.5	0.7		0.4	0.3
COUNT	3									
Sample 50										

	Fe	Ag	S	Mn	Si	Pb	Cu	Zn	Au	Total
Avg	16.6	51.7	20.9	0.30	b.d	3.0	0.8	0.2	1.9	95.5
Std	5.7	9.8	3.0	0.02		0.2	0.0	0.0	0.0	0.84
COUNT	2									
Sample 51										
Avg	8.4	59.5	14.9	0.17	b.d	5.2	7.3	0.1	0.4	96.0
Std	1.2	3.1	1.0	0.06		3.5	2.0	0.1	0.7	3.2
COUNT	3									
Sample 53										
Avg	3.7	75.6	14.2	0.14	b.d	0.4	1.8	0.1	b.d	95.9
Std	1.0	0.4	0.5	0.05		0.1	0.4	0.2		2.0
COUNT	4									

Appendix IV: Electrum Chemistry

Sample #				mols	mols	
Piece 3	Ag	Au	Total	Ag	Au	X_{Ag}
46	2.51	96.19	98.83	0.02	0.49	0.05
46	2.61	96.73	99.43	0.02	0.49	0.05
46	2.62	96.55	99.25	0.02	0.49	0.05
46	2.66	96.92	99.67	0.02	0.49	0.05
46	2.55	96.30	98.95	0.02	0.49	0.05
46	2.78	96.80	99.68	0.03	0.49	0.05
46	2.92	96.38	99.40	0.03	0.49	0.05
46	2.98	95.96	99.01	0.03	0.49	0.05
46	3.07	96.25	99.42	0.03	0.49	0.05
46	3.15	96.84	100.06	0.03	0.49	0.06
46	3.65	95.31	99.02	0.03	0.48	0.07
46	3.61	95.91	99.61	0.03	0.49	0.06
46	3.61	95.68	99.36	0.03	0.49	0.06
46	3.53	95.77	99.37	0.03	0.49	0.06
46	3.54	95.25	98.86	0.03	0.48	0.06
46	3.56	95.40	99.03	0.03	0.49	0.06
46	3.55	95.89	99.52	0.03	0.49	0.06
46	3.55	95.99	99.63	0.03	0.49	0.06
46	3.60	95.95	99.69	0.03	0.49	0.06
46	3.64	95.96	99.67	0.03	0.49	0.06
46	3.67	95.49	99.22	0.03	0.49	0.07
Piece 4						
46	2.61	98.98	101.68	0.02	0.50	0.05
46	2.70	97.97	100.73	0.03	0.50	0.05
46	2.88	94.49	97.45	0.03	0.48	0.05
46	2.94	98.90	101.95	0.03	0.50	0.05
46	3.08	98.34	101.50	0.03	0.50	0.05
46	3.26	98.79	102.15	0.03	0.50	0.06
Sample #	Ag	Au	Total	mols Ag	mols Au	X_{Ag}
47	0.28	99.93	100.28	0.00	0.51	0.01
47	0.30	99.94	100.29	0.00	0.51	0.01
47	0.31	100.33	100.67	0.00	0.51	0.01

Sample #	Ag	Au	Total	mols Ag	mols Au	X_{Ag}
47	0.36	100.12	100.53	0.00	0.51	0.01
47	0.41	99.92	100.39	0.00	0.51	0.01
47	0.35	99.86	100.28	0.00	0.51	0.01
Piece 1						
47	0.25	97.32	97.70	0.00	0.49	0.00
47	0.41	100.91	101.39	0.00	0.51	0.01
47	0.42	100.42	100.91	0.00	0.51	0.01
47	0.39	100.71	101.17	0.00	0.51	0.01
47	0.43	99.81	100.29	0.00	0.51	0.01
47	0.42	100.23	100.72	0.00	0.51	0.01
47	0.39	100.44	100.88	0.00	0.51	0.01
47	0.45	100.15	100.66	0.00	0.51	0.01
47	0.47	100.06	100.62	0.00	0.51	0.01
47	0.49	100.19	100.74	0.00	0.51	0.01
Piece 2						
47	12.65	85.72	98.43	0.12	0.44	0.21
47	11.57	85.49	97.10	0.11	0.43	0.20
47	11.66	86.03	97.73	0.11	0.44	0.20
47	11.78	86.20	98.04	0.11	0.44	0.20
47	11.29	86.64	97.99	0.10	0.44	0.19
47	11.82	86.75	98.60	0.11	0.44	0.20
47	11.66	86.80	98.50	0.11	0.44	0.20
47	12.37	86.96	99.37	0.11	0.44	0.21
47	12.09	87.13	99.29	0.11	0.44	0.20
47	12.81	87.00	99.84	0.12	0.44	0.21

Sample #	Ag	Au	Total	mols Ag	mols Au	X_{Ag}
Piece 1						
49	9.33	90.35	99.75	0.09	0.46	0.16
49	8.99	90.55	99.60	0.08	0.46	0.15
49	8.59	90.82	99.49	0.08	0.46	0.15
49	8.53	90.90	99.48	0.08	0.46	0.15
49	8.51	87.88	96.47	0.08	0.45	0.15
49	8.85	90.48	99.38	0.08	0.46	0.15
49	9.41	89.89	99.39	0.09	0.46	0.16
49	10.01	88.49	98.59	0.09	0.45	0.17
49	10.55	88.74	99.36	0.10	0.45	0.18
49	10.96	87.96	98.98	0.10	0.45	0.19

Sample #	Ag	Au	Total	mols Ag	mols Au	X_{Ag}
49	8.47	83.70	92.39	0.08	0.43	0.16
49	9.36	88.42	97.87	0.09	0.45	0.16
49	8.71	87.99	97.01	0.08	0.45	0.15
Piece 2						
49	13.22	84.43	97.72	0.12	0.43	0.22
49	13.19	84.29	97.55	0.12	0.43	0.22
49	13.30	84.05	97.39	0.12	0.43	0.22
49	11.40	83.48	94.98	0.11	0.42	0.20
49	13.35	85.04	98.45	0.12	0.43	0.22
49	13.62	82.07	95.75	0.13	0.42	0.23

Sample #	Ag	Au	Total	mols Ag	mols Au	X_{Ag}
Piece 1						
50	7.03	93.77	100.92	0.07	0.48	0.12
50	7.00	93.20	100.30	0.06	0.47	0.12
50	7.34	93.63	101.06	0.07	0.48	0.12
50	7.61	92.93	100.64	0.07	0.47	0.13
50	8.82	91.79	100.71	0.08	0.47	0.15
50	9.49	91.12	100.69	0.09	0.46	0.16
50	10.10	90.91	101.08	0.09	0.46	0.17
50	10.43	90.36	100.86	0.10	0.46	0.17
50	10.89	89.47	100.42	0.10	0.45	0.18
Piece 2						
50	11.64	87.81	99.51	0.11	0.45	0.19
50	11.69	87.57	99.35	0.11	0.45	0.20
50	11.61	88.59	100.28	0.11	0.45	0.19
50	11.65	86.99	98.73	0.11	0.44	0.20
50	11.60	87.49	99.13	0.11	0.44	0.19
50	11.42	87.65	99.13	0.11	0.45	0.19
50	11.64	88.09	99.82	0.11	0.45	0.19
50	11.62	88.65	101.09	0.11	0.45	0.19
Piece 2						
50	11.72	87.42	100.20	0.11	0.44	0.20
50	10.68	86.96	101.34	0.10	0.44	0.18
50	11.55	86.75	99.45	0.11	0.44	0.20

Sample #	Ag	Au	Total	mols Ag	mols Au	X_{Ag}
Piece 1						
51	15.55	79.50	95.42	0.14	0.40	0.26
51	16.17	80.18	96.75	0.15	0.41	0.27
51	16.27	80.29	96.97	0.15	0.41	0.27
51	16.24	80.62	97.27	0.15	0.41	0.27
51	15.67	79.84	95.89	0.15	0.41	0.26
Piece 1						
51	16.34	82.90	99.66	0.15	0.42	0.26
51	16.28	82.94	99.67	0.15	0.42	0.26
51	16.14	83.40	99.92	0.15	0.42	0.26
51	16.25	82.99	99.66	0.15	0.42	0.26
51	16.07	82.98	99.45	0.15	0.42	0.26
51	16.28	83.11	99.77	0.15	0.42	0.26
Piece 1						
51	16.37	82.31	100.42	0.15	0.42	0.27
51	14.85	73.44	104.07	0.14	0.37	0.27
51	16.45	77.11	98.92	0.15	0.39	0.28
51	15.82	82.81	100.04	0.15	0.42	0.26
51	15.75	82.53	99.38	0.15	0.42	0.26

Sample #	Ag	Au	Total	mols Ag	mols Au	X_{Ag}
Piece 1						
52	0.01	99.78	99.86	0.0001	0.51	0.0002
52	0.02	99.68	99.75	0.0001	0.51	0.0003
52	0.02	100.52	100.59	0.0002	0.51	0.0003
52	0.01	99.98	100.03	0.0001	0.51	0.0002
52	0.01	99.71	99.78	0.0001	0.51	0.0002
52	0.01	100.04	100.15	0.0001	0.51	0.0002
Piece 1						
52	0.03	99.81	99.93	0.0003	0.51	0.0005
52	0.03	99.86	99.98	0.0003	0.51	0.0006
52	0.03	99.63	99.76	0.0003	0.51	0.0005
52	0.03	100.08	100.24	0.0003	0.51	0.0005
Piece 2						
52	0.07	100.04	100.14	0.0006	0.51	0.0013
52	0.12	99.44	99.61	0.0012	0.51	0.0023
52	0.07	99.88	100.03	0.0007	0.51	0.0013
52	0.07	100.32	100.42	0.0007	0.51	0.0013

Sample #	Ag	Au	Total	mols Ag	mols Au	X_{Ag}
Piece 2						
52	0.31	100.21	100.62	0.0029	0.51	0.0056
52	0.32	99.46	99.91	0.0030	0.51	0.0059
52	0.33	99.07	99.49	0.0030	0.50	0.0060
52	0.33	99.09	99.55	0.0031	0.50	0.0061
52	0.36	99.41	99.96	0.0033	0.51	0.0065

Sample #	Ag	Au	Total	mols Ag	mols Au	X_{Ag}
Piece 1						
53	0.04	99.21	99.41	0.0003	0.50	0.0006
53	0.03	100.36	100.54	0.0003	0.51	0.0006
53	0.04	99.34	99.52	0.0004	0.51	0.0007
53	0.04	99.35	99.52	0.0003	0.51	0.0007
53	0.05	98.75	98.98	0.0004	0.50	0.0009
53	0.04	99.10	99.29	0.0004	0.50	0.0007
Piece 2						
53	0.01	100.39	100.48	0.0001	0.51	0.0003
53	0.01	100.40	101.05	0.0001	0.51	0.0003
53	0.01	100.62	100.71	0.0001	0.51	0.0002
53	0.02	99.95	100.02	0.0002	0.51	0.0003
53	0.02	100.20	100.30	0.0002	0.51	0.0004
53	0.02	100.12	100.19	0.0001	0.51	0.0003

Sample #	Ag	Au	Total	mols Ag	mols Au	X_{Ag}
Piece 1						
54	0.41	98.74	99.22	0.0038	0.50	0.0075
54	0.40	98.83	99.31	0.0037	0.50	0.0074
54	0.40	99.60	100.07	0.0037	0.51	0.0072
54	0.40	98.62	99.13	0.0037	0.50	0.0073
54	0.39	98.59	99.04	0.0037	0.50	0.0072
54	0.43	98.61	99.11	0.004	0.50	0.008
Piece 2						
54	0.08	99.06	99.19	0.0007	0.50	0.0014
54	0.07	99.45	99.56	0.0007	0.51	0.0013
54	0.08	98.99	99.13	0.0008	0.50	0.0015

Sample #	Ag	Au	Total	mols Ag	mols Au	X_{Ag}
54	0.07	99.45	99.63	0.0007	0.51	0.0013
54	0.07	99.98	100.08	0.0006	0.51	0.0012
54	0.08	99.68	99.81	0.0007	0.51	0.0014

Sample #	Ag	Au	Total	mols Ag	mols Au	X_{Ag}
Piece 1						
55	14.55	83.91	98.49	0.13	0.43	0.24
55	14.13	83.59	97.74	0.13	0.43	0.24
55	14.56	83.79	98.41	0.13	0.43	0.24
Piece 2	11.31	86.98	98.39	0.10	0.44	0.19
55	11.36	87.41	98.81	0.11	0.44	0.19
55	11.33	87.08	98.46	0.11	0.44	0.19
55	11.40	87.66	99.12	0.11	0.45	0.19
55	11.22	87.81	99.11	0.10	0.45	0.19
55	11.21	87.39	98.64	0.10	0.44	0.19
55	11.27	87.63	98.94	0.10	0.45	0.19
55	12.03	83.88	98.43	0.11	0.43	0.21
55	10.18	81.20	95.28	0.09	0.41	0.19

Sample #	Ag	Au	Total	mols Ag	mols Au	X_{Ag}
Piece 1						
56	14.06	82.54	96.84	0.13	0.42	0.24
56	13.99	82.95	97.00	0.13	0.42	0.24
56	14.40	82.77	97.18	0.13	0.42	0.24
56	14.30	83.27	97.60	0.13	0.42	0.24
56	14.41	83.77	98.24	0.13	0.43	0.24
56	14.46	83.90	98.38	0.13	0.43	0.24
56	14.50	83.82	98.33	0.13	0.43	0.24

Sample #	Ag	Au	Total	mols Ag	mols Au	X_{Ag}
Piece 1						
57	8.48	89.61	98.15	0.08	0.46	0.15
57	8.44	89.72	98.24	0.08	0.46	0.15
57	8.43	89.71	98.18	0.08	0.46	0.15
57	8.58	89.73	98.37	0.08	0.46	0.15
57	8.68	89.96	98.72	0.08	0.46	0.15
57	8.57	89.59	98.21	0.08	0.46	0.15

Sample #	Ag	Au	Total	mols Ag	mols Au	X_{Ag}
57	8.35	90.94	99.35	0.08	0.46	0.14
57	8.37	91.02	99.45	0.08	0.46	0.14
57	8.15	89.71	97.92	0.08	0.46	0.14
57	8.40	90.21	98.75	0.08	0.46	0.15
57	8.72	89.24	98.00	0.08	0.45	0.15
Piece 2						
57	13.89	84.72	98.65	0.13	0.43	0.23
57	13.96	85.09	99.08	0.13	0.43	0.23
57	13.95	84.82	98.82	0.13	0.43	0.23
57	13.78	84.50	98.31	0.13	0.43	0.23
57	13.88	84.58	98.51	0.13	0.43	0.23
57	13.70	84.11	97.83	0.13	0.43	0.23
57	13.63	84.08	97.76	0.13	0.43	0.23

Sample #	Ag	Au	Total	mols Ag	mols Au	X_{Ag}
Piece 1						
58	0.22	99.85	100.17	0.0020	0.51	0.0039
58	0.22	99.92	100.23	0.0020	0.51	0.0039
58	0.25	99.90	100.28	0.0024	0.51	0.0046
58	0.21	99.87	100.17	0.0019	0.51	0.0038
58	0.21	99.43	99.76	0.0019	0.51	0.0038
58	0.22	100.72	101.08	0.0021	0.51	0.0040
Piece 2						
58	0.22	99.51	99.84	0.0021	0.51	0.0041
58	0.22	99.23	99.54	0.0021	0.50	0.0041
58	0.23	98.74	99.07	0.0022	0.50	0.0043
58	0.23	100.10	100.44	0.0022	0.51	0.0043
58	0.26	99.03	99.39	0.0024	0.50	0.0047
58	0.27	99.91	100.27	0.0025	0.51	0.0050

Sample #	Ag	Au	Total	mols Ag	mols Au	X_{Ag}
Piece 1						
59	0.45	99.27	99.82	0.0042	0.50	0.0082
59	0.41	99.29	99.78	0.0038	0.50	0.0075
59	0.40	98.91	99.41	0.0037	0.50	0.0073
59	0.39	99.31	99.78	0.0036	0.51	0.0070
59	0.39	100.19	100.74	0.0037	0.51	0.0071
59	0.51	98.69	99.31	0.0047	0.50	0.0093

Sample #	Ag	Au	Total	mols Ag	mols Au	X_{Ag}
Piece 2						
59	0.47	99.64	100.29	0.0044	0.51	0.0086
59	0.45	98.64	99.24	0.0042	0.50	0.0083
59	0.45	98.82	99.47	0.0041	0.50	0.0082
59	0.47	99.37	99.97	0.0043	0.51	0.0085
59	0.43	98.70	99.28	0.0040	0.50	0.0079
59	0.49	98.95	99.56	0.0045	0.50	0.0089

Appendix V: Silicate Glass Chemistry

Sample #	SiO2	Al2O3	Na2O	K2O	CaO	FeO	Cl	Total
1	71.3	9.4	3.8	6.3	b.d	3.0	0.15	94.1
1	73.1	11.8	2.8	7.8	0.02	0.6	0.11	96.3
1	73.9	11.4	3.0	6.6	0.11	0.2	0.17	95.5
1	75.5	10.7	3.0	6.6	b.d	0.1	0.15	96.2
1	75.6	10.4	3.4	6.9	0.03	1.4	0.23	97.8
1	75.6	10.8	3.2	6.8	0.08	0.5	0.23	97.4
1	75.9	10.5	2.9	6.3	b.d	0.7	0.15	96.8
1	71.9	11.7	2.9	8.0	0.08	1.3	0.21	96.2
1	67.5	11.5	3.3	9.9	0.00	4.7	0.20	96.9
1	67.4	14.5	2.7	11.2	b.d	3.2	0.09	99.1
1	68.7	10.1	3.8	6.6	0.06	2.7	0.19	92.2
1	71.9	10.9	3.1	6.6	0.04	1.8	0.16	94.6
1	72.9	8.6	3.7	6.5	0.01	4.7	0.26	96.7
1	73.6	7.5	3.5	6.3	0.04	4.0	0.22	95.4
1	70.1	9.3	4.0	6.4	0.01	4.7	0.04	94.6
Average	**72.3**	**10.4**	**3.3**	**7.3**	**0.03**	**2.3**	**0.17**	**96.0**
STDEV	**2.8**	**1.6**	**0.4**	**1.4**	**0.04**	**1.7**	**0.06**	**1.7**
ASI	**0.80**							

Sample #	SiO2	Al2O3	Na2O	K2O	CaO	FeO	Cl	Total
2	67.5	7.7	4.0	6.6	0.03	10.5	0.57	96.9
2	66.90	7.4	4.0	7.0	0.03	9.8	0.55	95.7
2	67.6	7.6	4.1	6.7	0.05	9.9	0.59	96.6
2	68.5	7.1	3.9	6.7	0.07	9.5	0.60	96.5
2	68.7	6.5	3.8	6.5	0.03	9.8	0.55	95.9
2	68.8	6.2	3.8	6.4	0.04	9.4	0.58	95.4
2	68.5	5.5	3.9	6.3	0.05	10.9	0.60	95.7
2	68.6	4.7	3.8	6.1	0.06	11.5	0.64	95.4
2	66.7	6.9	3.9	6.6	0.09	8.9	0.59	93.7
2	67.2	7.1	3.8	6.7	0.07	9.0	0.58	94.5
2	66.9	7.2	4.0	6.5	0.06	9.2	0.59	94.5
2	67.6	7.1	4.1	6.7	0.03	9.1	0.57	95.3
2	67.1	7.3	3.8	6.9	0.09	8.5	0.60	94.2
2	66.3	7.6	3.9	6.6	0.28	8.4	0.64	93.7
2	67.2	7.7	3.8	6.6	0.06	8.3	0.57	94.3
2	68.2	7.8	3.7	6.8	0.04	8.4	0.53	95.5
2	68.0	7.5	3.8	6.8	0.00	8.6	0.52	95.1
2	67.5	7.7	3.8	6.7	0.04	8.7	0.52	94.9
2	67.6	7.5	3.6	6.6	0.04	8.5	0.54	94.3
2	68.1	7.0	3.8	6.7	0.03	9.8	0.53	96.0
2	67.9	7.0	3.9	6.6	0.03	9.6	0.56	95.7
2	67.8	7.0	3.8	6.6	0.02	9.9	0.48	95.6
2	66.6	6.7	3.7	6.4	0.03	9.3	0.50	93.3
Average	**67.7**	**7.1**	**3.9**	**6.6**	**0.06**	**9.4**	**0.57**	**95.2**
STDEV	**0.7**	**0.75**	**0.1**	**0.2**	**0.05**	**0.8**	**0.04**	**1.0**
ASI	**0.50**							

Works Cited

Albinson, T., Norman, D., Cole, D., Chomiak, B. 2001. Controls on Formation of Low- Sulphidation Epithermal Deposits in Mexico: Constraints from Fluid Inclusions and Stable Isotope Data. In: New Mines and Discoveries in Mexico and Central America, Ed: Nelson, C, Society of Economic Geologists, 1-32.

Anderko, A., Pitzer, K.S., 1993. Phase equlibria and volumetric properties of the systems KCl-H2O and NaCl-KCl-H2O above 573K : Equation of state representation. *Geochimica et Cosmochimica Acta*, 57, 4885-4897.

Audetat, A., Gunther, D., Heinrich, C.A., 1998. Formation of Magmatic-Hydrothermal Ore Deposit: Insights with LA-ICP-MS Analysis of Fluid Inclusions. *Science*, 279, 2091-2094.

Audetat, A., Pettke, T., 2003. The magmatic-hydrothermal evolution of two barren granites: A melt and fluid inclusion study of the Rito del Medio and Canada Pinabete plutons in Northern New Mexico (USA). *Geochimica et Cosmochimica Acta,* 67, 97-121.

Ballantyne, G.H, Smith, T. W., Redmond, P.E., 1997. Gold and silver in the Bingham Canyon porphyry copper deposit, Utah. In: GSA Abstracts with Programs, 29, 283.

Barton, M.D., 1996. Granitic magmatism and metallogeny of the southwestern North America, *Transactions of the Royal Society of Edinburgh: Earth Sciences,* 87, 261-280.

Barton, P. B., Toulmin, P., 1964. The electrum-tarnish method for the determination of fugacity of sulfur in laboratory sulfide systems. *Geochimica et Cosmochimica Acta.*, 28, 619-640.

Blevin, P.L, Chappell, B.W., Allen, C.W., 1996. Intrusive metallogenic provinces in eastern Australia based on granite source and composition, *Transactions of the Royal Society of Edinburgh: Earth Sciences,* 87, 281-290.

Blundy, J., Wood, B., 2003. Partitioning of trace elements between crystals and melts, *Earth and Planetary Science Letters,* 210, 383-397.

Bodnar, R.J,. Sterner, S.M., 1985. Synthetic fluid inclusions in natural quartz. II. Application to PVT studies. *Geochimica et Cosmochimica Acta*, 49, 1855-1859.

Brown, K.L., 1986. Gold Deposition from Geothermal Discharges in New Zealand, *Econ. Geol.,* 81, 979-983.

Burnham, C.W., 1975. Waters and magmas; a mixing model. *Geochimica et. Cosmochimica Acta.,* 39, 1077-1084.

Burham, C.W., Magmas and hydrothermal fluids. In: H.L. Barnes, Geochemistry of Hydrothermal Ore Deposits (2nd ed.). John Wiley & Sons, pp 71-136.

Candela, P.A., 1992. Controls on ore metal ratios in granite-related ore systems: an experimental and computational approach, *Transactions of the Royal Society of Edinburgh: Earth Sciences*, 83, 317-326.

Candela, P.A., Bouton, S.L, 1990. The influence of oxygen fugacity on Tungsten and Molybdenum Partitioning between silicate melts and Ilmenite, *Econ. Geol.,* 85, 633-640.

Candela, P.A, and Holland, H.D., 1984. The partitioning of copper and molybdenum between silicate melts and aqueous fluids. *Geochimica et Cosmochimica Acta,* 48, 373-380.

Candela, P.A., and Holland, H.D., 1986. A mass transfer model for copper and molybdenum in magmatic hydrothermal systems; the origin of porphyry-type ore depostis. *Econ. Geol*., 81, 1-19.

Candela, P.A, Piccoli, P.M., 1995. Model ore-metal partitioning from melts into vapor and vapor/melt mixtures. In: Magma, Fluids, and Ore deposits, Ed: Thompson, J.F.H., Mineralogical Association of Canada, 23, 101-127.

Chou, I-M, 1987, Phase relations in the system NaCl-KCl-H2O; III, Solubilities of halite in vapor-saturated liquids above 445°C and redetermination of phase equilibrium properties in the system NaCl-H2O to 1000° and 1500 bars. *Geochimica et. Cosmochimica Acta,* 51, 1965-1975.

Cygan, G.L, Candela, P.A., 1995. Preliminary study of gold partitioning among pyrrhotite, pyrite, magnetite, and chalcopyrite in gold-saturated chloride solutions at 600 and 700°C, 140 MPa. In: Magmas, Fluids, and Ore Deposits, Ed: Johnson, J.F.H., Mineralogical Associated of Canada, 23, 129-137.

Czamanske, G.K., 1969, The stability of argentopyrite and sternbergite. *Econ. Geol*., 64, 459-461.

Deer, W.A., Howie, R.A., Zussman, J. Spinels and Pyrrhotite. In: An Introduction to rock-forming minerals. Longmans, 1966, 424-434, 450-452.

Ewart, A. and Griffin, W.L. 1994. Application of Proton-Microprobe Data to Trace-Element Partitioning in Volcanic-Rocks. *Chemical Geology,* 117, 251-284.

Frank, M.R., Candela, P.A., Piccoli, P.M, 2003. Alkali exchange between a silicate melt and coexisting magmatic volatile phase: An experimental study at 800°C and 100 MPa, *Geochimica et Cosmochimica Acta.* 67, 1415-1427.

Frank, M.R., Candela, P.A., Piccoli, P.M., Glascock, M.D., 2002. Gold solubility, speciation, and partitioning as a function of HCl in the brine-silicate-melt-metallic gold system at 800°C and 100 MPa. *Geochimica et Cosmochimica Acta.,* 66, 3719-3732.

Frank, M. R., 2001. An experimental investigation of ore metals in silicate melt-volatile phase systems. Pd.D. Dissertation, University of Maryland, College Park: 242 pp.

Gammons, C.H., Barnes, H.L., 1989. The solubility of Ag2S in near-neutral aqueous sulfide solutions at 25 to 300°C. *Geochimica et Cosmochimica Acta*, 53, 279-290.

Giggenbach, W.F., Corrales, R., 1992. The isotopic and chemical composition of water and steam discharges from volcanic-magmatic-hydrothermal systems of the Guanacaste geothermal province, Costa Rica. *Appl. Geochemistry*, 7, 309-332.

Gunther, D., Audetat, A., Frischknecht, R., Heinrich, C.A., 1998. Quantitative analysis of major, minor and trace elements in fluid inclusions using laser ablation-inductively coupled plasma mass spectrometry. *Journal of Analytical Atomic Spectrometry,* 13, 263-270.

Hedenquist, J.W., 1995. The ascent of magmatic fluid: Discharge versus Mineralization. In: Magmas, Fluids, and Ore deposits, Ed: Thomposon, J.F.H., Mineralogical Society of Canada, 23, 263-289.

Hedenquist, J.W, Lowenstern, J.B., 1994. The role of magmas in the formation of hydrothermal ore deposits. *Nature*, 370, 519-527.

Heinrich, C.A., Ryan, C.G., Mernagh, T.P., Eadington, P.J., 1992. Segregation of Ore Metals between Magmatic Brine and Vapor: A Fluid Inclusion study using PIXE Microanalysis. *Econ. Geol*., 6, 1566-1583.

Ishihara, S., 1981. The granitoids series and mineralization. In: Economic Geology, 75th Anniversary Edition, 458-484.

Ishihara, S., Imai, A., 2000. Geneses of high chlorine and Ag-Pb-Zn mineralized granitoids in Tsushima, Japan. *Resource Geology,* 50, 169-178.

Jugo, P., 1997. Experimental study of the behavior of copper and gold in the system: Haplogranite-$CuFeS_2$-FeS-Au-H_2O-HCl-O_2. M.S. Thesis, University of Maryland, College Park: 93 pp.

Jugo, P.J., Candela P.A., Piccoli, P.M., 1999. Magmatic sulfides and Au:Cu ratios in porphyry deposits: an experimental study of copper and gold partitioning at 850°, 100 MPa in a haplogranitic melt – pyrrhotite –intermediate solid solution – gold metal assemblage at gas saturation. *Lithos*, 46, 573-589.

Kullerud, G.,. Experimental techniques in Dry Sulfide Research, in: Research techniques for High Pressure and High Temperature. Springer-Verlag, 1971.

Luhr, J.F., 1990. Experimental phase relations of water and sulfide saturated Arc Magmas and the 1982 eruption of El Chichon volcano. *Journal of Petrology*, 31, 1071-1114.

Metrich, N., Rutherford, M.J., 1992. Experimental study of chlorine behavior in hydrous silicate melts. *Geochimica et Cosmochimica Acta.* 56, 607-616.

Morimoto, N., Nakazwa, H., Nishiguchi, K., Tokonami, M., 1974. Pyrrhotites: Stoichoimetric Compounds with the composition $Fe_{n-1}S_n$ ($n \geq 8$). *Science,* 168, 964-966.

O'Neil, J.R., Silberman, M.L, 1974. Stable Isotope Relations in Epithermal Au-Ag deposits. *Econ. Geol.,* 69, 902-909.

Robb, L. Introduction to Ore-forming processes. Blackwell Publishing, 2005, pgs. 373.

Rudnick, R.L, Gao, S., 2003. The Crust, In:Treatise on Geochemistry. Elsevier Publishing, 2003, Volume 3, pgs. 659.

Sheppard, S.M.F., Taylor, H.P., 1974. Hydrogen and Oxygen Isotopic Evidence for the Origins fo Water in the Boulder Batholith and the Butte Ore Deposit, Montana, 1974. *Econ. Geol.,* 69, 926-946.

Simmons, S.F., 1995. Magmatic contributions to low-sulphidation epithermal deposits. In: Magma, Fluids, and Ore deposits, Ed: Thompson, J.F.H., Mineralogical Association of Canada, 23, 101-127.

Simon, A.C., Candela, P.A., Piccoli, P.M., Pettke, T, Heinrich, C.A., 2002. Gold solubility in magnetite, *Geological Society of America, 2002 annual meeting Abstracts with Programs.*

Simon, A.C., 2003. An experimental study to elucidate magnetite solubility and metal partitioning in a magnetite-silicate melt-vapor-brine-gold metal assemblage. PhD. Thesis, University of Maryland, College Park. 190 pp.

Simon, A. C., Candela, P.A., Piccoli, P.M., Pettke, T., Heinrich, C.A., 2003. Vapor-brine partitioning of iron and magnetite solubility as a function of pressure in the magmatic-hydrothermal environment. *GAC-MAC Programs with Abstracts.*

Simon A.C., Pettke, T., Candela, P.A, Piccoli, P.M., Henirich, C.A., 2003. Experimental determination of Au solubility in rhyolite melt and magnetite: Constraints on magmatic Au budgets. *American Mineralogist,* 88, 1644-1651.

Simon, A.C., Pettke, T., Candela, PA., Piccoli, P.M., Heinrich, C.A., 2004. Magnetite solubility and iron transport in magmatic-hydrothermal environments. *Geochimica et Cosmochimica Acta.* 68, 4905-4914.

Simon, A.C., Candela, P.A., Piccoli, P.M., 2004. The effect of iron on the chlorine concentration in felsic melts, AGU abstracts.

Singer, D.A, Berger, V.I., Moring, B.C., 2005. Porphyry Copper Deposits of the World: Database, Map, and Grade and Tonnage Models. USGS website: http://pubs.usgs.gov/of/2005/1060/.

Stefansson, A., Seward, T.M., 2003. Experimental determination of the stability and stoichiometry of sulfide complexes of silver (I) in hydrothermal systems to 400°C. *Geochim. Cosmochim. Acta*, 67, 1395-1413.

Takagi, T., 2004. Origin of magnetite and ilmenite series-bearing granitic rocks in the Japan Arc. *American Journal of Science,* 304, 169-202.

Titley,S.R., 2001. Crustal affinities of metallogenesis in the American Southwest. *Econ. Geol.,* 6, 1323-1341.

Thompson, J.F.H., Newberry, R., 2000. Gold deposits related to reduced granitic intrusions, In: SEG Reviews, 13, 377-400.

Toulmin, P., Barton, P.B., 1964. A thermodynamic study or pyrite and pyrrhotite. *Geochimica et Cosmochimica Acta.* 28, 641-671.

Webster, J.D., De Vivo, B., 2002. Experimental and modeled solubilities of chlorine in aluminosilicate melts, consequences of magma evolution, and implications for exolution of hydrous chloride melt at Mt. Somma-Vesuvious. *The American Mineralogist*, 87, 1046-1061.

White, J.L, Orr, R.L, and Hultgren, R., 1957. The thermodynamic properties of silver-gold alloys. *Acta Metallurgica,* 5, 747-760.

Williams, T.J., Candela, P.A., Piccoli, P.M, 1995. The partitioning of copper between silicate melts and two-phase aqueous fluids: An experimental investigation at 1 kbar, 800°C and 0.5 kbar, 850°C. *Contributions to Mineralogy and Petrology*, 121, 388-399.

Whitney, J.A., 1984. Fugacities of sulfurous gases in pyrrhotite-bearing silicic magmas. *The American Mineralogist*, 69, 69-78.